Engineering 59 (2026) 82–117

Contents lists available at ScienceDirect

Engineering

journal homepage: www.elsevier.com/locate/eng

Research
Low Carbon Transformation for Conventional Energies—Review

A Review on Liquid-Ammonia Injection and Combustion for Engine Applications

Hao Wu [a,*], Fahad Almatrafi [a], Moez Ben Houidi [a], Tiegang Fang [b], William L. Roberts [a]

[a] Clean Energy Research Platform (CERP), King Abdullah University of Science and Technology (KAUST), Thuwal 23955-6900, Saudi Arabia
[b] Department of Mechanical and Aerospace Engineering, North Carolina State University, Raleigh, NC 27695, USA

ARTICLE INFO

Article history:
Received 23 March 2025
Revised 4 July 2025
Accepted 9 September 2025
Available online 20 September 2025

Keywords:
Liquid ammonia
Flash-boiling spray
Alternative fuels
Dual-fuel combustion
Internal-combustion engines

ABSTRACT

This comprehensive review examines the application of liquid-ammonia injection and combustion in engine systems, highlighting the potential of liquid ammonia as a carbon-neutral fuel alternative. The study synthesizes recent advancements in liquid-ammonia injection and combustion technologies, addressing critical domains such as fundamental fuel properties, injection and spray dynamics, combustion behavior, and engine performance. Key challenges are identified, including ammonia's high latent heat of vaporization, slow flame-propagation speed, narrow flammability range, and elevated NO_x emissions, while emphasizing the need for optimized injection strategies and nozzle designs to enhance atomization and mixing. The research findings indicate that liquid-ammonia injection can significantly reduce greenhouse gas emissions, with dual-fuel modes (e.g., ammonia–diesel) proving effective in overcoming ammonia's low reactivity. Studies show that both low-pressure and high-pressure dual fuel-injection modes can achieve substantial emission reductions, with high-pressure injections offering better thermal efficiency and lower NO_x emissions. Innovative approaches, such as turbulent jet ignition, stratified fuel injection, and hydrogen co-injection, have been explored to improve ignition efficiency and combustion stability. Future research should prioritize the development of integrated solutions that combine advanced combustion technologies, optimized engine designs, and effective emission-control strategies. Collaboration between academia, industry, and policymakers will be crucial in driving the adoption of ammonia as a sustainable fuel alternative.

1. Introduction

1.1. Background

The adoption of carbon-free energy sources and vectors has emerged as a pivotal strategy to mitigate carbon emissions and address climate-related challenges [1–3]. In recent years, ammonia (NH_3) has garnered significant attention as a potential energy source due to its unique properties and the urgent need for sustainable alternatives in the global energy transition [4,5]. Historically, ammonia has been predominantly used as a fertilizer, with about 70% of global production allocated to this purpose [6]. Traditional ammonia production relies heavily on the Haber–Bosch process, which is highly energy-intensive, accounting for about 2% of global energy consumption and approximately 450 Mt of carbon dioxide (CO_2) emissions in 2020 [7]. The focus on ammonia has driven a shift toward "green ammonia" production, which utilizes renewable electricity, water, and air to produce hydrogen for synthesizing ammonia, thereby reducing the latter's carbon footprint [8–11].

Fig. 1 highlights the role of ammonia as an energy carrier in a future energy system. Ammonia has a high volumetric (108 $kg \cdot m^{-3}$ H_2 in liquid NH_3 at 20 °C and 8.6 bar) and gravimetric (17.8 wt%) energy density [12], making it an efficient energy-storage medium. It also offers a lower cost per unit of energy stored (0.54 $USD \cdot kg^{-1}$ H_2, 182 days) [13], compared with hydrogen (14.95 $USD \cdot kg^{-1}$ H_2). Unlike hydrogen, ammonia can be stored and transported relatively easily at reasonable temperatures and pressures, making it particularly attractive for maritime shipping and long-term energy storage [14,15]. Additionally, ammonia can be catalytically decomposed into CO_x-free hydrogen [16–18] or directly used in power-generation devices such as engines, turbines, and fuel cells

* Corresponding author.
E-mail address: wu.hao@kaust.edu.sa (H. Wu).

https://doi.org/10.1016/j.eng.2025.09.008

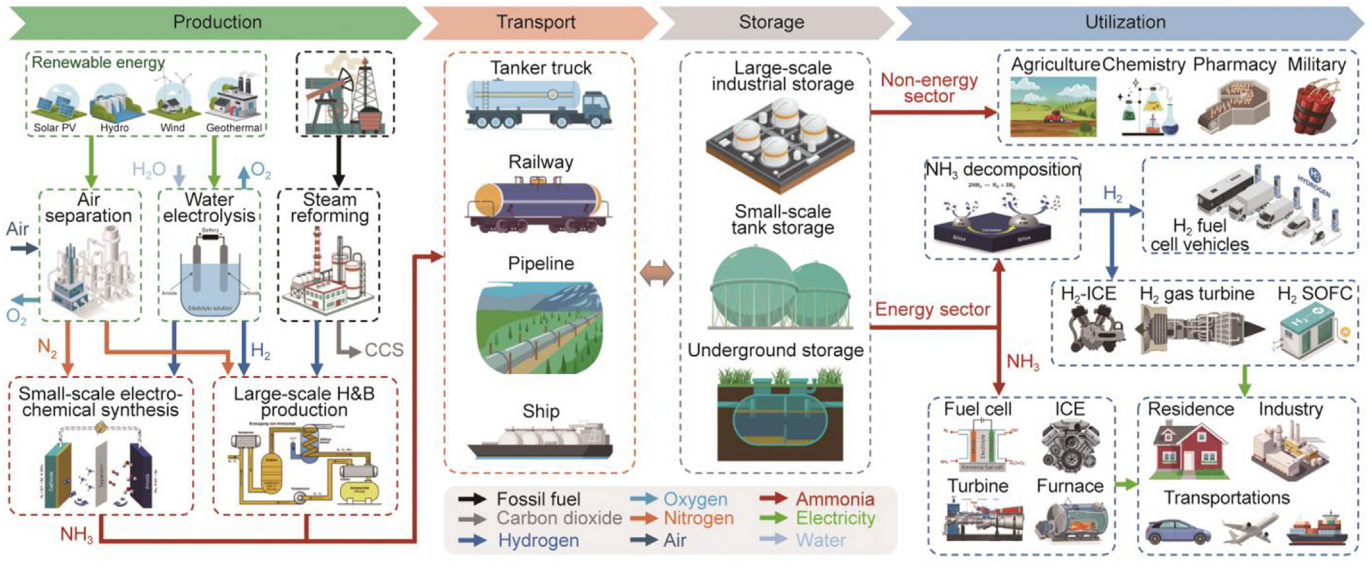

Fig. 1. The key role of ammonia as an energy carrier in a future energy system. ICE: internal combustion engines; SOFC: solid oxide fuel cells; PV: photovoltaic; CCS: carbon capture and storage; H&B: Haber–Bosch process.

[19,20]. Furthermore, ammonia has been manufactured and transported globally for more than a century, benefiting from an existing high-capacity infrastructure [21]. The shipping industry, in particular, views ammonia as a promising alternative to traditional marine fuels, given its potential to reduce emissions [22].

The use of ammonia as a fuel traces its origins to the early 20th century, with notable experiments conducted during the 1940s and later periods [23–27]. However, recent advancements in renewable energy technologies and the growing emphasis on sustainability have rekindled interest in ammonia as an energy source. By 2050, it is projected that over 50% of global ammonia manufacturing capacity will be dedicated to energy decarbonization [28]. Despite its potential, ammonia's widespread adoption still presents challenges, including high green-production costs, the need for technology to address renewable-energy intermittency [29], and safety concerns regarding its hazardous nature [6]. Ongoing research and development and robust policy support are essential to overcome these barriers and realize ammonia's potential as a sustainable energy carrier.

1.2. Ammonia as a sustainable fuel

Ammonia presents several key advantages as a fuel in transportation and industrial processes [30]. As a carbon-free compound composed only of nitrogen and hydrogen, ammonia produces no direct CO_2 emissions when combusted, making it an attractive option for reducing greenhouse gas (GHG) emissions [31]. Its liquefiability at relatively modest pressures and temperatures makes it practical for storage and transportation, offering superior energy density and manageable infrastructure requirements [32]. Additionally, ammonia's versatility allows it to be utilized across multiple sectors, including maritime transport, power generation, and industrial processes, with the potential for "green ammonia" production using renewable electricity [33]. Its versatility in application methods, ranging from direct use in modified gas turbines to co-firing with traditional fuels, offers flexible pathways for adoption while leveraging existing infrastructure [21].

Ammonia shows significant promise as a fuel across various sectors, with particular applicability in maritime transportation [34,35]. Its low reactivity and slower burn rate suit low-speed engines, enabling ocean vessels to transition from carbon-intensive bunker fuel to ammonia power, thereby reducing shipping's environmental impact. Several major shipping companies and engine manufacturers have already begun developing and testing ammonia-powered marine engines [36–40]. In the power-generation sector, ammonia can be utilized in modified gas turbines or fuel cells. Some power companies are synchronously exploring co-firing ammonia with coal or natural gas in existing power plants as a transitional solution [41–43]. Industrial processes are another key application, where ammonia serves as both fuel and chemical feedstock. The fertilizer industry's extensive ammonia-handling experience provides a natural expansion starting point. Research continues into stationary power applications and specialized vehicles, although vehicular use presents greater technical and safety challenges due to ammonia's toxic nature [5,13].

Ammonia combustion is a complex process with unique characteristics that make it both promising and challenging. Table 1 [23,44–47] summarizes the fundamental physical and chemical properties of ammonia compared with those of other commonly used fuels. Ammonia is characterized by its well-known low reactivity, which results in poor ignition characteristics and a narrow flammability range (15%–28% by volume in air) [48,49]. Its minimum ignition energy is significantly greater than that of hydrogen and other hydrocarbon fuels, making it difficult to ignite under normal conditions. This poses a particular challenge for internal-combustion engines, where rapid and reliable ignition is essential for stable operation [50,51]. However, ammonia has a high-octane number of 110, indicating its superior anti-knock properties compared with gasoline [44]. The narrow flammability range means that ammonia combustion is more sensitive to variations in the air-to-fuel ratio; thus, maintaining stable combustion becomes more challenging [52]. As a result, precise control of the fuel injection and mixing processes is crucial for efficient ammonia combustion. Another significant challenge associated with ammonia combustion is its slow flame-propagation speed [53], which makes it difficult for the flame to propagate efficiently through the fuel mixture. This results in longer combustion duration and lower thermal efficiency. Additionally, the adiabatic flame temperature of ammonia is only approximately 1800 °C, lower than those of hydrogen, natural gas, and other traditional liquid fuels [54]. This lower temperature, combined with the absence of CO_2 in the exhaust, reduces radiative heat transfer and causes combustion delay [55].

Table 1
Physical and chemical properties of various types of fuels [23,44–47].

Fuel	Density ($kg·m^{-3}$)[a,b]	Lower heating value ($MJ·kg^{-1}$)	Octane number	Boiling point (°C)	Latent heat of vaporization ($kJ·kg^{-1}$)	Minimum ignition energy (mJ)[a,c,d]	Maximum laminar flame speed ($cm·s^{-1}$)[a,b]	Flammability limit (vol%)[d]	Auto-ignition temperature (K)	Adiabatic flame temperature (K)
Ammonia	681	18.80	110	−33.4	1369	8.00	7	15–28[e]	923	1800
Hydrogen	71.1	120.10	130	−253	431	0.02	291	4–75.6	850	2390
Methane	424	50.00	108	−161	510	0.29	37	5.3–15	813	2225
Ethanol	791	26.95	100–130	78.4	838	0.23	40	4.3–19	698	2193
Methanol	792	20.09	109	64.6	1100	0.14	55	6–36	738	2143
Gasoline	750	42.40	90–98	30–200	300–350	0.24	58	1.4–7.6	~623	2580
Diesel	845	43.50	40–55	180–230	250–270	0.24	87	0.6–5.5	~523	2300

[a] Pressure at 1 atm, 1 atm = 1 bar = 101325 Pa.
[b] Temperature at 300 K.
[c] At stoichiometry.
[d] In air.
[e] Gas phase.

In addition to these technical challenges, ammonia combustion produces unique emissions requiring careful management. Ammonia's high nitrogen content leads to increased NO_x emissions during combustion [44,48]. Specifically, both nitric oxide (NO) and nitrous oxide (N_2O) are formed during ammonia combustion, with N_2O being particularly problematic due to its high global warming potential (GWP) (265–298 times that of CO_2) [56]. Moreover, incomplete ammonia combustion can result in significant unburned NH_3 emissions, posing environmental and health risks [57]. To mitigate these emissions, various strategies have been explored, including optimizing combustion conditions, using exhaust-gas recirculation (EGR), and employing selective catalytic reduction (SCR) systems [58]. While the characteristics of ammonia combustion pose significant challenges for its practical application, ongoing research and technological advancements are gradually overcoming these obstacles. Given its potential to contribute to a low-carbon future, ammonia combustion remains an area of active investigation and development.

1.3. Overview of liquid-ammonia injections and applications

Liquid ammonia presents numerous advantages as a combustion fuel, making it a practical option for a wide range of applications [59–61]:

Higher volumetric energy density. Liquid ammonia has a significantly higher volumetric energy density than gaseous ammonia. Thus, liquid ammonia can store more energy in a given volume, making it more efficient for transportation and storage. This is particularly advantageous in applications with limited space and infrastructure.

Simplified supply system. Using liquid-phase ammonia at terminals eliminates the need for additional devices (i.e., vaporizers, electric heaters, and accumulators) for gaseous conversion. This full-chain liquid-ammonia path from supply to application reduces evaporation-related energy consumption. Liquid ammonia also enables more accurate fuel metering and flow control than gaseous ammonia.

Compatibility with direct-injection systems. Direct injection (DI) of liquid fuels is well-established in internal-combustion engines and gas turbines. High-pressure liquid ammonia can utilize existing injectors, enabling liquid-ammonia DI. This method is a primary approach for investigating liquid-ammonia spray and combustion, given the absence of mature ammonia-specific injectors. However, the use of conventional gasoline and diesel direct injectors for liquid-ammonia injections poses reliability concerns.

Cost efficiency. Liquid ammonia can be transported using existing infrastructure—such as pipelines, trucks, and ships—with minimal modifications. Storage and transportation costs for liquid ammonia are lower than those for gaseous ammonia. This can make liquid ammonia more economically viable as a fuel, particularly in applications where fuel must be transported over long distances.

Fig. 2 maps liquid-ammonia injection test conditions from the current literature onto an ambient pressure–temperature phase diagram, with colors indicating research methods. Current research focuses on three aspects: liquid-ammonia injection into low-pressure, low-temperature environments, with an emphasis on flash-boiling spray characteristics; injection into high-pressure, low-temperature environments that characterize non-reactive spray behavior; and injection into high-temperature, high-pressure environments to examine spray combustion characteristics that simulate engine operating conditions and reactive states. Table 2 summarizes practical liquid-ammonia injection applications within specific ambient pressure and temperature ranges based on these test conditions.

Prior to 2021, relatively few studies were conducted on liquid-ammonia injections. However, in recent years, this area has seen exponential growth. The trends shown in Fig. 3 indicate that flash-boiling studies—in which ammonia is injected into a low-pressure ambient—have gained more momentum than high-pressure injection studies, likely due to the relative ease of experimental setup. However, in 2024, flash-boiling studies were fewer than elevated-pressure studies, likely due to the additional time required to establish safer high-pressure experimental setups. Additionally, the consensus on ammonia being more suitable as a retrofit fuel for dual-fuel, diesel-based engines may have contributed to this shift.

In addition to the fundamental challenges associated with burning ammonia as a fuel, another non-negligible issue related to the DI and combustion of liquid ammonia pertains to its high latent heat of vaporization [23,58]. The high latent heat of vaporization of liquid-ammonia spray significantly impacts the combustion process by creating a strong local cooling effect as droplets evaporate [62]. This cooling effect substantially reduces the temperature in the spray region, inhibiting flame propagation and slowing chemical reaction rates [63]. In extreme cases, it may even lead to flame extinction [64]. To address these challenges, ammonia combustion systems often require additional energy input to maintain stable combustion. Strategies such as increasing compression ratios (CRs) [65,66], preheating air [67,68], or using pilot fuels [69,70], have been explored to counteract the strong evaporative cooling effect and ensure efficient and stable combustion.

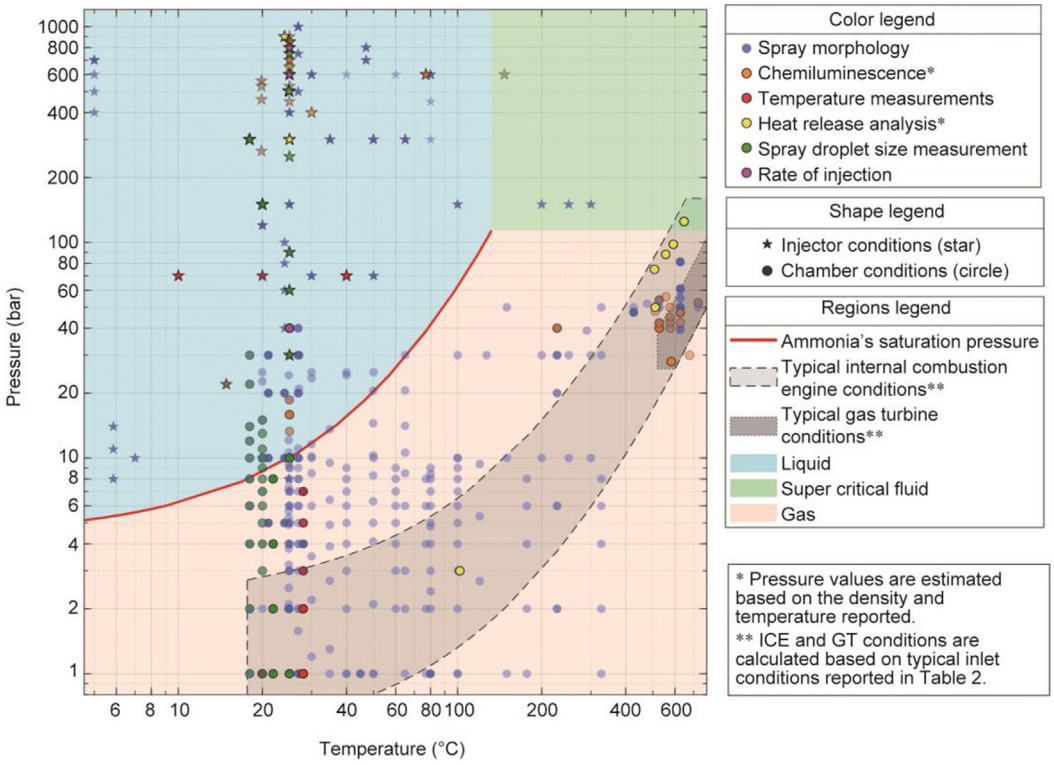

Fig. 2. Test conditions of experimental liquid-ammonia injection in the literature, plotted on an ammonia injection pressure–temperature phase diagram.

Table 2
Ambient pressure and temperature range of liquid-ammonia injection in different applications.

Application	Ambient pressure range (bar)	Ambient temperature range (°C)
PFI[a]-ICE	0.5–2.5	15–100
DI-ICE (early injection)	0.5–5.0	15–100
DI-ICE (late injection)	50–150	300–700
GT	1–30	300–600

PFI: port fuel injection; GT: gas turbine.
[a] Port fuel injection.

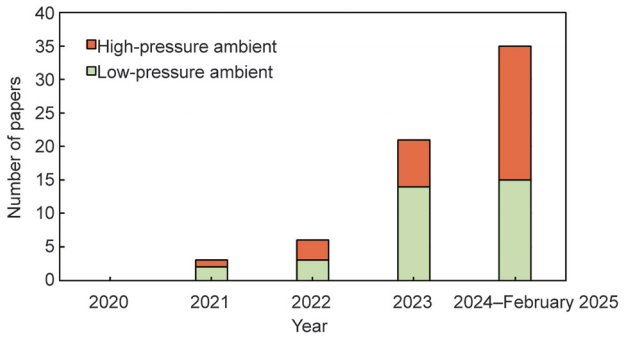

Fig. 3. Trends in ammonia injection research over the years, categorized by ambient pressure.

1.4. Motivation and outline

This paper reviews recent research progress on the injection of liquid ammonia as a fuel and its application in combustion engines. It does not further discuss the topics of where, when, or whether liquid ammonia should be used as an energy carrier. The preceding sections have summarized the attractiveness of using ammonia as a fuel, the growing interest in ammonia combustion, and potential technical challenges. Previous articles have already extensively covered gaseous ammonia combustion, with excellent reviews and research work on chemical reaction mechanisms [71–74], basic combustion characteristics [48,49,75–77], combustion instability [78–81], combustion emissions and control [44,51,82], combustion applications [58,83–85], and combustion modeling [86–89].

This paper synthesizes recent liquid-ammonia research from fundamental spray characteristics to engine implementation. Section 2 examines liquid-ammonia injections in low-pressure environments, emphasizing flash-boiling spray behavior. Section 3 explores spray dynamics under high-pressure, high-temperature conditions, covering both non-reacting sprays and combustion phenomena. Section 4 analyzes practical liquid-ammonia DI applications in engine systems. Section 5 identifies literature knowledge gaps, highlights key contemporary findings, and provides future research directions in this rapidly evolving field.

2. Liquid-ammonia injection into low pressure

Spray flash boiling occurs when pressurized liquid is rapidly depressurized below its saturated vapor pressure, causing instantaneous, explosive liquid-to-vapor phase change [90]. In this process, the pressurized liquid (or typically preheated to near boiling point) is injected through a nozzle into a lower-pressure environment. The sudden pressure drop creates superheat and thermodynamic instability [91]. This triggers rapid vapor bubble nucleation throughout the liquid, disrupting its structure and causing explosive vaporization. The rapid expansion significantly alters the spray characteristics, typically resulting in wider initial spray angles, smaller droplet sizes, enhanced atomization, and increased

rapid mixing and heat transfer [92,93]. Flash boiling in sprays is still an active area of research, with relevant research progress summarized in the latest reviews [94–96].

Fig. 4 shows the ammonia phase diagram with the gas–liquid saturation line. Two pathways induce liquid-ammonia boiling: increasing the temperature at constant pressure above the saturation temperature (A → S_1 → C) or decreasing the pressure at constant temperature below the saturation pressure (B → S_2 → C).

The extent of flash boiling is characterized using two methods: pressure/temperature difference or pressure ratio [96]. The first uses the superheat degree (SD), which is defined as the difference between the saturated vapor pressure and the ambient pressure ($P_{S2} - P_c$) or between the fuel temperature and the boiling temperature ($T_a - T_{S1}$). The second uses the superheat index, a dimensionless ratio expressed as either P_{S2}/P_a or P_a/P_{S2} [97]. For an injected superheated liquid, $P_a/P_{S2} < 1$ [92,98], with values near 0.3 marking the onset of flash boiling [99]. For an injected subcooled liquid, $P_a/P_{S2} > 1$. To maintain consistency, this review adjusts all reported values to match the first definition. Additionally, the term "superheat degree" is sometimes used interchangeably to describe both parameters.

2.1. Liquid-ammonia injection using single-hole injectors

Single-hole injectors provide a simplified, controlled environment for spray analysis by eliminating plume interactions, enabling precise measurements of spray evolution, penetration, and atomization. They minimize pattern variability, allowing the isolation of parameters such as injection pressure and nozzle geometry. Table 3 [100–111] summarizes extensive recent experimental research on liquid-ammonia spray.

Li et al. [100] (Fig. 5) reported superheated ammonia spray characteristics across different saturation-ambient pressure ratios (R_p), identifying three flashing regimes: initial-flashing ($1.0 < R_p \leq 2.0$), transitional-flashing ($2.0 < R_p \leq 5.0$), and flare-flashing ($R_p > 5.0$). Near-field analysis showed that the bubble explosion intensity depends on the SD and fuel viscosity. Far-field penetration exhibited three stages—flashing-dominated, transitional, and quasi-steady—with time-dependence exponents deviating from traditional spray models. While ammonia spray penetration resembles that of diesel under critical- and initial-flashing conditions, bubble behavior increasingly dominates penetration evolution under transitional- and flare-flashing conditions.

The team's subsequent investigation [101] of near-field characteristics and two-phase distribution in superheated ammonia sprays revealed exponential spray-volume expansion when the non-dimensional SD fell below 0.5. At a fuel temperature of 338 K, the spray volume increased by 200% within 1 mm below the nozzle. The maximum gasification ratio reached 3.5% at high temperatures, demonstrating the significant impact of bubble puffing and micro-explosions in the near-field region.

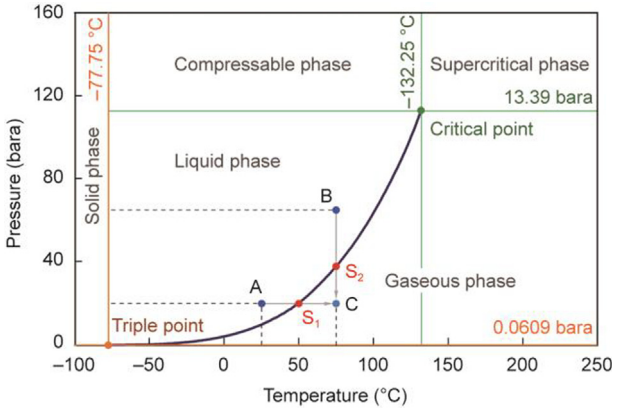

Fig. 4. Ammonia phase diagram and vapor pressure at gas–liquid equilibrium. bara: bar absolute.

Ma et al. [102] studied flash-boiling spray characteristics and jet fluctuation in high-pressure liquid-ammonia injection, identifying three axial-development stages dominated sequentially by flash boiling, unbroken liquid-core acceleration, and broken liquid-core inertia (Fig. 6). The first and third stages negatively correlated with the SD, while the second correlated positively with the initial velocity. High-speed shadowgraphy revealed a decreasing spray area with increasing ambient temperature, disappearing swirling vortices, and increased asymmetry. Near-nozzle regions exhibited significant instability under flare flash-boiling conditions, with fluctuations intensifying up to 59% at elevated temperatures due to thermal disturbances.

Fang et al. [103] experimentally investigated high-pressure liquid-ammonia injection under non-flash and flash-boiling conditions, revealing a "spray-resistance phenomenon" characterized by suppressed liquid penetration and spray tip velocity during initial injection, particularly below 0.7 MPa ambient pressure. This phenomenon, attributed to needle-lift-induced cavitation and subsequent vapor formation, obstructed the nozzle hole, reducing the mass flow rate and spray tip velocity. Flash-boiling conditions caused near-nozzle spray expansion and bubble explosion, rapidly increasing the spray width and altering aerodynamic behavior. Under non-flash conditions, the Hiroyasu and Arai's model [112] predicted liquid penetration within 3% accuracy at 4 MPa ambient pressure, outperforming the Naber and Siebers' model [113]. Additionally, this team [104] measured the droplet diameter and velocity of high-pressure liquid-ammonia sprays up to 75 MPa using a phase Doppler particle analyzer, which determines particle velocity and size by measuring phase differences between Doppler signals from intersecting laser beams [114]. Compared with that of diesel at 1 MPa ambient pressure, ammonia's Sauter mean diameter (SMD) was 50%–70% smaller across injection pressures of 25–75 MPa, attributed to its lower viscosity and higher evaporation rate. Above an injection pressure of 25 MPa, ammonia's SMD remained below 12 μm.

Liu et al. [105] employed particle-droplet image analysis based on shadowgraphy to measure liquid-ammonia spray droplets and characterize their microscopic properties, although this method is limited to localized dilution zones and requires accurate individual droplet identification. Microscopic statistics revealed that the most probable droplet size increased from about 13 μm at R_p = 0.12 to approximately 26 μm at R_p = 1.06 (ambient to saturated pressure ratio), with corresponding SMD growth from about 20 to about 60 μm and significant reduction in droplet number density. While ambient temperature minimally affected the macroscopic spray morphology, it significantly increased evaporation, particularly at 373 K, where droplet density reached minimum values.

Li et al. [106] employed high-resolution microscopic drop-size imaging to measure liquid-ammonia spray droplet-size distributions (Fig. 7). Under flare-flashing conditions (P_a = 0.1 MPa), the distribution exhibited an M-shaped cumulative volume curve, best fitted by the BIDoseResp function. This bimodal distribution resulted from vertex recirculation, with numerous small droplets dominating the probability density, while fewer large droplets contributed significantly to the cumulative volume, confirmed by dual volume density peaks. The bimodal pattern reflects complex spray–air interactions under flare-flashing conditions. As the ambient pressure increased from 0.2 to 0.8 MPa, flash boiling transitioned from transitional to initial flashing regions, with the probability densities showing corresponding rightward shifts in droplet-size distribution.

Table 3
Summary of recent experimental investigations of liquid-ammonia spray using single-hole injectors.

Reference	Injector		Condition		Methods	Key conclusions
	Hole type	Hole diameter (mm)	Injection	Ambient		
Li et al. [100]	Single	0.28	300 bar, 35–65 °C	1.0–29.5 bar, 298 K	CVC, DBI	Quantified near-field bubble explosion and far-field penetration dynamics across flashing regions; highlighted viscosity-driven bubble explosion and atypical penetration scaling
Li et al. [101]	Single	0.28	300 bar, 35–65 °C	1.0–29.5 bar, 298 K, 1.17–34.5 kg·m^{-3}	CVC, DBI, micro-imaging; Schlieren imaging	Quantified near-field gasification ($\leq$ 3.5%) and its exponential impact on two-phase distribution; highlighted bubble puffing as the primary vaporization mechanism
Ma et al. [102]	Single	0.32	300 bar, 291 K	0.1–0.8 MPa, 291–600 K	CVC, high-speed shadowgraphy	Spray exhibits three-stage axial penetration: flash-boiling-dominated, unbroken liquid core acceleration, inertia-dominated
Fang et al. [103]	Single	0.168	50–100 MPa, 300 K	0.1–4.0 MPa, 300 K	CVC, DBI	The "spray resistance phenomenon" occurs under P_{amb} < 0.7 MPa; liquid penetration and tip velocity are suppressed during 0–0.05 ms ASOI due to cavitation inside the nozzle from needle lift effects
Fang et al. [104]	Single	0.168	25–75 MPa, 298 K	0.1–1.0 MPa, 198 K	CVC, PDPA	The SMD of liquid ammonia is 50%–70% smaller than that of diesel due to lower viscosity and higher evaporation rate; flash boiling reduces the SMD further
Liu et al. [105]	Single	0.7	10 bar, 293 K	1.0–9.0 bar, 293–373 K	CVC, PDIA, Schlieren imaging	Spray morphology transitions from radial expansion (flare) to axial contraction (transition) as pressure ratio increases. Reported microscopic droplet statistics for ammonia spray under flash-boiling conditions
Li et al. [106]	Single	0.186	3.0–9.0 MPa, 295 K	0.1–0.8 MPa, 295 K	CVC, DBI, MDSI, LIBS	Performed LIBS-based quantitative ammonia concentration measurement. Flare-flashing generates bimodal droplets due to micro-explosions and recirculation; slow evaporation under flare-flashing due to ammonia's high latent heat
Zhong et al. [107]	Single	0.12, 0.32, and 0.52	30 MPa, 291 K	0.1–3.0 MPa, 291 K	CVC, high-speed shadowgraphy	SMD increases with larger nozzle diameters; with a 0.32-mm nozzle, shows optimal spray characteristics (balanced penetration, cone angle, and atomization)
Shen and Leach [108]	Single	0.55	150 bar, 20 °C	3–11 bar, 20 °C	CVC, DBI, laser diffraction	Observed a "plume-necking" phenomenon downstream of the injector tip under various conditions. Transition between flash and non-flash-boiling regions appeared abrupt for droplet size
Colson et al. [109]	Single	0.10–0.21	0.60–1.4 MPa, 270–293 K	1.0 bar	Backlit imaging	High nozzle aspect ratio and superheat trigger flashing, drastically increasing spray angles
Desclaux et al. [110]	Single	0.165	70 bar, −10–50 °C	1.0–7.0 bar, 28 °C, 1.12–8 kg·m^{-3}	CVC, Schlieren imaging, K-type thermocouples	Higher SD reduces axial penetration, increases spray angle, and enhances lateral expansion. Minimum spray temperature reached –60 °C under flash boiling
Bjørgen et al. [111]	Single	0.17	70 bar, −10–50 °C	0.15–7.0 bar, 28 °C, 0.11–8 kg·m^{-3}	CVC, Schlieren, K-type thermocouples	SD alone is insufficient to fully characterize flash-boiling state. Observed shock waves in the ammonia spray for very high SD

ASOI: after start of injection; CVC: constant-volume chamber; DBI: diffuse background illumination; LIBS: laser-induced breakdown spectroscopy; MDSI: microscopic drop size imaging; PDIA: particle droplet image analysis; PDPA: phase Doppler particle analyzer; SMD: Sauter mean diameter.

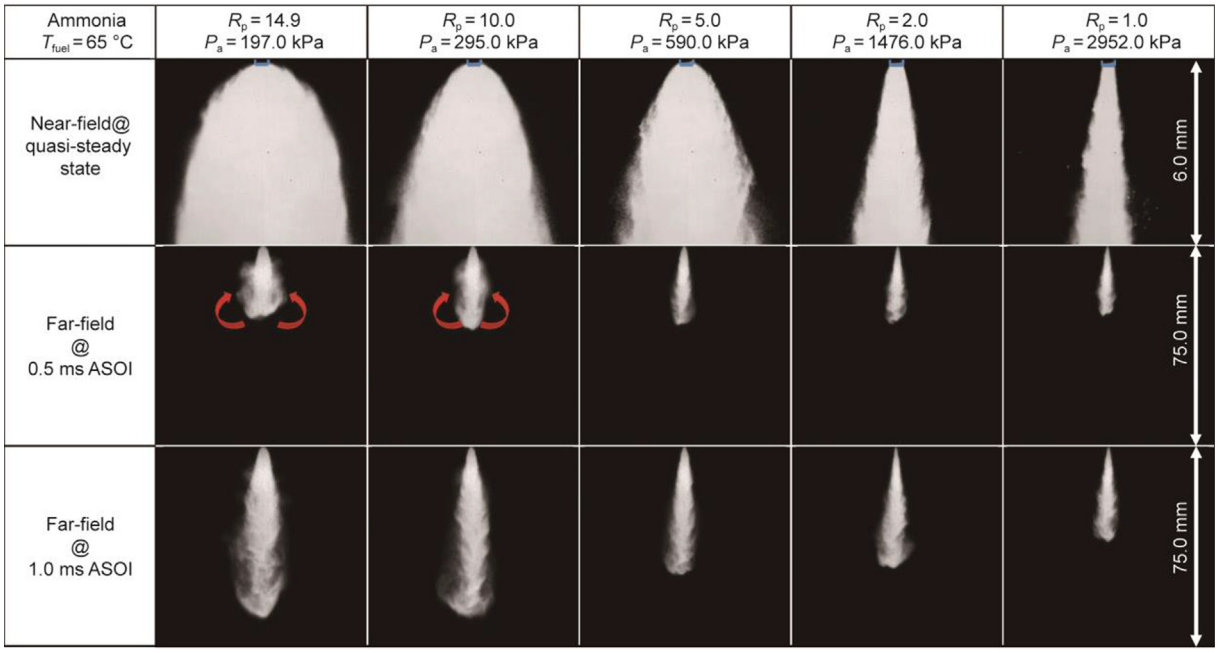

Fig. 5. Morphological features of superheated ammonia spray under different pressure ratios. P_a: ambient pressure; T_{fuel}: fuel temperature. Reproduced from Ref. [100] with permission.

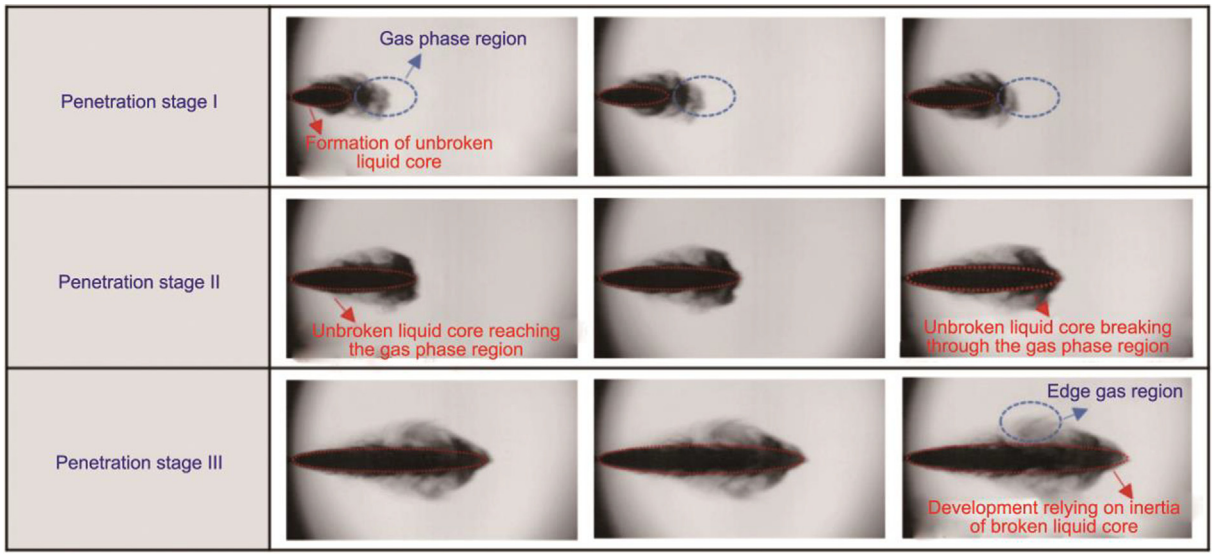

Fig. 6. Stage development process of spray under 0.2 MPa ambient pressure. Reproduced from Ref. [102] with permission.

Zhong et al. [107] examined nozzle diameter effects on the macroscopic and microscopic characteristics of flash-boiling liquid-ammonia sprays. High-speed shadowgraphy revealed that smaller diameters (0.12 mm) promoted intense radial expansion and vortex formation through enhanced thermodynamic fragmentation under low SDs, while larger nozzles (0.52 mm) produced asymmetric spray structures and larger droplets due to higher flow rates and weaker bubble nucleation. Microscopic analysis revealed non-monotonic droplet-size distribution trends, with the most probable droplet size increasing marginally for the largest diameter (0.52 mm). Spray SMD increased with nozzle diameter, particularly during non-flash boiling, where it rose up to 35%. Optimal spray performance balancing atomization, penetration, and radial dispersion was achieved using a 0.32-mm nozzle. Shen and Leach [108] also investigated liquid-ammonia spray atomization characteristics through droplet-diameter analysis. Flash-boiling conditions at low ambient pressure produced significant radial expansion, shortened penetration lengths, and reduced droplet sizes, with an SMD reaching 16 μm at 3 bar ambient pressure. Higher ambient pressures suppressed flash boiling, yielding longer penetration lengths and larger droplets (SMD of ~30 μm at 15 bar). A bimodal droplet-size distribution emerged, with smaller droplets predominating under flash-boiling conditions.

Colson et al. [109] studied injection temperature and nozzle geometry effects on liquid-ammonia spray flashing transitions using single-hole nozzles. The transition between non-flash and flash boiling strongly depended on the nozzle aspect ratio *L/D*, with a critical threshold of *L/D* = 5 identified for flash-boiling onset,

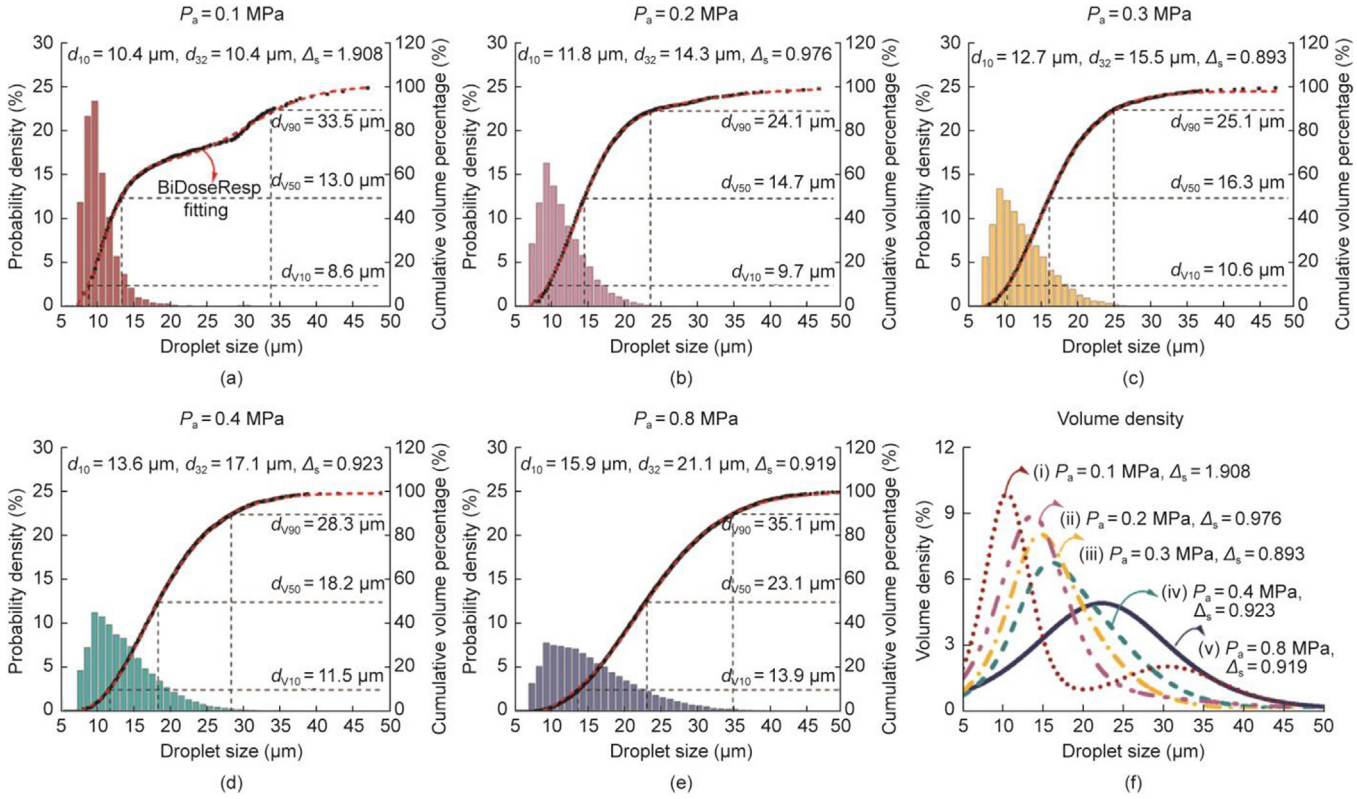

Fig. 7. (a–e) Statistic results for drop-size characteristics under different ambient conditions; (f) summary of volume density under injection pressure P_{inj} = 9.0 MPa. d_{10}: linear average diameter; d_{32}: Sauter mean diameter; Δ_s: dimensionless span number; d_{v10}, d_{v50}, and d_{v90}: the volumes of all droplets smaller than 10%, 50%, and 90%. Reproduced from Ref. [106] with permission.

attributed to increased heterogeneous nucleation near nozzle walls. Jacob and Weber number transition criteria were validated but showed deviations, due to ammonia's low viscosity and surface tension promoting bubble nucleation. Glass nozzle observations revealed that minor geometry variations, such as orifice tapering, could trigger internal flashing and enhance atomization.

Desclaux et al. [110] investigated the behavior of superheated ammonia sprays under flash-boiling conditions. With Schlieren imaging and thermocouples, they demonstrated that reducing R_p significantly amplifies radial spray expansion, with a notable change observed at $R_p > 8.85$, resulting in distinct flaring of the liquid plume. Spray penetration exhibited a non-linear relationship with R_p, initially increasing before stabilizing due to increased bubble formation and droplet fragmentation near the nozzle. The cooling effect induced by flash boiling led to temperature reductions of up to −60 °C near the spray core, indicating a correlation with the latent heat vaporization.

Bjørgen et al. [111] further investigated the flash-boiling dynamics of superheated liquid-ammonia sprays. Their results showed that higher SDs led to significant radial spray expansion and reduced penetration, primarily due to increased bubble nucleation within droplets. At $R_p > 4$, radial expansion dominated over penetration, effectively decoupling spray morphology from ambient density effects. Near-field analysis revealed that, for high R_p, the liquid core became less dense and exhibited shock-wave formation, with shocks becoming more pronounced as R_p increased beyond 65, as presented in Fig. 8. In-spray temperature measurements highlighted substantial cooling within the spray core, with minimum temperatures reaching as low as −66 °C at low ambient pressures. This significant cooling was attributed to ammonia's high latent heat of vaporization.

In addition to the experimental investigations discussed above, several researchers utilized numerical methods to study the behavior of liquid-ammonia sprays from single-hole nozzles. A summary of these studies is presented in Table 4 [115–118].

Huang et al. [115] investigated high-pressure liquid-ammonia injection under flash-boiling and non-flash-boiling conditions. Lower ambient pressure produced longer spray penetration and higher gas-phase velocity, while the ammonia vapor mass fraction decreased with increasing ambient pressure, intensifying heat transfer and lowering the gas-phase temperature. Flash-boiling sprays exhibited high initial droplet velocity, significant radial expansion shortly after injection, and larger evaporation source terms compared with non-flash-boiling sprays, which showed lower droplet velocity, moderate velocity variation over time, and weaker radial expansion.

An et al. [116] numerically evaluated five phase-change models for liquid-ammonia flash sprays under various temperatures and pressures. The combined Zuo and Langmuir–Knudsen (LK) model (Eq. (1)) proved most suitable for superheated conditions, matching experimental penetration length and spray characteristics data (Fig. 9). Evaporation rate increased with decreasing pressure, significantly reducing droplet and gas-field temperatures. The ammonia vapor mass fraction showed complex temperature relationships: initially decreasing then increasing under low pressure, while positively correlating at high ambient pressure. These findings highlight vaporization cooling effects and pressure's influence on droplet–gas phase interactions, which are critical for liquid-ammonia combustion applications.

$$\chi_{neq,s} = \chi_{eq,s} - \left(\frac{2L_K}{d}\right)\beta \tag{1}$$

where $\chi_{neq,s}$ and $\chi_{eq,s}$ are vapor molar fraction at the droplet surface contains non-equilibrium and equilibrium term, respectively; L_K is the Knudsen layer thickness; d is the droplet diameter; β is the non-dimensional evaporation parameter.

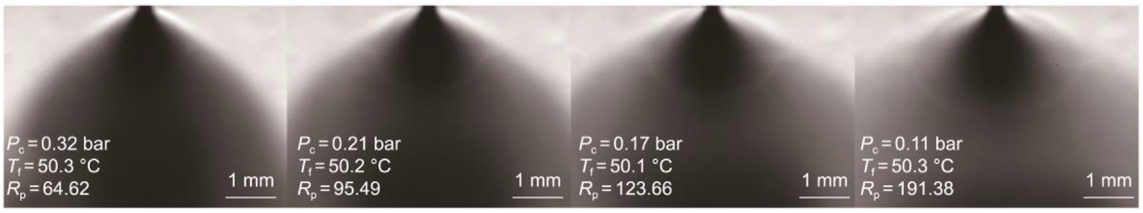

Fig. 8. Shock waves observed for high R_p cases in a Schlieren setup. Reproduced from Ref. [111] with permission.

Table 4
Recent simulation studies of liquid-ammonia spray using single-hole injectors.

Reference	Injector		Conditions		Methods	Key conclusions
	Hole type	Hole diameter (mm)	Injection condition	Ambient condition		
Huang et al. [115]	Single	0.168	50–100 MPa, 300 K	0.1–4.0 MPa, 300 K	CFD based on Eulerian–Lagrangian framework; LES using OpenFOAM	Flash sprays have higher initial droplet velocity (decaying rapidly), much higher evaporation rates, significant radial expansion early on, lower gas temperatures in the core, and stronger preferential concentration compared with non-flash sprays
An et al. [116]	Single	0.28	30 MPa, 308 and 338 K	0.101–2.952 MPa, 298 K	CFD based on Eulerian–Lagrangian framework; LES using OpenFOAM	The combined Zuo + LK model provided the best agreement with experimental data, capturing details such as spray collapse and droplet recirculation
Wang et al. [117]	Single	0.21	0.87–1.09 MPa, 270–295 K	0.1 MPa, 298 K	CFD based on Eulerian–Lagrangian framework; RANS with VOF	Flash-boiling mechanism: SD and orifice aspect ratio significantly affect spray expansion via internal bubble development. Higher superheat/longer orifices promote intense flash boiling
Zhou et al. [118]	Single	0.22	60 MPa, 298–350 K	298, 900, and 1000 K; 15, 18, and 21 kg·m^{-3}	CFD based on Eulerian–Lagrangian framework; RANS and LES	The evaporation process of liquid-ammonia spray under these conditions is mixing-controlled (fuel–air mixing), not controlled by local interphase transport at the droplet surface (consistent with diesel)

CFD: computational fluid dynamics; LES: large eddy simulation; RANS: Reynolds-averaged Navier-Stokes; VOF: volume of fluid; LK: Langmuir–Knudsen.

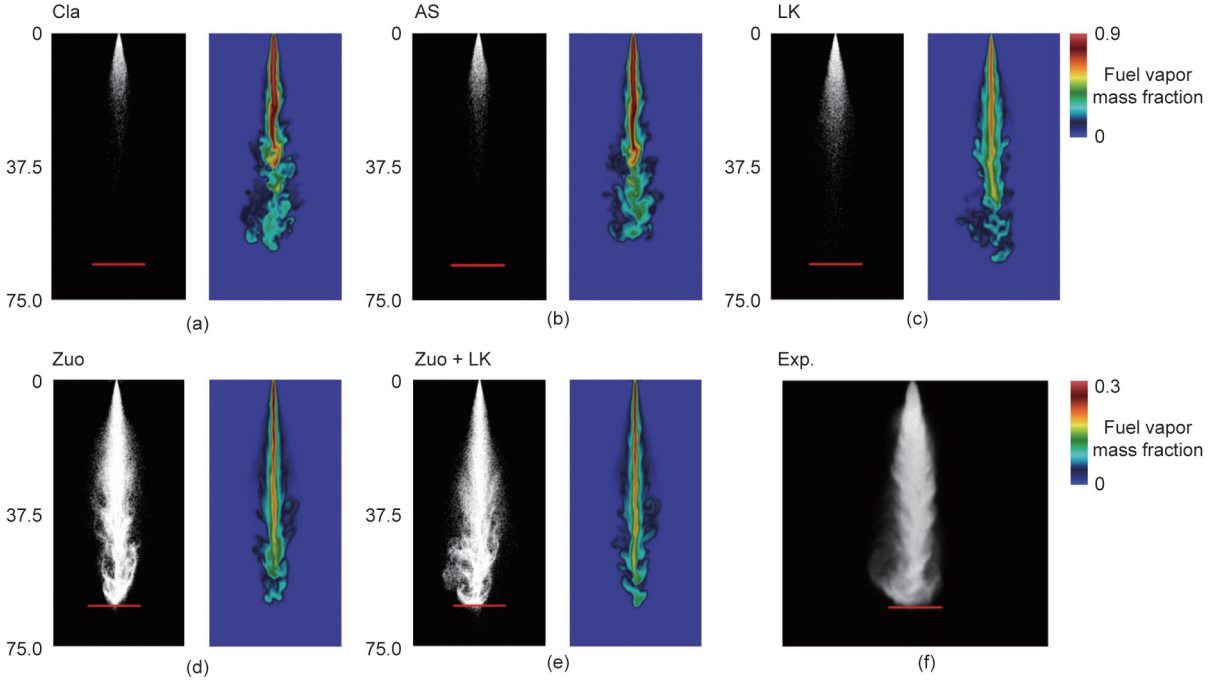

Fig. 9. Morphological features of superheated ammonia spray: experimental measurements and predictions using various phase-change models. (a)–(e) are simulation results, and (f) is experiment (Exp.) benchmark. Cla: classical; AS: Abramzon and Sirignano. Reproduced from Ref. [116] with permission.

Wang et al. [117] utilized 2D numerical simulations to investigate flash-boiling liquid-ammonia spray characteristics, focusing on orifice aspect ratios and SDs. They validated the Eulerian framework and homogeneous relaxation model (HRM) for simulating flash-boiling ammonia sprays through a comparison with experimental data from Colson et al. [109]. The rate of phase change is modeled by

$$dY_l = \left(Y_l^1 - Y_l^0\right)\left(1 - e^{-dt/\theta}\right) \quad (2)$$

where dY_l is the change in liquid mass fraction after timestep dt, and θ is the relaxation timescale over which the phase change is expected to occur.

Higher SDs significantly enhanced bubble growth and phase transitions, improving atomization and fuel-distribution uniformity. An aspect ratio (L/D) of 10 produced a unique gas-phase distribution with a lower void fraction near walls and a higher fraction near the center axis, indicating intense phase transitions at the nozzle exit. Fig. 10 [117] shows axial and radial temperature distributions for four sprays. Flash boiling significantly accelerates atomization while notably reducing the spray-area temperature, with the temperature decrease intensifying as the SD increases. A higher superheat causes internal flash boiling and rapid vaporization, creating sharp temperature drops downstream of the injection nozzle that gradually flatten. The radial temperature distribution exhibits an M-shaped profile from the competing effects of droplet evaporation and convective heat transfer with ambient gas. While flash boiling enhances atomization, it substantially reduces spray temperature.

In addition, Zhou et al. [118] conducted theoretical and numerical investigations on high-pressure DI liquid-ammonia spray similarity across different engine sizes and nozzle-hole dimensions. They established single-value conditions and two similarity laws for scaling liquid-ammonia sprays, demonstrating that both the speed law and pressure law achieve similarity in fuel-injection rate, spray breakup, spray tip penetration evolution, and maximum liquid length.

2.2. Liquid-ammonia injection using multi-hole injectors

Multi-plume sprays from multi-hole injectors closely represent actual engine applications, as these injectors ensure sufficient fuel delivery while synergizing with combustion chamber geometry to optimize mixing. Table 5 [119–124] summarizes recent studies on liquid-ammonia spray characteristics from multi-hole injectors.

Pelé et al. [119] conducted the first experimental study on liquid-ammonia spray characteristics using Schlieren imaging (Fig. 11). Ammonia sprays showed greater sensitivity to air density and temperature than conventional fuels, producing longer, narrower sprays under low-air-density conditions. Flash-boiling conditions near saturation pressure (8.8 bar at 20 °C) yielded wider spray angles at half penetration length, with notable collapse effects from vapor condensation. The researchers developed a semi-empirical correlation for spray-penetration prediction based on thermodynamic parameters, achieving high accuracy. Temperature-sensitivity quantification revealed exponential coefficient values of 0.46 for liquid ammonia, 0.30 for gasoline, and 0.21 for methanol, confirming ammonia's heightened temperature responsiveness.

Using a Bosch six-hole injector, Akram et al. [120] experimentally studied ammonia spray flash-boiling behavior. Ammonia exhibited significantly greater vaporization than methanol, ethanol, or gasoline, particularly as the injector tip temperature increased to 300 °C, which was consistent across chamber pressures of 10 and 30 bar. At a chamber pressure of 10 bar, ammonia showed the lowest penetration rates and spray areas, while other fuels demonstrated comparable values. Generally, increasing the injector tip temperature at a lower chamber pressure decreased the penetration rates and spray areas for all fuels. At a chamber pressure of 30 bar, ammonia and other fuels exhibited similar penetration rates and spray area ranges.

Scharl et al. [121] investigated fuel-temperature and injection-timing effects on ammonia DI, innovatively measuring injection mass and evaluating discharge coefficients through exhaust-gas composition analysis during engine operation with ammonia injection but without combustion. Increasing the fuel temperature decreased the ammonia injection mass up to 12.8%, while minimally impacting discharge coefficients during late injection timings and high in-cylinder pressures. However, early injection timings showed discharge coefficient decreases of up to 17.4% at elevated fuel temperatures. The study confirmed that temperature increases notably reduce the injection mass, primarily because ammonia's pronounced temperature sensitivity significantly affects its density.

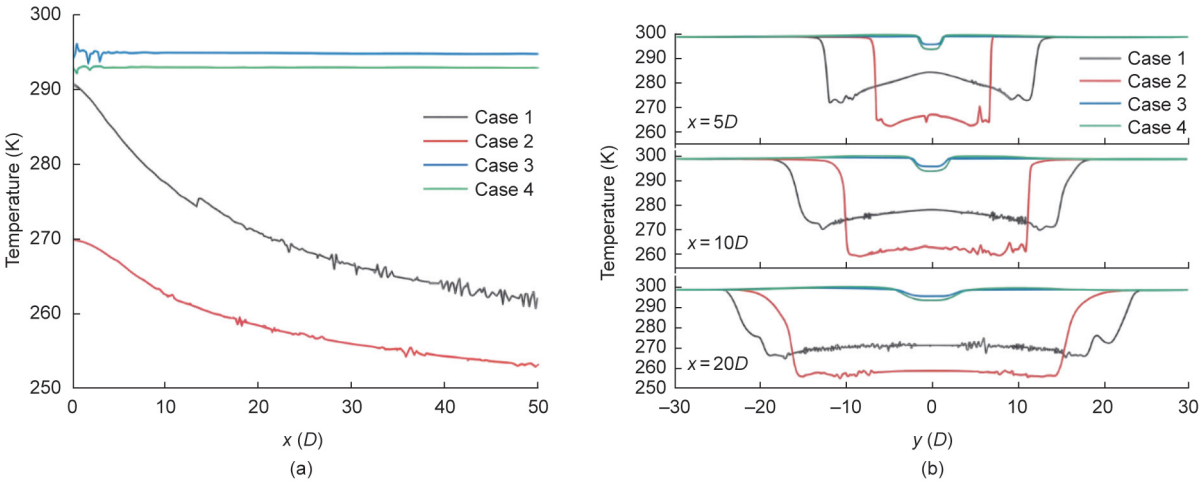

Fig. 10. Temperature distributions along (a) the nozzle center axis and (b) three different radial lines. Case 1: L/D = 10, R_p = 8.3; Case 2: L/D = 5, R_p = 9.0; Case 3: L/D = 2.5, R_p = 8.5; Case 4: L/D = 10, R_p = 3.9. Reproduced from Ref. [117] with permission.

Table 5
Summary of recent studies of liquid-ammonia spray using multi-hole injectors.

Reference	Injector		Conditions		Methods	Key conclusions
	Hole type	Hole diameter	Injection condition	Ambient condition		
Pelé et al. [119]	7 holes	365 μm	120 bar, 20 °C	2–25 bar, 20–120 °C, 2.38–29.75 kg·m^{-3}	CVC; Schlieren imaging	Ammonia spray is longer and narrower than gasoline/ethanol sprays. Ammonia is more sensitive to air density/temperature changes
Akram et al. [120]	6 holes	0.2 mm	150 bar, 25–300 °C	10 and 30 bar, 19–23 °C	CVC; Schlieren imaging	Superheating reduces spray penetration/area for all fuels, but ammonia shows the strongest reduction (especially at 10 bar) due to rapid vaporization
Scharl et al. [121]	6 holes	0.227 mm	2000 bar, 320–388 K	~4–7 and ~50 bar, ~450–650 and ~1000 K	Optical engine; DBI	Two spray-collapse mechanisms identified; 12.9% mass reduction with heating. Discharge coefficients drop by 17.4% for early injections at high temperatures (cavitation enhancement)
Zembi et al. [122]	7 holes	365 μm	120 bar, 20 °C	2–15 bar, 20 °C	CFD based on Lagrangian particle method within the RANS	Highlights the challenge of developing truly calibration-free models, especially for new fuels like ammonia whose properties differ significantly from those of hydrocarbons
Hu et al. [123]	Single hole/7 holes	280/150 μm	300/120 bar, 293–350 K	P_{amb}/P_{sat}: 0.035–1.24, 20 °C	CFD based on Lagrangian particle method with Blob injection	Demonstrates high-precision prediction of ammonia-spray characteristics across flash-boiling regimes using two dynamically adjusted variables based on flashing ratio
Rachakonda et al. [124]	8 holes	165 μm	20 MPa, 260–363 K	50, 600 kPa, 333–573 K, 0.5, 3.5 kg·m^{-3}	CFD (HRMFoam) based on foam-extend v4.1	Ammonia's high volatility and low Jakob number promote spray collapse, bell-shaped jets, and shock structures. Pressure ratio is the primary parameter governing spray behavior, followed by Jakob number

Zembi et al. [122,125] conducted numerical studies based on Pelé's multi-hole ammonia spray experiments [119]; they successfully compared numerical results with experimental data for liquid and vapor tip penetration, local SMD, and overall spray morphology, establishing a predictive simulation framework for ammonia injections. Their study highlighted challenges in capturing local spray details across different regimes—particularly flash-boiling phenomena crucial for understanding ammonia's unique properties. Standard breakup model constants for conventional fuels proved inadequate for ammonia, requiring significant tuning and specific calibration. The researchers investigated liquid-ammonia spray behavior under varying ambient pressures, focusing on transitions between flash-boiling and non-flashing regimes, and specifically calibrated Kelvin-Helmholtz and Rayleigh-Taylor (KH–RT) model constants for both conditions. The results demonstrated good agreement between the simulations and experiments for liquid spray tip penetration and local SMD (Fig. 12) [122].

Based on previous experimental and simulation studies, Hu et al. [123] conducted a numerical investigation of multi-plume liquid-ammonia spray. They developed a novel variable discharge coefficient C_d accounting for spray resistance from ammonia vaporization within the nozzle, achieving prediction errors below 1.5% for spray penetration at a fuel temperature of 308 K across all flashing ratios. A breakup model constant B_1 that strongly influences spray penetration was designed as a variable constant formula with an identical functional form to variable C_d (Eq. (3)), improving predictions at higher fuel temperatures. Using the variable C_d–B_1 model at a fuel temperature of 338 K, the spray penetration prediction error at an injection time of 1 ms remained below 5% for all ambient pressures and approached 0 during the flare flash-boiling stage, as shown in Fig. 13 [123].

$$\begin{cases} B_1 = 8.34 + 24.27 \cdot e^{-F_r/0.24} \\ C_d = \left(0.8 - 0.22 \cdot e^{-F_r/0.25}\right) \cdot \frac{T}{T_{ref}} \end{cases} \quad (3)$$

where F_r is the flashing ratio and T_{ref} is the reference temperature of 338 K.

Rachakonda et al. [124] compared the internal flow and near-nozzle behavior of iso-octane, methanol, and ammonia under flash-boiling and subcooled conditions. Flash-boiling sprays demonstrated greater steadiness than their subcooled counterparts and behaved as either under-expanded or over-expanded jets, depending on the operating conditions and fuel thermophysical properties. High R_p values (saturation to ambient pressure ratio) produced a "bell-shaped" morphology with significant spray collapse, characterized by strong under-expanded jets that generated shock fronts truncated by Mach disks perpendicular to the spray axes. The Mach disk appeared as an abrupt pressure rise, visible as darker regions in superheated ammonia spray pressure contours (Fig. 14 [124]). Rapid vaporization and expansion accelerated sprays beyond sonic velocities, creating low-pressure regions relative to ambient pressure. Shock cell boundaries formed through barrel shocks or constant pressure streamlines, followed by intercepting shocks as the flow turned inward. Triple point regions were clearly visible where the Mach disks intersected intercepting shocks, producing reflected shocks and slipstreams from both sides, as shown in the log-scaled density gradients in Fig. 14.

2.3. Summary

This section provides a comprehensive review of research on liquid-ammonia injection and spray characteristics, with a particular focus on flash-boiling phenomena and the behavior of ammonia sprays from both multi-hole and single-hole injectors. Key parameters influencing flash boiling include the saturation-ambient pressure ratio and degree of superheat.

Multi-hole injector studies show that ammonia sprays are highly sensitive to air density and temperature, producing longer, narrower sprays at low densities. Flash-boiling widens spray

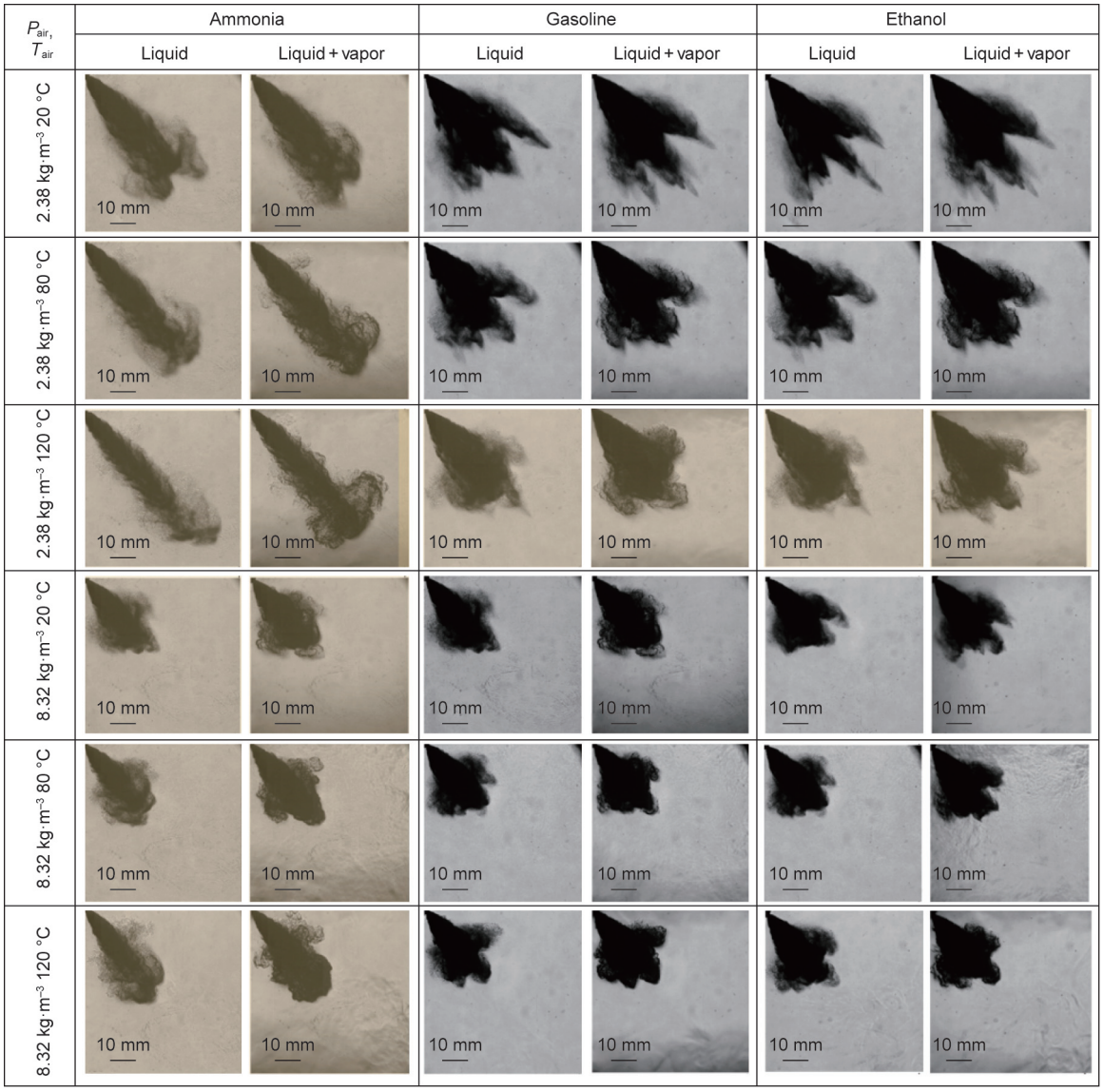

Fig. 11. Comparison of spray shapes for liquid and liquid + vapor under varying air densities and ambient temperatures (yellow section indicates flash boiling). P_{air}: air density; T_{air}: ambient temperature. Reproduced from Ref. [119] with permission.

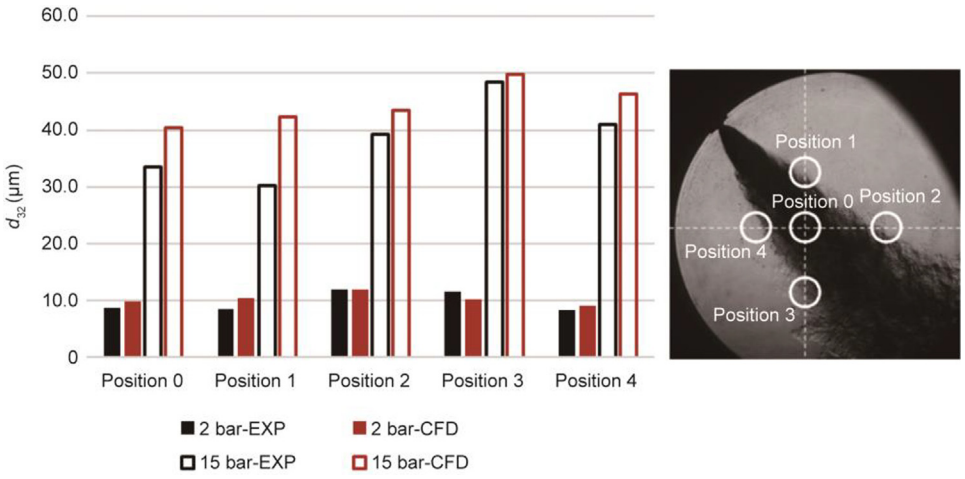

Fig. 12. Comparison of experiments and simulation regarding local SMD, under flashing (2 bar) vs non-flashing (15 bar) conditions. Reproduced from Ref. [122] with permission.

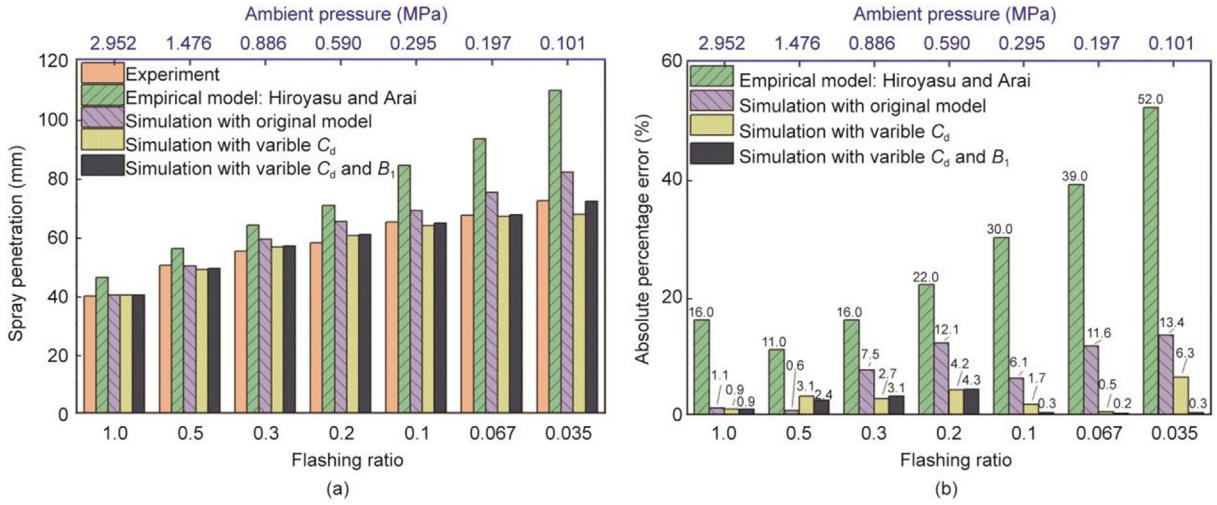

Fig. 13. Comparison of simulation and experimental results at t = 1 ms and T = 338 K: (a) spray penetration; (b) prediction errors. Reproduced from Ref. [123] with permission.

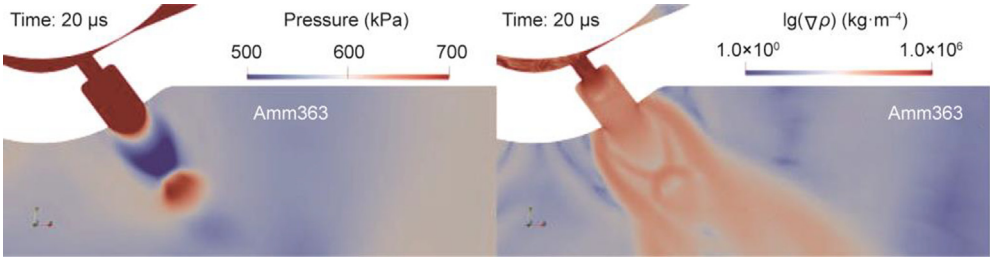

Fig. 14. Instantaneous shock structures observed in ammonia injection at 363 K, at 20 μs after the start of injection (ASOI), using the contours of pressure (linearly scaled) and gradient of mixture density (log-scaled). Pressure range: 500–700 kPa; ambient pressure: 600 kPa. Reproduced from Ref. [124] with permission.

angles and causes collapse from vapor condensation, while higher injector temperatures enhance vaporization and alter spray characteristics. Ammonia's temperature-sensitive density affects the injection mass and discharge coefficients. Single-hole injectors enable more precise spray analysis, revealing distinct flashing regions based on pressure ratios and showing the influence of bubble behavior on penetration during flash-boiling. Nozzle diameter, ambient pressure, and fuel temperature critically determine spray characteristics; smaller nozzles increase radial expansion, while larger ones produce larger droplets. Numerical and experimental studies developing predictive models reveal challenges in modeling ammonia sprays due to their unique thermodynamic properties, which require ammonia-specific breakup models. These findings emphasize optimizing injection parameters and nozzle design for efficient atomization and mixing in ammonia engines.

In addition, critical examination of the reviewed studies reveals several conflicting findings that warrant further investigation. For instance, while Pelé et al. [119] reported spray penetration lengths 44.7%–56.2% smaller than those of diesel, Payri et al. [126] found comparable penetration rates in the fully developed zone. This discrepancy likely stems from differences in experimental conditions and measurement techniques, as Pelé used Schlieren imaging in a constant-volume chamber, while Payri employed diffuse background illumination (DBI) in a constant-pressure flow vessel. In addition, discrepancies in spray penetration under similar conditions (e.g., 12% shorter penetration in Ref. [100] vs Ref. [102] at R_p = 5.0) arise from nozzle geometry variations (0.28 vs 0.32 mm diameter), emphasizing the need to non-dimensionalize the spray parameters with respect to the nozzle geometry. The robustness of numerical models also varies significantly; while the Lagrangian particle method shows good agreement for non-flash-boiling conditions, Zhang et al. [127] highlighted significant discrepancies under intense flash boiling, indicating that current models require substantial improvements for capturing thermal breakup effects. While large-eddy simulation (LES) models [115] robustly capture near-field flash boiling, Reynolds-averaged Navier-Stokes (RANS) approaches [122] struggle with plume-collapse effects due to unresolved turbulence–chemistry interactions, limiting their use in engine-scale simulations.

3. Liquid-ammonia injection into high pressure/temperature

This section examines liquid-ammonia injections in high-pressure, high-temperature environments that closely replicate engine operating conditions, building on the low-pressure spray studies previously discussed. This progression is essential for three reasons: Engine compression generates ambient pressures that exceed ammonia's saturation pressure, thereby suppressing flash boiling; elevated temperatures create competing effects between increased evaporation and reduced flash-boiling tendency; and reactive conditions fundamentally alter spray development through heat release and combustion-induced flow fields. Understanding these behaviors under engine-relevant conditions is critical for translating fundamental spray physics into practical combustion system designs.

3.1. Non-reactive ammonia injection and spray study

Research on non-reactive ammonia injection and spray is essential for optimizing injection strategies and ensuring efficient atomization and distribution in combustion systems. Non-reactive conditions allow researchers to isolate and analyze fundamental physical processes, including spray formation, droplet size distribution, and penetration. The constant volume combustion chamber (CVCC) provides controlled environments for studying spray characteristics under precise pressure and temperature conditions that simulate combustion device operations, while enabling high-quality optical access for advanced diagnostics [128]. Table 6 [126,127,129–132] lists recent non-reactive ammonia injection and spray studies.

Wang et al. [129] and Li et al. [130] investigated high-pressure ammonia spray combustion characteristics under diesel-like conditions. Under non-reacting conditions, ammonia sprays exhibited macroscopic characteristics similar to diesel sprays, with significant evaporation at room temperature. Empirical diesel spray correlations can be used to predict ammonia spray tip penetration by incorporating Reynolds number and Ohnesorge number. Microscopic imaging revealed that the ammonia sprays showed greater susceptibility to needle-motion-induced turbulence or cavitation during injection transients. Fig. 15 [130] shows that the ammonia spray liquid length was 44.7%–56.2% smaller than that of diesel, with differences increasing with ambient density. While liquid-phase development in ammonia sprays initially lagged behind that of diesel from the start of the injection, ammonia sprays showed pronounced liquid penetration increases during the quasi-steady state due to their large latent heat of evaporation.

Ma et al. [102] investigated the spray characteristics and jet fluctuations of high-pressure DI liquid ammonia across ambient temperatures of 291–600 K. Under high-temperature and high-pressure conditions, liquid-ammonia sprays were significantly influenced by the interplay between flash boiling and evaporation effects. Increasing the ambient temperature produced three-stage axial spray development: Initial stages dominated by flash boiling caused rapid spray area increase, while later stages showed high-temperature evaporation dominance, resulting in marked spray area reduction. At 600 K, pronounced evaporation reduced the spray, as intense heat transfer overcame liquid ammonia's latent heat of evaporation. Spray centroid oscillation deviations increased with rising temperatures, indicating greater jet instability, with maximum deviation growth rates reaching 59.16% in near-nozzle regions.

Payri et al. [126] experimentally investigated DI liquid-ammonia spray characteristics under non-reacting diesel-like conditions. Fig. 16 [126] shows spray images captured using DBI and Schlieren techniques for both fuels. Ammonia jets exhibited cone-like shapes similar to those of diesel, with narrower spray angles. Ammonia demonstrated slower initial penetration rates compared with diesel but achieved comparable rates in fully developed zones. Ammonia liquid length was shorter than that of diesel, influenced by ambient temperature, density, and nozzle diameter, but not injection pressure. A one-dimensional (1D) spray model originally developed for diesel fuels showed good agreement with experimental results for quasi-steady liquid length and vapor penetration when applied to ammonia.

Yang et al. [131] experimentally investigated high-pressure liquid-ammonia spray characteristics under various ambient conditions. Their results revealed significant differences in spray development across flash-boiling, transitional flash-boiling, and non-flash-boiling conditions. Under flash-boiling conditions, the spray tip velocity initially increased then gradually decreased, while non-flash-boiling conditions showed significant initial velocity decrease followed by forward penetration at a similar velocity. Higher ambient temperatures increased vaporization, shortening liquid spray penetration length. This research provides

Table 6
Recent literature on non-reactive ammonia injection and spray.

Reference	Injector		Conditions		Methods	Main findings
	Hole type	Hole diameter (mm)	Injection condition	Ambient condition		
Wang et al. [129]	Single hole	0.22	30–60 MPa, 298–420 K	800–1000 K; 15–21 kg·m^{-3}	CVCC; Schlieren; DBI	Successfully observed auto-ignition of high-pressure ammonia spray under diesel-like conditions (900/1000 K, 21% O_2). Ammonia flame luminosity is drastically lower (semi-transparent orange) than diesel
Li et al. [130]	Single hole	0.15, 0.18, and 0.28	30–60 MPa, 313–373 K	800–1000 K; 14.7–25.4 kg·m^{-3}	CVCC; DBI	LL of ammonia spray was 44.7%–56.2% smaller than that of diesel under identical conditions, decreasing further with higher ambient density
Payri et al. [126]	Single hole	0.25, 0.3	400–800 bar, 288 K	700–900 K; 22.8, 30.4 kg·m^{-3}	CPF rig, Schlieren; DBI	Observed slower initial penetration for ammonia due to needle lift dynamics, but similar quasi-steady behavior (mixing-controlled). Ammonia LL is shorter (vs diesel), decreases with higher ambient T/ρ, insensitive to injection pressure
Yang et al. [131]	Single hole	0.2	40–80 MPa, ~278 K	1–30 bar; 300–600 K	CVC; DBI	Flare flash boiling causes strong initial radial expansion, distorted spray contour, large dilute region, cavitation at spray edge. Transition flash boiling has less radial expansion than flare
Wu et al. [132]	Single hole	0.1, 0.3	40–80 MPa, 303 K	5 MPa; 423–800 K	CVC; DBI; Shadowgraphy	A distinct vortex ring structure forms at the spray front under high superheat flash-boiling. A "post-supercooling residual region" is formed downstream of ammonia spray due to its high latent heat, preventing complete droplet evaporation, unlike diesel
Zhang et al. [127]	Single hole/7 holes	0.365/0.22	120/600 bar, 293/350 K	293–393/900 K; 2.38–8.32/7.45–18 kg·m^{-3}	CFD based on Euler–Lagrange framework with Lagrangian particle tracking	Under strong flash boiling, models underestimate liquid penetration by 11%–35%. New flash-boiling models accounting for thermal breakup are needed for accurate predictions

CPF: constant-pressure flow; LL: liquid length.

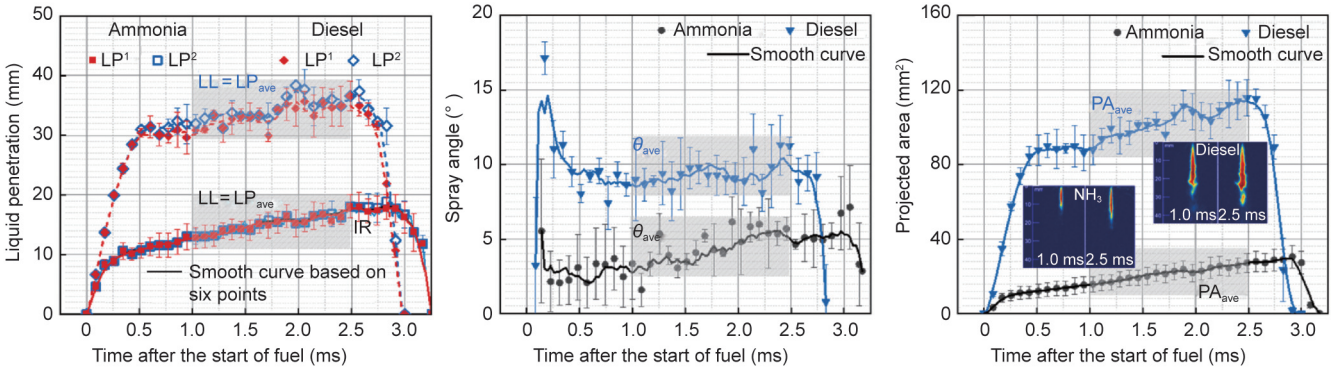

Fig. 15. Comparison of dynamic evolution of macroscopic morphology parameters according to fuel type. P_{inj} = 60 MPa, T_f = 353 K, P_{amb} = 6.0 MPa, T_{amb} = 900 K, ρ_{amb} = 21.9 kg·m^{-3}). Reproduced from Ref. [130] with permission.

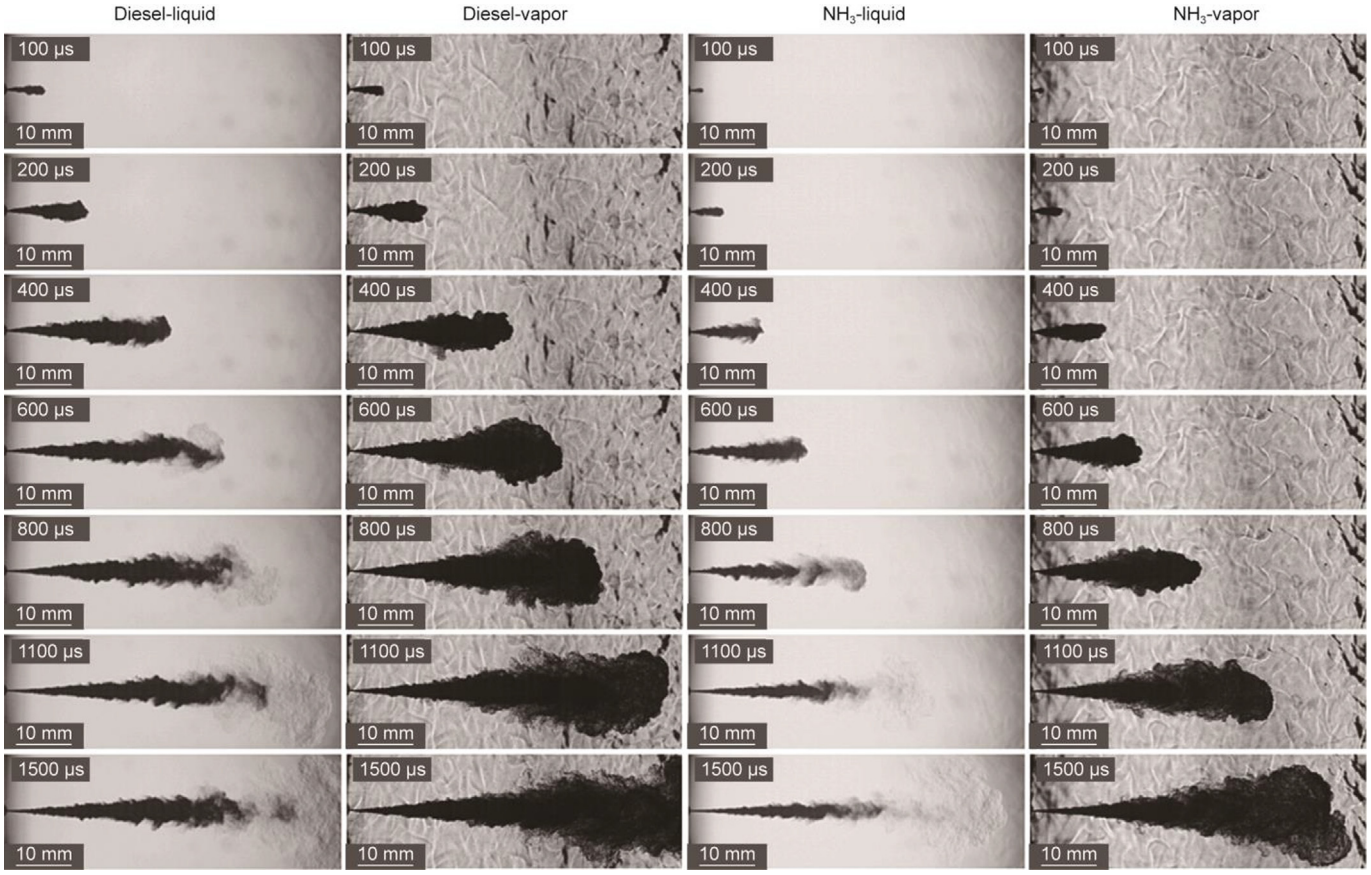

Fig. 16. Time sequence of spray images by DBI and Schlieren. The sequence from top to bottom consists of the transient region (first to fourth) and the stabilized liquid length region (1500 μs ASOI). Conditions: ρ_a = 22.8 kg·m^{-3}, T_a= 900 K, D_0 = 300 μm, P_r= 800 bar. Reproduced from Ref. [126] with permission.

comprehensive reference data for numerical simulations and valuable theoretical and practical guidance for ammonia spray combustion studies and ammonia-fueled engine development.

Wu et al. [132] investigated the spray and evaporation characteristics of high-pressure liquid-ammonia injection compared with those of diesel. Liquid penetration initially increased then decreased with rising ambient temperature, with large-nozzle sprays showing higher inflection-point temperatures. Small-nozzle sprays exhibited greater ambient condition sensitivity at high temperatures, reducing spray stability. Ammonia demonstrated higher axial diffusion rates but lower radial diffusion rates than diesel. At 800 K, distinct spray-structure differences emerged: Capturing and recirculation regions from pilot-evaporated ammonia prevented complete droplet evaporation, unlike diesel. Ammonia vapor cone angles were 4°–6° smaller than those of diesel under evaporating conditions, with liquid cone angle differences decreasing at higher ambient temperatures. Ammonia spray volume exceeded diesel spray volume due to ammonia's high latent heat of vaporization.

Zhang et al. [127] presented a computational fluid dynamics (CFD) study on the fuel/air mixing properties of liquid ammonia under DI engine conditions. Current Lagrange-based spray models effectively replicated liquid-ammonia spray characteristics under non-flash-boiling conditions but showed significant discrepancies

with experimental measurements under intense flash-boiling conditions. This finding highlights the need for more precise flash-boiling models incorporating thermal breakup effects to accurately predict ammonia fuel/air-mixing properties across the full spectrum of engine-relevant conditions.

Research on liquid-ammonia injections have employed established spray methods using a constant volume chamber (CVC) with optical techniques such as diffused back-illumination imaging to observe fundamental spray behavior under elevated pressure and temperature conditions. Studies have consistently examined how ambient temperature, pressure, and injection pressure affect ammonia spray characteristics, finding distinct differences from diesel sprays in penetration rates and evaporation characteristics. Ambient temperature has emerged as a significant influence on spray behavior and penetration length across all studies. These findings hold practical significance for ammonia-fueled engine development and sustainable transportation applications.

3.2. Ammonia spray combustion without reactive fuel

Igniting and sustaining liquid-ammonia spray combustion is challenging due to ammonia's high auto-ignition temperature, narrow flammability range, high latent heat of vaporization, and low laminar flame speed. Achieving single ammonia spray combustion without reactive fuel additives requires appropriate atomization through high-pressure injections and optimal nozzle design to control droplet size distribution, as smaller droplets facilitate faster evaporation and mixing. Maintaining ammonia concentration within its flammability range (15%–28% by volume in air) with sufficient oxygen is essential. Fuel and ambient air preheating compensate for cooling effects from ammonia's high vaporization latent heat. High-temperature and -pressure ambient conditions enhance combustion processes. Continued research into combustion dynamics, flame stability, and heat-release mechanisms remain vital for improving liquid-ammonia fuel combustion system performance and reliability.

An experimental investigation by Wang et al. [129] demonstrated successful high-pressure liquid-ammonia spray auto-ignition under diesel-like conditions, with 21% oxygen concentration and comparable temperature/pressure levels, marking the first observation of this phenomenon. Fig. 17 [129] shows the temporal morphology of the ammonia spray flames at various ambient and fuel temperatures. Ammonia combustion intensity was significantly lower than that of diesel and more sensitive to ambient temperature than initial fuel temperature. The lift-off length at 1000 K remarkably exceeded that at 900 K, while the apparent heat-release rate (AHRR) increased by 40% at 1000 K because of increased after-burning and earlier ignition. Ammonia's spray flame lift-off length exceeded diesel's, indicating slower combustion. The AHRR exhibited a sharp initial spike followed by slow heat release, suggesting a transition from premixed to mixing-controlled combustion. The cumulative heat from ammonia diffusive combustion was less than one-fourth of that from diesel spray combustion.

Wu et al. [133] experimentally investigated the ignition and flame-development characteristics of high-pressure liquid-ammonia spray combustion using simultaneous high-speed imaging of OH^* and NH_2^* chemiluminescence with flame luminosity (FL) under controlled conditions (3 MPa ambient pressure, 950 K temperature, 40 MPa injection pressure). The combustion process comprised four stages—ignition with auto-ignition kernels, flame propagation, fully developed combustion, and post-combustion—with key radical distributions characterized throughout. Fig. 18 [133] shows the temporal evolution of OH^*, NH_2^*, and FL images. During fully developed combustion, all signals covered the spray core region, with NH_2^* showing a smaller distribution and lower intensity than OH^* except at the core region and flame front. OH^* intensity peaked centrally, diminishing toward the flame sides. Post-combustion showed a significant FL decrease, OH^* contour alignment with the flame front, and rapid NH_2^* reduction, disappearing before OH^*. Combustion lasted approximately 5.6 ms. The study identified unique small-scale auto-ignition phenomena after main combustion, providing insights into chemical kinetics—including OH and NH_2 radical formation—and contributing valuable knowledge for developing numerical models and increasing ammonia fuel efficiency.

In addition to ammonia spray combustion, Matsuura et al. [134] investigated individual ammonia-droplet combustion using hot-wire ignition and back-illumination high-speed imaging under high-pressure microgravity conditions. Their study revealed unique combustion behaviors, including droplet disruption, puffing, and re-expansion (Fig. 19 [134]). Initially, droplets vaporized at consistent rates that decreased over time, reducing the flame standoff ratio. These phenomena resulted from water vapor accumulation on droplet surfaces, which suppressed ammonia vaporization and caused superheating, leading to bubble nucleation and growth. This pioneering research on ammonia-droplet combustion provides insights into designing ammonia spray combustors and developing carbon-neutral fuel technologies for gas turbines and marine diesel engines.

3.3. Ammonia spray combustion with pilot-ignited reactive fuel

Liquid ammonia exhibits modest reactivity and limited combustion characteristics under standard conditions due to high activation-energy barriers and slow reaction kinetics, making stable flame maintenance challenging. Its substantial latent heat requires considerable vaporization energy before combustion initiation, collectively limiting standalone fuel utilization. To overcome these limitations, dual-fuel strategies employ higher-reactivity fuels such as hydrogen or hydrocarbons as combustion promoters. These active fuels react first, providing the initial energy and chemical pathways to overcome ammonia's combustion challenges by generating heat and free radicals that break down ammonia molecules, sustaining the chain reactions necessary for continuous stable combustion. Table 7 [69,70,135–144] presents a summary of recent studies on liquid-ammonia spray combustion using pilot-ignited reactive fuels.

Although gasoline [145] and DME [146,147] have been explored as dual-fuel combustion partners to enhance liquid-ammonia combustion characteristics, recent research predominantly focuses on diesel-piloted ignition strategies. When diesel serves as a pilot fuel, it overcomes ammonia's poor combustion properties through multiple mechanisms: providing reliable ignition due to a lower ignition temperature than ammonia [148,149], creating local high-temperature zones facilitating ammonia decomposition, and generating hydrocarbon radicals promoting ammonia oxidation reactions. Diesel's higher energy density and established fuel-delivery systems make it practical for dual-fuel applications. Combining diesel's reliable ignition properties with ammonia's carbon-free fuel potential makes this pairing particularly suitable for internal-combustion engine applications [150].

Scharl and Sattelmayer [70] investigated diesel-piloted ammonia ignition and combustion characteristics by systematically varying temporal and spatial spray interactions, diesel pilot amounts, and injection durations. Using independent single-hole injectors, they achieved variable spray interaction angles from –22.5° (converging) to 15° (diverging) parallel to the cylinder head. Their experiments demonstrated reliable ammonia ignition using pilot-ignited diesel with a lower heating value (LHV) fraction as small as 3.2%. Strong diesel-ammonia spray interaction proved crucial for effective ignition, with injection sequence adjustments

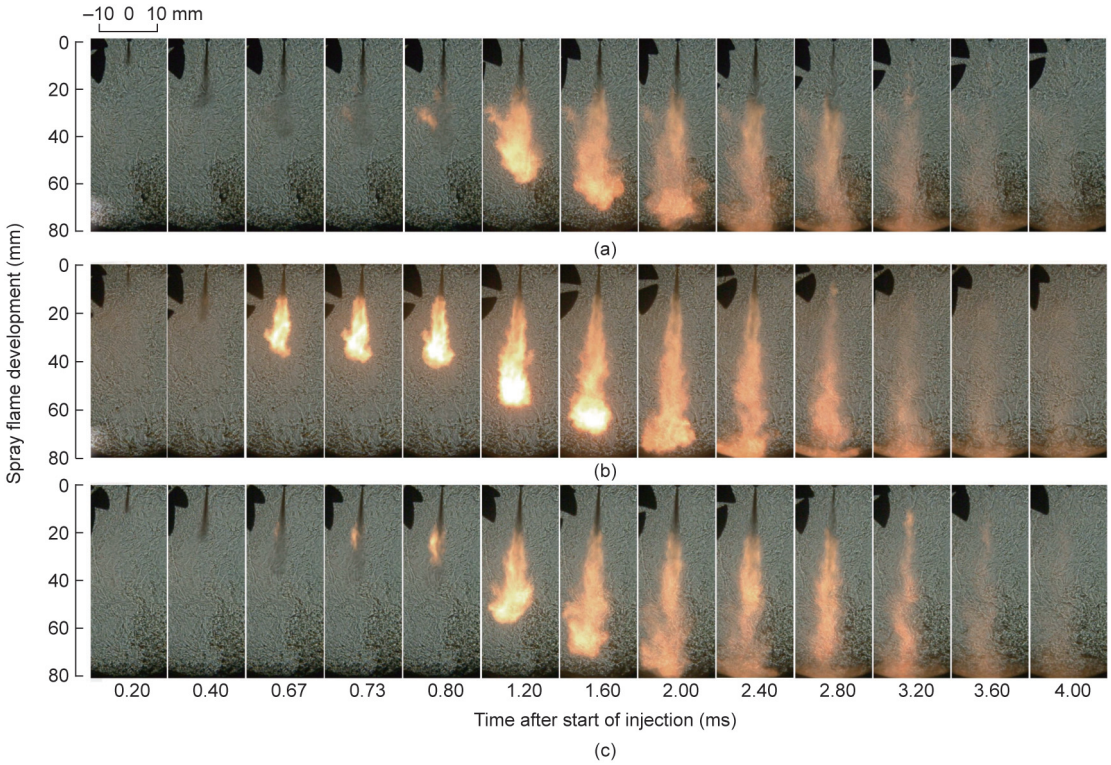

Fig. 17. Temporal morphology development of ammonia spray flames at different ambient and initial fuel temperatures. (a) T_a = 900 K, T_{fuel} = 350 K; (b) T_a = 1000 K, T_{fuel} = 350 K; (c) T_a = 900 K, T_{fuel} = 420 K. ND filter: 40%; [O_2] = 21%, P_{inj} = 60 MPa, ρ_a = 18 kg·m^{-3}. Reproduced from Ref. [129] with permission.

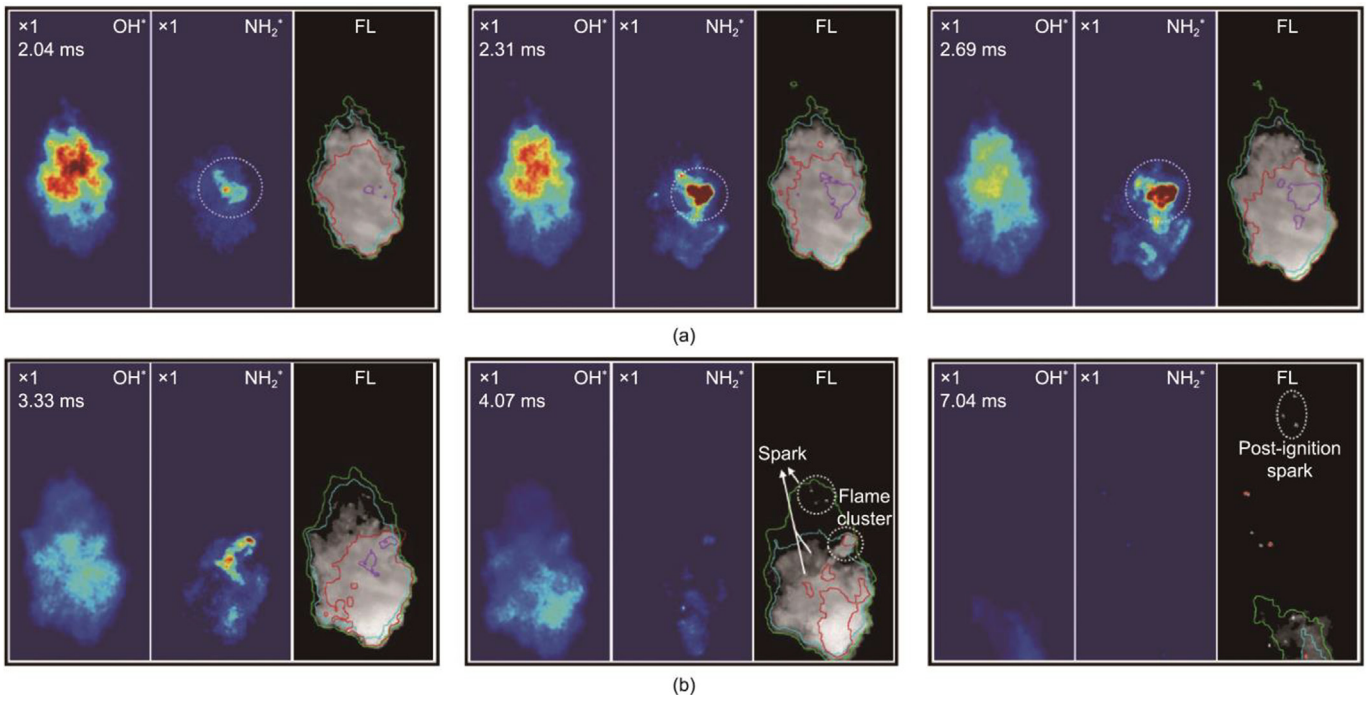

Fig. 18. Temporal evolution of OH*, NH_2*, and FL images during (a) the fully developed combustion process and (b) the post-combustion process. Reproduced from Ref. [133] with permission.

mitigating misfiring. Low-load conditions showed less effective combustion, indicating ammonia's potential limitations in certain engine operations, despite its carbon-free benefits. This research contributes valuable insights for understanding ammonia's feasibility as a sustainable fuel alternative, addressing NO_x emissions and combustion efficiency challenges while informing future engine design and fuel strategies for GHG reduction.

Based on the same rapid compression expansion machine (RCEM) system, Scharl et al. [69] explored ammonia spray combustion characteristics and mixture formation under high-pressure DI

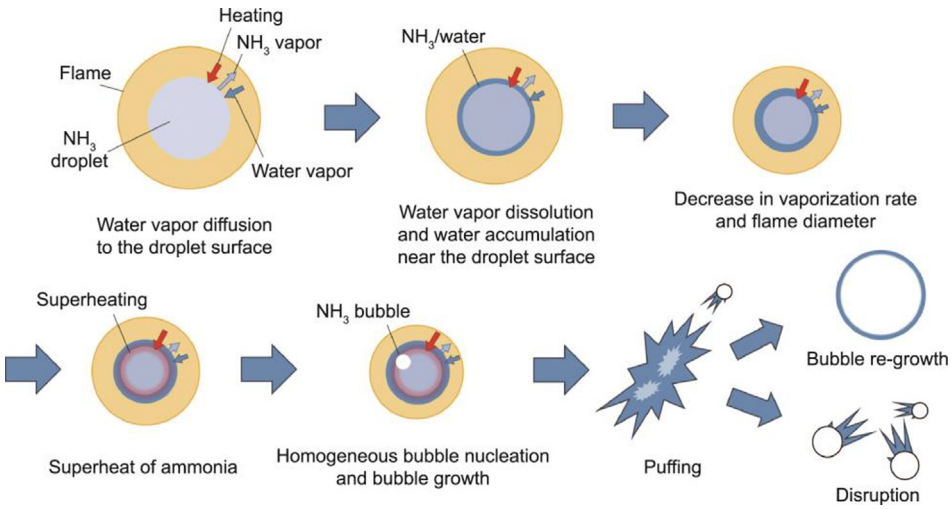

Fig. 19. Schematic diagram of the mechanism of vaporization suppression and bubble generation caused by water dissolution to the droplet in ammonia-droplet combustion. Reproduced from Ref. [134] with permission.

conditions. Fig. 20 [69] shows simultaneous shadowgraph and OH* chemiluminescence images of diesel-piloted ammonia combustion. Diesel-piloted ammonia spray behavior was analyzed via heat-release rate (HRR) analysis and a validated 1D spray model. The results revealed that diesel-ignited ammonia spray flames failed to stabilize, causing a continuously increasing lift-off length throughout injection, which was evident from parametrized HRR, OH*-intensity, and lift-off length data. This resulted from ammonia's high mixing requirements for auto-ignition, influenced by its physical properties and diesel combustion product interactions. Ammonia sprays quickly became lean, with mean equivalence ratios well below stoichiometry, further complicating flame stabilization. These findings highlight ammonia fuel challenges in internal-combustion engines, suggesting that diesel post-injections and fuel pre-heating strategies may reduce pollutant formation.

Scharl and Sattelmayer [135] reported recent findings on diesel-piloted ammonia spray combustion flame emissions under internal-combustion engine conditions. The combustion process showed distinct phases, with ammonia combustion contributing to most heat release. Fig. 21 [135] displays background-corrected OH* and NH* intensities. OH*, NH*, and NH_2* emissions significantly influenced FL, with NH_2*-chemiluminescence (CL) primarily contributing to visible emissions during ammonia combustion. The OH*-radiation intensity from the ammonia spray was significantly lower than that from the diesel pilot combustion, despite diesel comprising only 5% of the supplied LHV. For low-soot-formation cases, the authors recommend focusing on wavelengths capturing NH_2*-CL, which provide strong signals originating mainly from the flame front during ammonia combustion.

Zhang et al. [136] investigated ammonia and diesel combustion characteristics in dual DI mode, focusing on flame propagation and distribution. Fig. 22 [136] shows combustion processes at 0 and −0.5ms intervals. Simultaneous diesel and ammonia injections significantly increased combustion efficiency while minimizing unburned ammonia emissions. At an ambient temperature of 850 K, substantial diesel injection pressure created prominent flame kernels but delayed the concentrated flames from ammonia combustion on one side of the injection axis, impeding opposite-side combustion participation and causing low HRR and elevated unburned emissions. Increasing the ambient temperature to 900 K notably improved these issues. Larger spray cone angles and higher injection rates produced wider ammonia spray distribution, preventing flame backpropagation to spray junctions and improving combustion stability.

Wu et al. [137] investigated ammonia-polyoxymethylene dimethyl ether (PODE) combustion characteristics in dual-fuel DI systems, focusing on spray interaction, ignition, and flame development. Fig. 23 [137] shows radial integral OH* intensity below the theoretical interaction point versus axial distance and time, revealing gradual downstream shifts in the reaction center. The simultaneous injection (APDI-S) strategy exhibited larger axial spatial spans than PODE-pilot injection (APDI-P). During spray interaction, insufficient air mixing in collision sprays created high-equivalence-ratio regions in collision cores, delaying reactions. OH* signals weakened at 1.4–1.7 ms after the PODE injection started (ASOPI) for APDI-S and 1.9–2.1 ms for APDI-P. APDI-S showed longer OH* duration, with persistent bands below the interaction points post-combustion. Radial intensity distributions revealed three peaks with larger spatial spans in APDI-P, where the reactions occurred more on the liquid-ammonia sides. APDI-S demonstrated extended reaction durations with dispersed centers, while APDI-P showed concentrated reaction areas with earlier core region initiation. The injection timing significantly affected flame development: Simultaneous injection promoted aligned flames, while pilot injection resulted in vertical growth. Longer overlapping injection durations increased combustion efficiency.

Pathak et al. [138] investigated the temperature dependence of flame behavior in high-pressure dual-fuel diesel-piloted liquid-ammonia spray combustion, validating against optical and heat-release-rate data from RCEM experiments [69,70]. Ammonia's lower stoichiometric air requirement created lean combustion downstream of flame lift-off, reducing combustion product temperatures. Hot combustion-product entrainment into a cool ammonia spray proved insufficient for early autoignition. Diesel combustion products addressed this by serving as heat reservoirs near the ammonia spray, facilitating liquid-ammonia evaporation and vapor autoignition but necessitating sophisticated diesel injections and combustion strategies. Across all temperatures, ammonia combustion initiated through H-abstraction via OH radicals from diesel combustion. After OH radical consumption, the chemical contribution of diesel became negligible, particularly at elevated temperatures. Rising ambient temperatures increased the significance of direct ammonia oxidation through oxygen reactions.

Table 7
Summary of recent studies on liquid-ammonia spray combustion with pilot-ignited reactive fuel.

Reference	Conditions				Methods	Main findings
	Injector	Pilot fuel	Ammonia injection condition	Ambient condition		
Scharl and Sattelmayer [70]	Single	Diesel	480–530 bar	75–125 bar; 780–920 K	RCEM	HPDF combustion of ammonia is feasible for real engines but is sensitive to spray interaction, charge conditions, and pilot characteristics. Strong spatial (converging sprays) and temporal (diesel injected first) interaction is crucial for reliable ammonia ignition and burnout
Scharl et al. [69]	Single	Diesel	265–530 bar, 293 K	125 bar; 920 K; 44.5 kg·m^{-3}	RCEM; Shadowgraphy; Mie-Scattering; OH* CL	Pilot-diesel-ignited ammonia spray flames do not stabilize at a fixed lift-off length under engine-like conditions. High unburned ammonia emissions in the wake of the spray. Formation of pollutants (NO_x, N_2O) in lifted, lean reaction zones or unburned regions
Scharl and Sattelmayer [135]	Single	Diesel	503 bar, 293 K	98, 125 bar; 865, 920 K	RCEM; FL; Shadowgraphy; OH* CL	Combustion includes three identified phases: pilot ignition, flame transition, and ammonia combustion. Background-corrected OH*, NH*, and NH_2* intensities reveal the evolution of individual contributions to the flame emissions. NH_2*-CL is the main contributor to visible ammonia flame
Zhang et al. [136]	Single	Diesel	85 MPa	4.0–4.5 MPa; 800–900 K; 17.3 kg·m^{-3}	CVCC; Shadowgraphy	Optimal injection strategy is simultaneous diesel/ammonia injection with ammonia fully injected before flame extinction. Flame must backpropagate to the diesel/ammonia spray junction for complete ammonia combustion
Wu et al. [137]	Single	PODE	40 MPa	5 MPa; 850 K	CVCC; OH* CL; FL; NH_2* CL	Upon ammonia ignition, OH* forms first, followed by NH_2*. OH* has wider distribution and longer duration; NH_2* dissipates earlier and is concentrated near the spray head. Longer overlapping injection duration increases combustion efficiency
Pathak et al. [138]	Single	Diesel	530 bar, 293 K	125 bar; 920–1300 K	CFD based on Lagrangian–Eulerian approach with KH–RT breakup model	Ammonia flame fails to stabilize below 1100 K; drifts downstream. At 1300 K, flame stabilizes near the injector (lift-off length ~30 mm). NO_x emissions rise with temperature, while N_2O decreases
Zhang et al. [139]	Single	n-heptane	46 MPa, 293 K	10–15 MPa; 820–1000 K	CFD with LES and LPT	Proposed a new flame index combining species gradients and heat-release rate, providing better identification of combustion regimes in ammonia-diesel spray combustion
Yu et al. [140]	Single	n-heptane	150 MPa, 373 K	4.2 MPa; 1000 K	CFD based on LES (in OpenFOAM)	Ammonia delays n-heptane ignition nonlinearly due to competition for OH radicals. Chemical pathways: > 80% of NO_2 and N_2O generated via NO-involved reactions
Tian et al. [141]	Single	Diesel	65–85 MPa, 373 K	~28 bar; ~855 K	CVCC; RCEM; DBI	Injecting ammonia into the established diesel flame promotes more complete combustion of ammonia. Increasing ammonia injection pressure increases air entrainment and fuel–air mixing, leading to a more effective increase in peak HRR
Chen et al. [142]	Single	Diesel	60, 80 MPa, 373 K	4 MPa; ~800 K	CVCC; Schlieren	Increasing injection intervals decrease ignition delay and combustion duration but increase flame lift-off length. DI enables high ammonia substitution ratios (up to 97%) with lower soot/CO_2 emissions
Zhang et al. [143]	Single	Diesel	70 MPa	5.2–5.4 MPa; 750–800 K; ~23.4 kg·m^{-3}	CVC; DBI; FL	Stable ammonia diffusion combustion requires the entrainment of both the diesel flame and surrounding ambient gas into the effective ignition zone by the ammonia spray. Ammonia diffusion combustion is characterized by high thermal/combustion efficiencies, low NO_x, high burning rate, and high ammonia energy replacement
Sharma et al. [144]	Single	Dodecane	150 MPa	60 bar; 1000 K	CFD based on LES	Ignition delay is caused by NH_3 competing for OH radicals via NH_3 + OH = NH_2 + H_2O, suppressing dodecane's LTC chain-branching pathways·NH_3 combustion is initiated by dodecane's LTC activation. The flame evolves from LTC regions through high-temperature combustion and stabilizes near the stoichiometric mixture fraction, where NH_3 is fully consumed

CL: chemiluminescence; HPDF: high-pressure dual-fuel injection; LIBS: laser-induced breakdown spectroscopy; LTC: low-temperature chemistry; PODE: polyoxymethylene dimethyl ether; RCEM: rapid compression expansion machine.

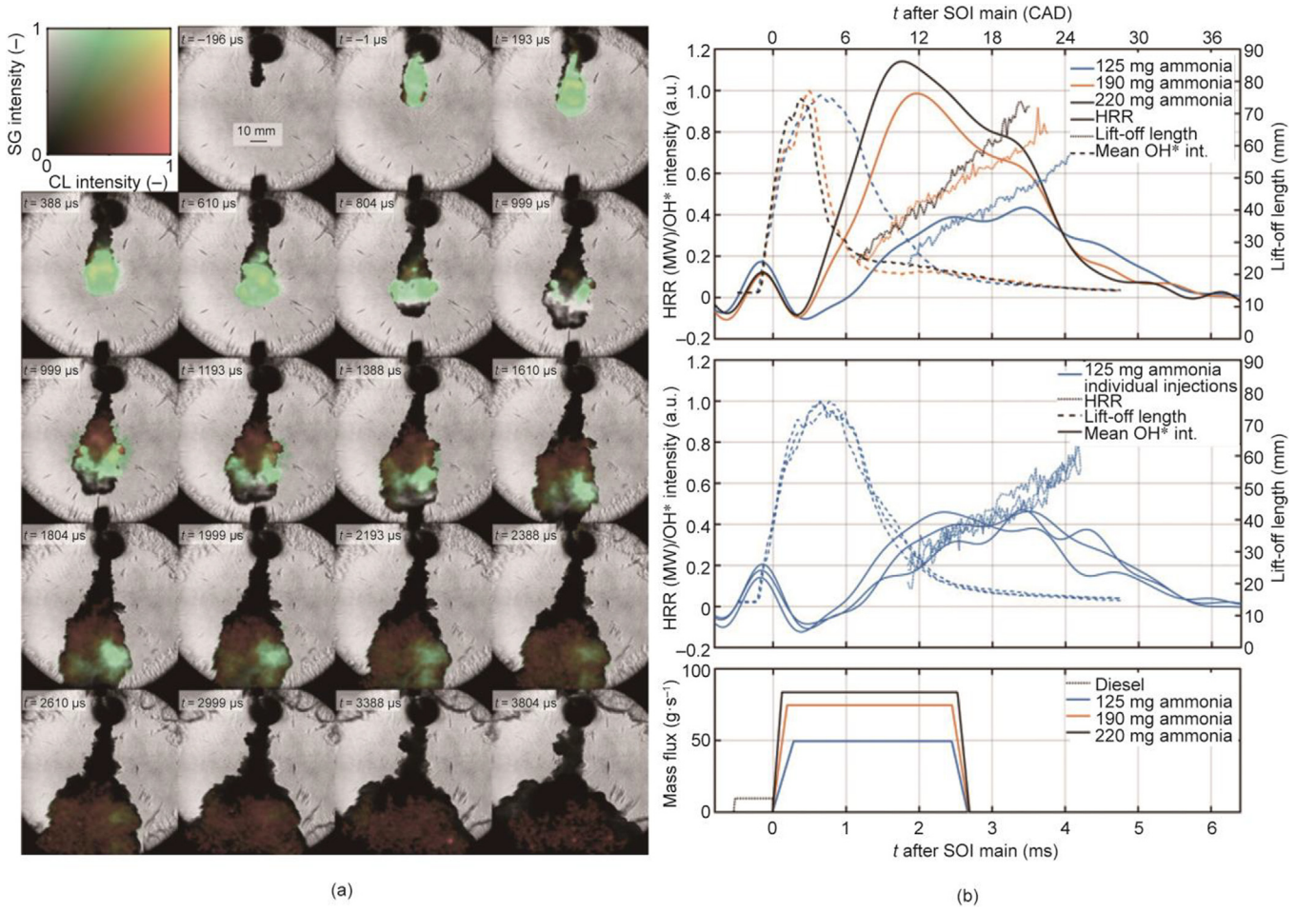

Fig. 20. (a) Series of simultaneously acquired and superimposed shadowgraph (SG) and chemiluminescence (CL) images of diesel-piloted ammonia combustion. (b) Averaged HRR, normalized mean OH*-intensity and lift-off length (top), individual HRR, normalized mean OH*-intensity and lift-off length for 125-mg injections (middle), and parametrized injection mass fluxes of diesel and ammonia (bottom) for ammonia mass and injection pressures of 125 mg/265 bar, 190 mg/460 bar, and 220 mg/560 bar. Reproduced from Ref. [69] with permission.

Zhang et al. [139] investigated ammonia-diesel high-pressure-injection dual-fuel combustion ignition characteristics under varying ambient conditions. The pilot ignition delay for diesel showed sensitivity to ambient conditions, with lower temperatures and pressures increasing delays, while the main ammonia ignition delay was primarily influenced by spray interactions and was less ambient-sensitive. The flame progression transitioned from diesel to two-layer to ammonia flame, following the ammonia injection direction (Fig. 24 [139]). This research introduced a new flame index definition for ammonia spray combustion, enhancing current understanding of the combustion regime. Increasing the ambient pressure showed no significant ignition improvement and had a potentially negative impact on reliability. The EGR strategy primarily affected ignition through ambient oxygen concentration. High ammonia energy fractions posed misfire risks due to increased mixing requirements and reduced flame temperature and HRR.

Yu et al. [140] used a validated LES model in OpenFOAM to examine ignition and pollutant formation in ammonia/n-heptane dual-fuel spray combustion under various ammonia concentrations ϕ_{NH_3}. Fig. 25 [140] displays the spatial and temporal pollutant distribution under different ϕ_{NH_3} conditions. For ϕ_{NH_3} = 0.25, 0.5, and 0.75, NO_2 was concentrated mainly at the spray base below 1150 K where first-stage ignition occurred, with NO_2 regions widening as ϕ_{NH_3} increased. NO_2 distribution remained relatively stable temporally within the cases, being transported downstream with the n-heptane spray flow and converted to N_2O and NO via the reactions $NO_2 + NH_2 = N_2O + H_2O$ and $NO_2 + H = NO + OH$. N_2O appeared downstream of NO_2 in the dual-fuel cases, followed by NO at the spray tips. NO_2 production occurred in the inner spray regions between 1150–1500 K (marked by red and black lines), increasing temporally in dual-fuel cases but remaining negligible at ϕ_{NH_3} = 0.

The above diesel-piloted ammonia spray combustion research primarily examines configurations where single-hole diesel and liquid-ammonia injectors are positioned proximally on the same side. This arrangement facilitates rapid spray-plume convergence at small angles (< 15°), ensuring effective diesel-ammonia spray intersection and interaction.

Tian et al. [141] conducted visualization studies on ammonia/diesel dual DI combustion characteristics with increased spray interaction angles of 60° (Fig. 26). Higher ammonia injection pressure increased air entrainment and fuel–air mixing. Optimal combustion required an ammonia injection close to the flame. Fuel-injection rates critically determined HRR in the high-pressure dual-fuel mode. Increasing the ammonia nozzle diameter and injection pressure significantly boosted ammonia injection rates and peak HRR through increased air entrainment and mixing. Pre-diesel ammonia injections produced mixed effects, forming combustible mixtures that increased peak HRR, while causing incomplete combustion due to rapid ammonia evaporation. Higher diesel injection pressure minimally impacted ammonia

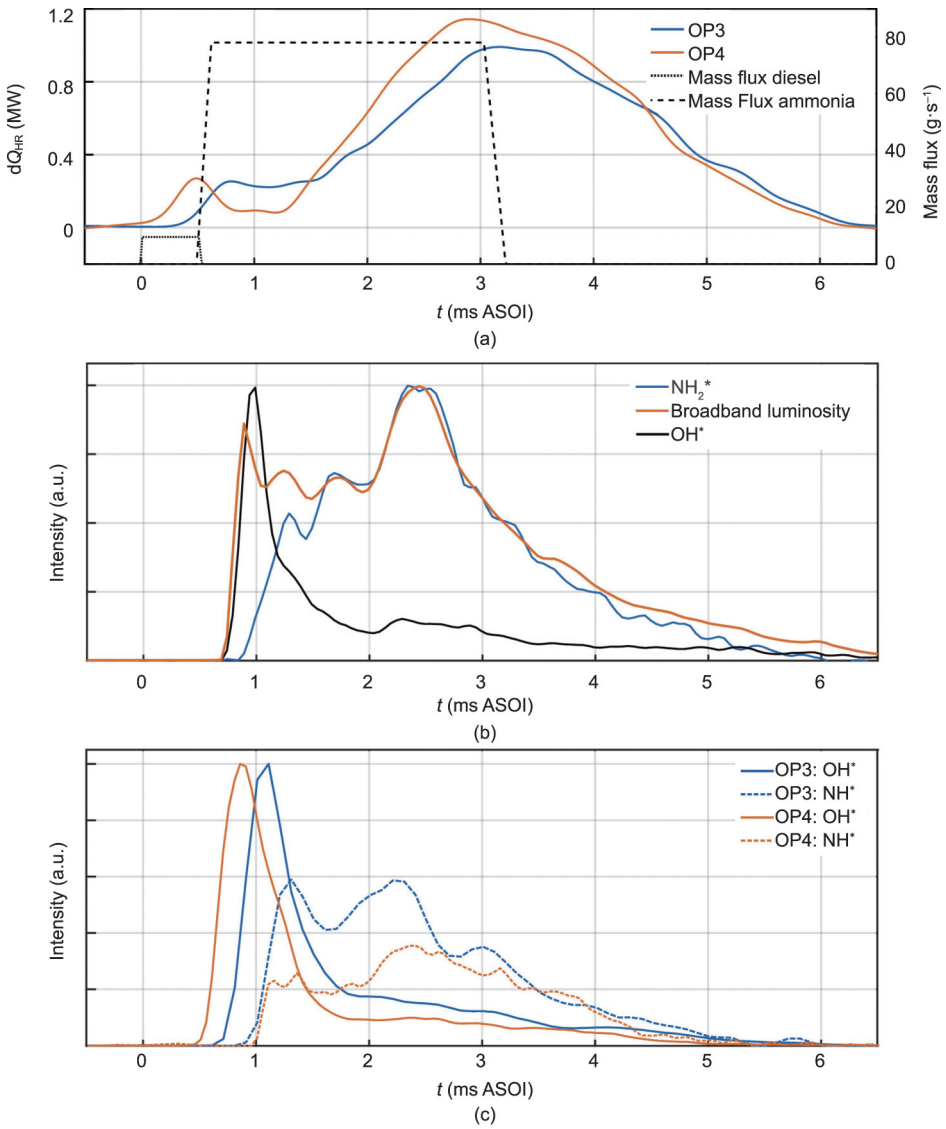

Fig. 21. Temporal evolution of normalized background-corrected CL intensities. (a) HRRs and mass fluxes to facilitate the allocation of flame emissions to the combustion phases; (b) OH* and NH*, as well as broadband luminosity for the less-reactive operating point (OP3); (c) OH* and NH* for OP3 and the highly reactive operating point (OP4). Reproduced from Ref. [135] with permission.

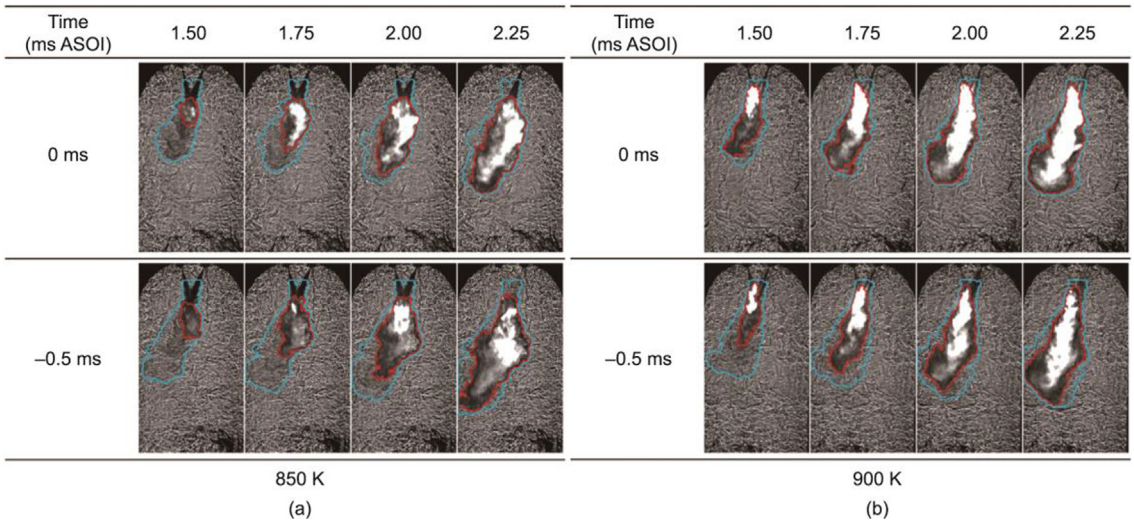

Fig. 22. Images of combustion processes at injection intervals of 0 and –0.5 ms, at (a) 850 K, 4.25 MPa and (b) 900 K, 4.5 MPa. Reproduced from Ref. [136] with permission.

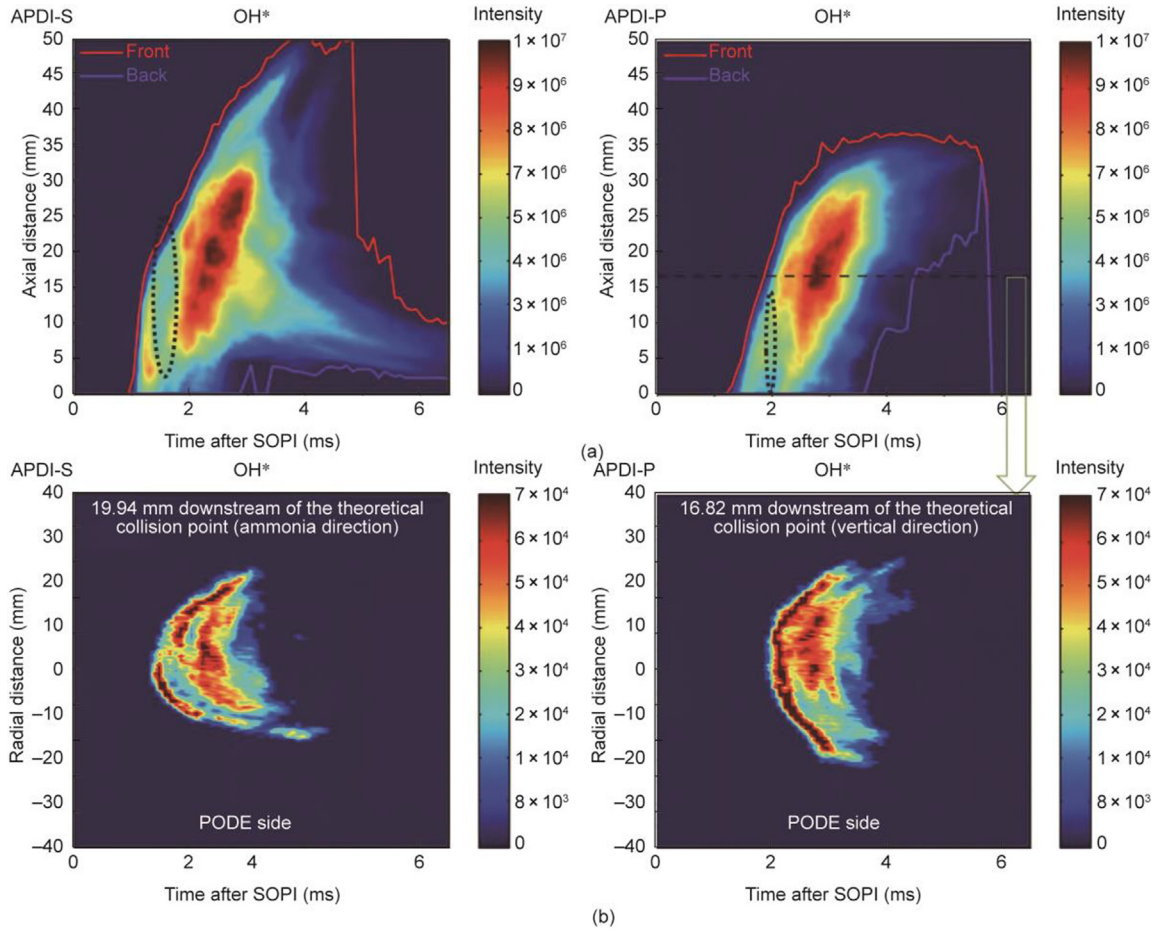

Fig. 23. (a) Radial integral intensity of OH* in the region below the theoretical interaction point in the APDI scheme as a function of axial distance and time; (b) radial intensity distribution of OH* at a specific distance as a function of time. Reproduced from Ref. [137] with permission.

combustion and was inhibited by the presence of ammonia. In the high-pressure dual-fuel mode, converged diesel and ammonia sprays followed the ammonia spray direction, although higher diesel pressure could cause directional deviation.

Chen et al. [142] experimentally investigated cross-spray and combustion behaviors in diesel–ammonia dual-fuel DI systems with diesel injectors positioned atop the CVCC and liquid-ammonia injectors on the side, creating 90° spray intersection angles. High-speed Schlieren imaging revealed that ammonia exhibited lower axial penetration, higher evaporation rates, and smaller diffusion rates than diesel, which were attributed to ammonia's lower density, viscosity, and boiling point. Diesel-ammonia spray collision increased the overall spray diffusion and fuel–air mixing. Vertical sprays showed larger liquid-phase penetration, with adjustments to the injection intervals improving atomization. Increasing the diesel-ammonia injection intervals initially delayed ignition but subsequently reduced combustion duration and soot emissions, suggesting that appropriate interval adjustments optimize combustion efficiency and reduce emissions.

Zhang et al. [143] positioned diesel and ammonia injectors on opposing CVC sides, creating collision patterns between sprays. Various nozzle-hole tilt angles produced diverse spray intersections. Fig. 27 [143] shows a spray interaction where ignition occurs at the upper and lower plume-collision points. High-pressure ammonia injection created gas entrainment and pushed-out zones, with effective ignition occurring 16–35 mm from the nozzle in entrainment zones. Diesel flames surrounding liquid ammonia were extinguished by ammonia gasification, while pushed-out zone flames failed to ignite the ammonia. Reliable ammonia ignition and diffusion combustion, achieving 74.4% energy replacement, were obtained by entraining the diesel flame and surrounding air into ignition zones. Increased ammonia injection or prolonged diesel-flame suspension was necessary for stable combustion. Premixed diesel flames igniting the ammonia spray increased the combustion efficiency and flame consistency compared with diffused diesel flames due to the leaner, more homogeneous air–fuel mixtures.

Xu et al. [64] combined optical experiments and LES to examine diesel–ammonia flame interaction and pollutant formation mechanisms (NO and N_2O) under two scenarios. Fig. 28 [64] shows the local equivalence ratio (Φ), ammonia/diesel mixture fraction (Z), heat-release rate (Qdot), and mass fractions of CO, NH_3, NO, and N_2O in spray cross-sections at different times. The ammonia–air mixtures displayed distinct pre-combustion characteristics between injection cases. Early interaction scenarios showed fuel-rich ammonia–air mixtures igniting directly from diesel flames, enabling self-sustained flame propagation and significant heat release that maintained high-temperature regions for continuous combustion. Late interaction scenarios resulted in rapid ammonia evaporation, which created fuel-lean ammonia/air mixtures that failed to ignite from diesel flames, causing flame extinction. NO_x and N_2O emissions proved highly sensitive to diesel–ammonia flame interaction. N_2O formed predominantly at ammonia flame-quenching fronts, presenting significant challenges due to ammonia's fast evaporation and slow oxidation rates in fuel–lean mixtures.

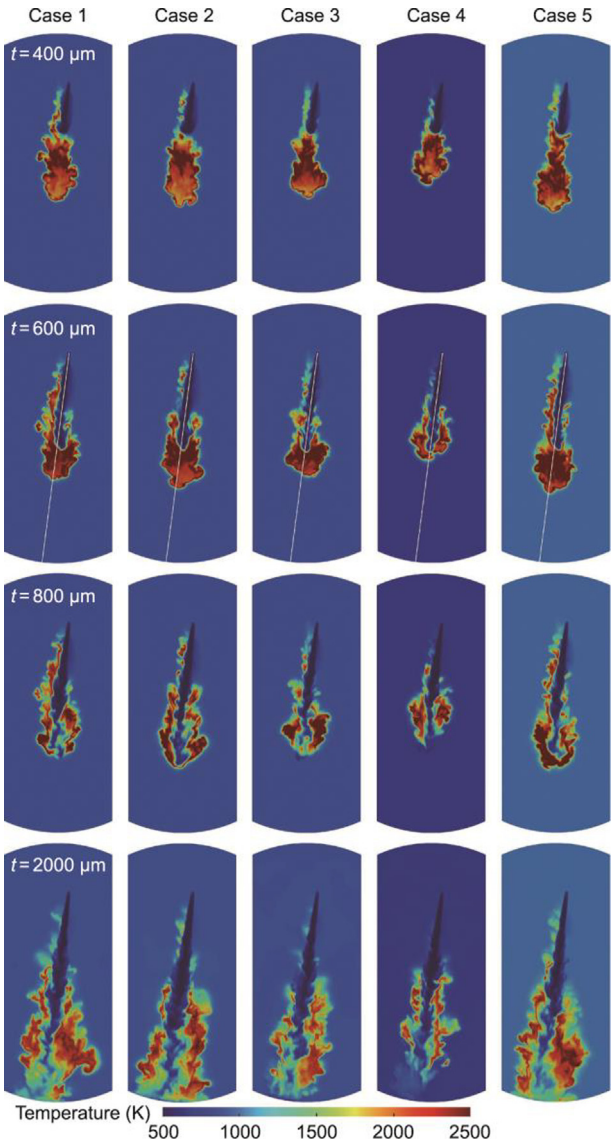

Fig. 24. Temporal evolution of instantaneous temperature under diesel-engine conditions (white line represents sampling position). Reproduced from Ref. [139] with permission.

In addition, Sharma et al. [144] examined the incorporation of ammonia as a low-reactivity fuel in diesel-assisted dual-fuel combustion under reactivity-controlled compression ignition (RCCI) conditions using LES. Through flamelet analysis, they investigated the flame-structure evolution and combustion modes of dodecane/ammonia mixtures. Their results showed that ammonia combustion initiated through dodecane low-temperature combustion activation, transitioning to high-temperature combustion, with ammonia consumption occurring as flames evolved toward stoichiometric conditions. Under fuel-lean conditions, ammonia exhibited no autoignition behavior.

3.4. Ammonia spray combustion with other emerging methods

Aside from pilot-diesel ignition, researchers have explored the use of turbulent jet injection (TJI) to enhance liquid-ammonia spray combustion. Zhong et al. [151] investigated transient ammonia spray flames using pre-chamber TJI, as illustrated in Fig. 29. Hydrogen injected into the pre-chamber generated high-speed jet flames. TJI-induced ammonia spray flames progressed through three phases: pre-chamber combustion, partially premixed combustion, and mixing-controlled combustion. Pre-chamber mixture enrichment greatly enhanced TJI ignition capability, causing earlier ignition- and combustion-mode transitions. Larger nozzle diameters with lower turbulent jet velocities improved the ignition ability and extended the critical oxygen concentration for stable ignition, which was attributed to the increased jet-ammonia spray interaction and mixing behavior enabling full ignition-energy utilization. Reduced turbulence intensity decreased heat dissipation, supporting ignition processes.

Researchers have explored improved liquid-ammonia injection methods. Ichikawa et al. [152] proposed a three-layer stratified fuel-injection approach for compression-ignition engines, involving sequential injections of a high-reactivity supporting fuel ($nC_{16}H_{34}$), liquid ammonia, and a second supporting fuel through a single nozzle (Fig. 30). CVCC verification confirmed that the system effectively produced two- or three-layer sprays, evidenced by injection energy rate measurements. First-layer $nC_{16}H_{34}$ ignited ammonia sprays, although the ammonia ignition delays slightly exceeded those of 100% $nC_{16}H_{34}$ sprays. Third-layer $nC_{16}H_{34}$ facilitated second-layer ammonia combustion, creating high HRR peaks at the combustion end and significantly shortening the late combustion periods. Third-layer $nC_{16}H_{34}$ combustion drastically reduced N_2O emissions by eliminating low-temperature regions in the liquid-ammonia spray diffusion flames where N_2O typically forms through active combustion.

Following previous work, researchers experimentally studied ammonia stratified spray combustion using high-speed direct imaging [153]. Fig. 31 [153] shows high-speed images of ammonia stratified and 100% $nC_{16}H_{34}$ spray flames. Ammonia's spray flame penetration lengths and cone angles matched those of 100% $nC_{16}H_{34}$, but the ammonia stratified spray flame lift-off positions moved downward, differing from those of 100% $nC_{16}H_{34}$ spray. This resulted from the second ammonia layer's low reaction rate, large latent heat, and specific heat compared with those of $nC_{16}H_{34}$. The initially formed burnt gas lump significantly influenced the flame lift-off position in the ammonia-dominated jet-stream second layer. The researchers concluded that developing initial burnt gas lump formation methods and third-layer combustion control is crucial for ammonia stratified spray flames.

Bakir et al. [154] computationally investigated the autoignition enhancement of liquid-ammonia spray with dissolved hydrogen to simplify engine hardware and infrastructure for ammonia–hydrogen dual-fuel combustion. Trace dissolved hydrogen successfully facilitated ammonia ignition within reasonable residence times, with complete flame development being achievable through extended injection duration. Ignition timing was controlled by spray evaporation and mixing rather than H_2 concentration. Chemical kinetic pathway analysis revealed that the OH radicals from H_2 oxidation dominantly and necessarily oxidized the NH_3, generating highly reactive intermediates and promoting the desired ignition. The emissions contained high NO_x and N_2O concentrations before and after ignition, particularly NO. This dissolved hydrogen–liquid ammonia blend offers cost and convenience advantages for improving liquid-ammonia spray combustion.

Cheng et al. [84] recently proposed a twin-fuel co-injection strategy using hydrogen as a combustion enhancer (Fig. 32). Their system blends high-pressure liquid NH_3 (> 300 bar) with gaseous H_2 (> 100 bar) before injection, enabling precise liquid-to-gas ratio control and creating homogeneous high-/low-reactivity fuel mixtures with controlled stratification. The advantages include flexible NH_3/H_2 ratio control based on injection pressure and duration, enhanced liquid NH_3 atomization and fuel–air mixture quality through premixed injection, and improved combustion stability due to homogeneous NH_3–H_2 mixtures reducing the flame instability. The system can incorporate pre-chambers as volumetric

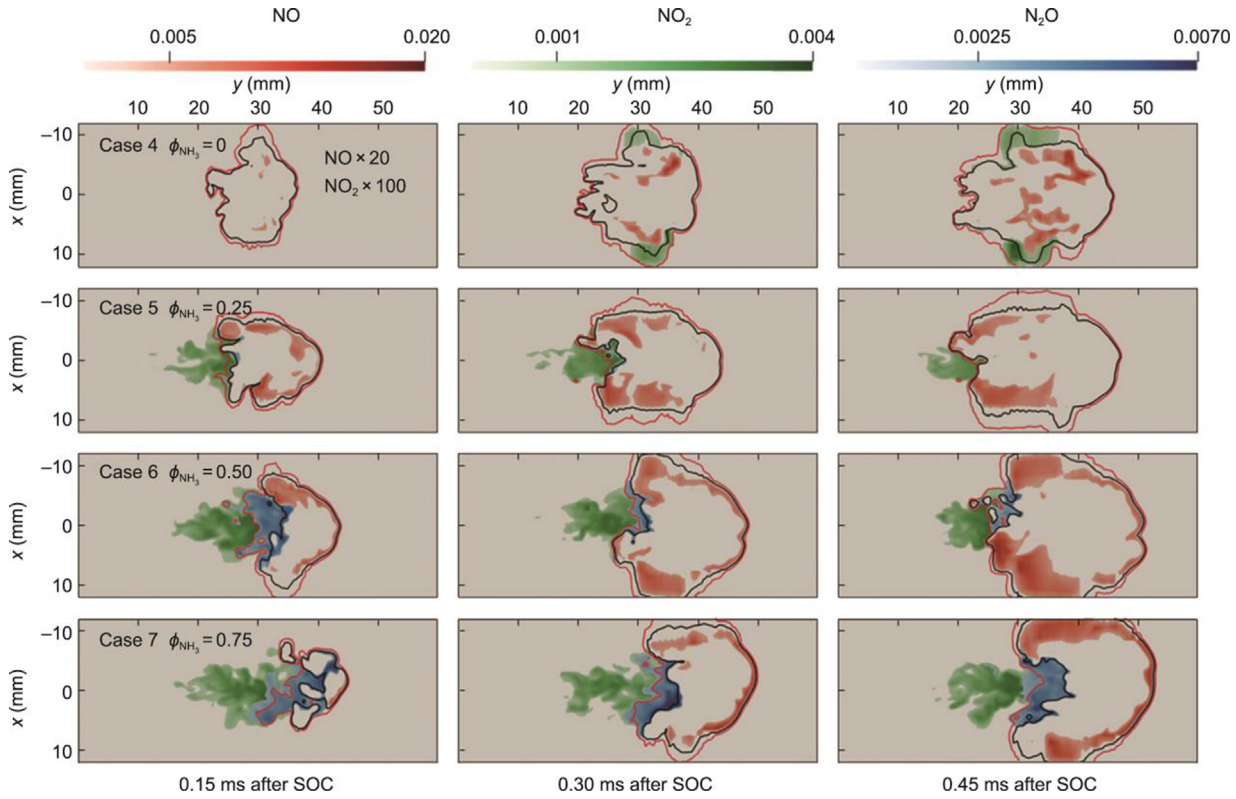

Fig. 25. Distribution of NO, NO_2, and N_2O mass fractions under different ϕ_{NH_3} with temporal evolution (nozzle exit located at $x = 0$, $y = 0$). Red and black lines represent $T = 1150$ and 1500 K. Reproduced from Ref. [140] with permission.

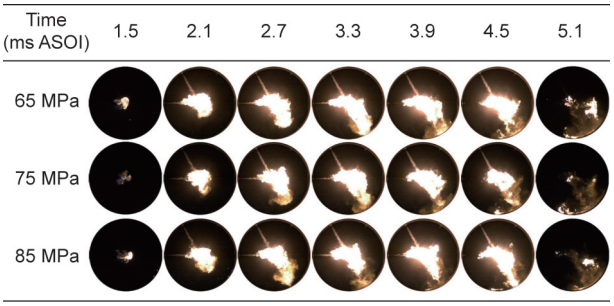

Fig. 26. Images of combustion processes with different ammonia injection pressures (65–85 MPa). Reproduced from Ref. [141] with permission.

ignition sources for NH_3–H_2 blends, further enhancing ignition and combustion stability.

Although the twin-fuel co-injection strategy offers significant advantages—such as superior combustion control with faster burn rates and lower cycle-to-cycle variations—and despite aligning with decarbonization goals by eliminating carbon-based pilot fuel, it presents several practical challenges. These include the complexity of storing liquid NH_3 and gaseous H_2 in dual tank systems with different safety requirements, which may increase system volume and weight by 40%–60% compared with conventional diesel systems. Precise control of the NH_3/H_2 ratio under transient engine conditions is difficult, with potential variations exceeding ±15%, which could lead to combustion instability or excessive NO_x formation. Additionally, the initial cost of the dual-fuel system is estimated to be 2.5–3.0 times higher than that of diesel systems due to the high-pressure hydrogen components and sophisticated control systems, with the hydrogen infrastructure requirement further limiting its near-term adoption.

3.5. Summary

This section reviews liquid-ammonia injections and spray characteristics under high-pressure, high-temperature conditions, covering both non-reactive and reactive scenarios. CVC studies show that ammonia spray behavior is highly sensitive to ambient conditions, with penetration and evaporation rates differing significantly from those of diesel, necessitating optimized injection strategies and nozzle designs. Ammonia's high auto-ignition temperature and low reactivity require pilot ignition strategies, typically using diesel. While diesel-piloted combustion achieves stable ignition, flame stabilization remains challenging due to ammonia's slow kinetics and high vaporization heat. Optical techniques and models have been used to analyze flame development, heat release, and pollutant formation (particularly NO_x and N_2O). Innovative approaches include TJI, stratified injections, and blending ammonia with hydrogen or reactive fuels to increase combustion efficiency and stability while reducing emissions. These findings provide crucial insights for developing ammonia-fueled engines and sustainable transportation systems.

Comparing the maturity levels of various combustion-enhancement technologies, TJI appears most promising for immediate implementation due to its ability to extend the critical oxygen concentration for stable ignition. In addition, TJI ignition [151] achieves 40% faster flame propagation than stratified injection [152]; however, its scalability to multi-cylinder engines remains unproven. Stratified injection systems, while theoretically superior in reducing N_2O emissions by 60% [152] through optimized temperature gradients, present practical challenges in precise fuel layer control and near-term adoption. The hydrogen co-injection approach offers excellent ignition enhancement but introduces significant infrastructure complexity. Based on the reviewed literature, pilot-ignited diesel injection remains the most

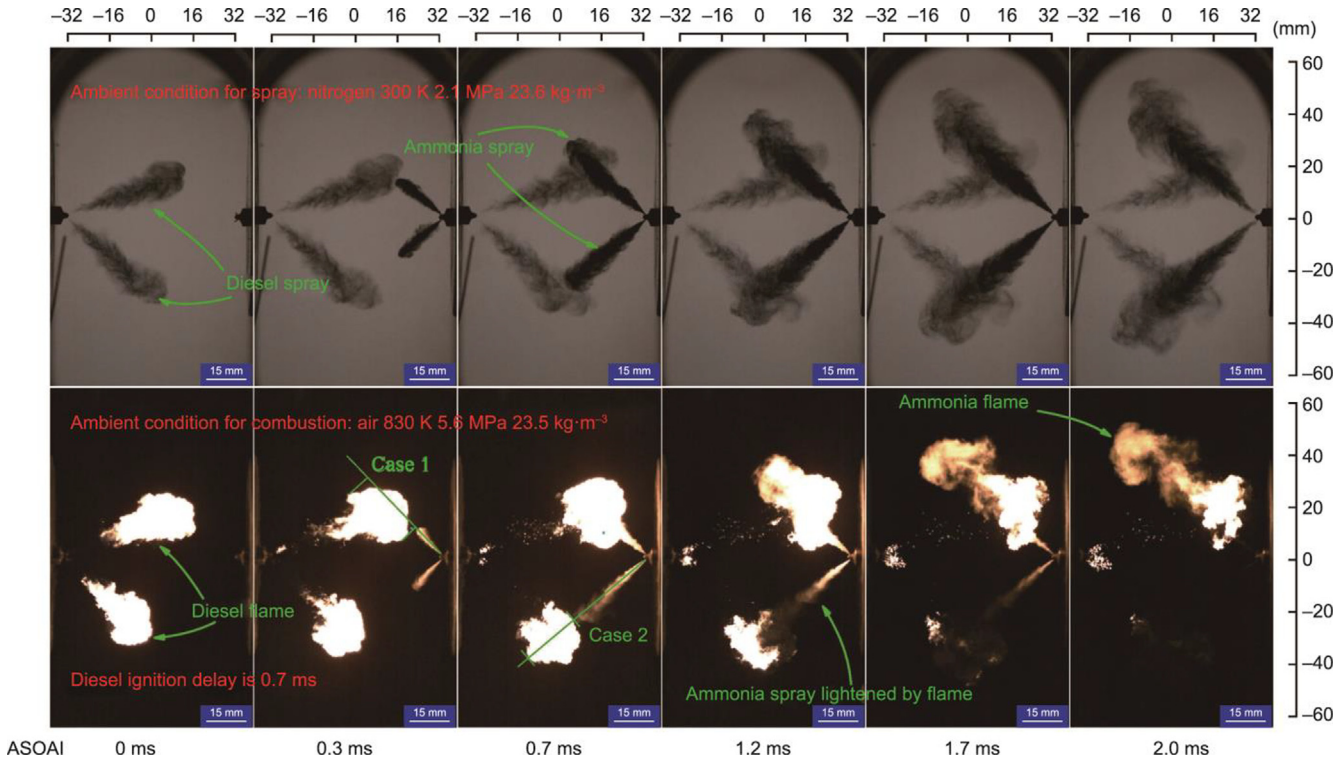

Fig. 27. Images of spray and combustion for a spray-plume arrangement with two ignition locations. Reproduced from Ref. [143] with permission.

mature technology, although it contradicts the carbon-neutral objective unless renewable diesel alternatives are employed.

4. Application of liquid-ammonia injection in engines

Research on liquid-ammonia applications in real engines began around 2022, prior to which ammonia was predominantly used in a gaseous state as engine fuel. Since 2022, researchers have explored liquid-ammonia injection feasibility and effectiveness in engine combustion. Due to ammonia's low reactivity, single-fuel-mode combustion remains unfeasible, making dual-fuel mode the currently recognized effective approach for ammonia engine combustion. A summary of ammonia dual-fuel engine performance and emissions from other relevant references [165–172] is provided in Table S1 in the Appendix.

4.1. Research progress

Zhou et al. [155] conducted a comparative analysis of the low-pressure injection dual-fuel (LPDF) mode and high-pressure injection dual-fuel (HPDF) mode, as illustrated in Fig. 33. In LPDF mode, low-pressure ammonia injection into intake ports or cylinders creates premixed combustible mixtures with air. High-reactivity diesel initiates combustion, with premixed turbulent flame-propagation speed controlling the process, particularly at small diesel fractions. Conversely, HPDF mode involves injecting both diesel and liquid ammonia near the top dead center, where fuel–air mixing rates dominate in-cylinder heat-release processes, similar to conventional diesel engines.

In addition, the researchers developed numerical models for pilot diesel-ignited ammonia dual-fuel engines in premixed and high-pressure spray combustion modes, based on commercial low-speed marine diesel engines and validated against experimental data on spray mixture formation, ignition delay, in-cylinder pressure, and pollutant emissions. Fig. 34 [135] compares the indicated thermal efficiency (ITE) and emissions across diesel-only, LPDF, and HPDF modes. Both dual-fuel modes achieved approximately 97% GHG reduction compared with diesel-only operation through substantial diesel replacement with carbon-free ammonia. Optimized LPDF increased the ITE by 5.1% through reduced cooling losses but raised NO_x emissions 140.6% above diesel-only levels. Optimized HPDF achieved a diesel-comparable ITE while reducing NO_x emissions by 47%. Both optimized configurations maintained 97% GHG reduction, with negligible unburned ammonia emissions.

Nadimi et al. [156] developed and validated a CFD model to study ammonia/biodiesel sprays, combustion characteristics, and emissions formation. Direct liquid-ammonia injection with biodiesel in single-cylinder diesel engines significantly reduced GHG emissions and combustion chamber temperatures. A maximum 50% ammonia energy ratio (AER) was achievable without significant performance drops. Retarding the ammonia injection timing from −25 to −10 crank angle degrees (CAD) reduced NO_x, CO, and ammonia emissions by 31.4%, 39.6%, and 31.3%, respectively. Optimal conditions occurred with ammonia injection at −10 CAD and biodiesel at −16 CAD with 50% AER. In addition, this team modified a single-cylinder diesel engine with dual common rail systems for direct liquid-ammonia/pilot biodiesel injection [157]. Welding three nozzles from six-nozzle injectors reduced NH_3 and CO emissions by 29.2%. Late fuel injection increased the particulate matter from 10.5 to 15.2 $mg \cdot m^{-3}$ due to fuel-rich high-temperature zones but reduced NO_x and CO emissions by 1.4 and 4.4 $g \cdot (kW \cdot h)^{-1}$, respectively, compared with early biodiesel start of injection (SOI).

Zhang et al. [158] experimentally validated ammonia/diesel dual DI in two-stroke low-speed engines using a diesel jet-controlled compression ignition (JCCI) concept, examining engine performance and emissions under various ammonia injection quantities, timings, and diesel injection timings. The study verified feasibility, demonstrating precise liquid-phase ammonia ignition

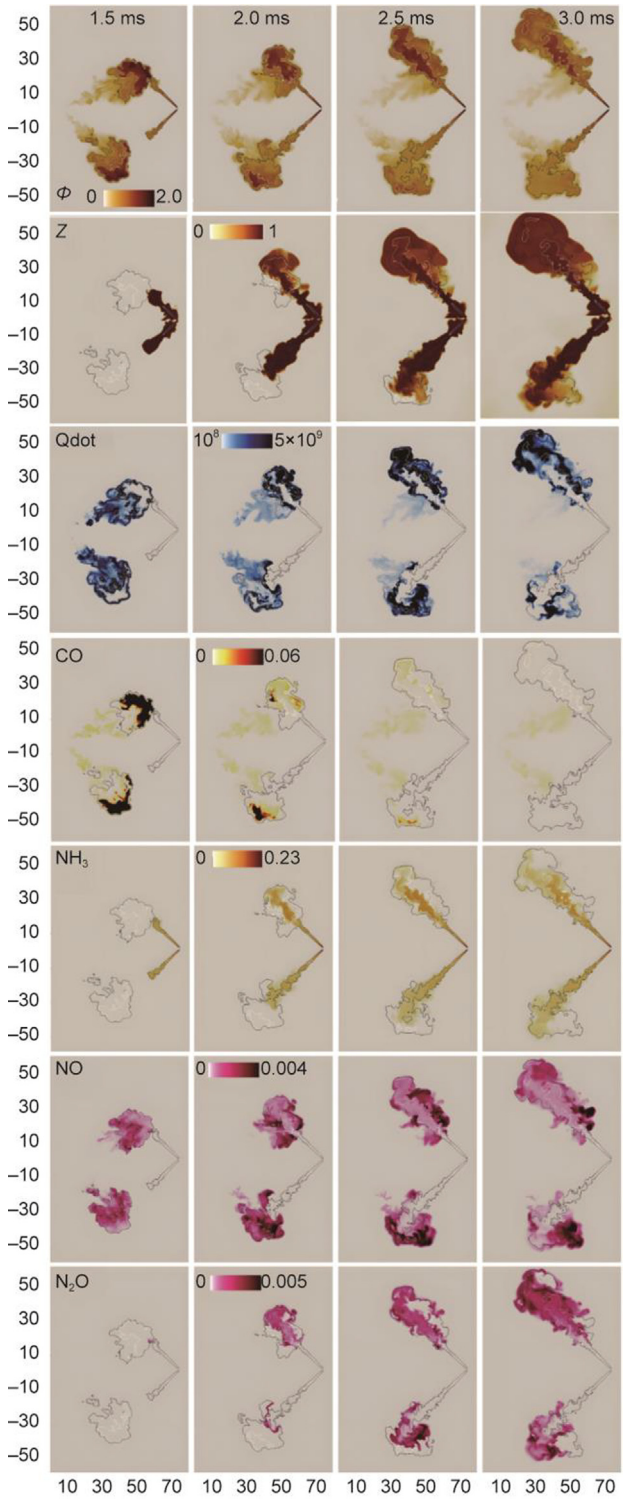

Fig. 28. Distribution of local equivalence ratio (Φ), ammonia/diesel mixture fraction (Z), HRR (QDot), and mass fractions of CO, NH_3, NO, and N_2O in the central cross-section of the spray at different times. White and black iso-lines represent Φ values of 1.0 and 0.5, respectively. Reproduced from Ref. [64] with permission.

control by diesel jets resulting in two-stage combustion dominated by diesel then ammonia. Adjusting the ammonia injection timing enabled different combustion modes: premixed, diffusion, and premix-diffusion co-combustion. Excessive timing advancement created super-lean mixtures, while absolute diffusion combustion extended the total combustion duration. The combustion phase showed high sensitivity to diesel injection timing. Robust ammonia combustion control shortened the total combustion duration compared with that of pure diesel, improving the ITE. Soot and CO emissions decreased through enhanced spray plume interaction and improved diesel atomization/evaporation promoting oxidation during ammonia combustion. NO_x emissions increased due to the combined thermal NO_x (diesel) and fuel NO_x (ammonia) contributions. Adjusting the diesel injection timing or extending the combustion duration managed emissions but negatively impacted the ITE. Injection timing at −8° crank angle after top dead center (CA ATDC) provided optimal ITE and emission performance balance for both fuels.

In 2024, research on liquid-ammonia spray engines began to increase. Dong et al. [159] developed and validated a numerical model for ammonia/diesel dual DI two-stroke engines using bench test results. Their findings showed that optimizing the spray spatial arrangement, intake temperatures, and EGR rates effectively controlled nitrogenous and GHG emissions while maintaining high thermal efficiency. Optimal conditions included an 8° spray arrangement angle, 355-K intake temperature, and 20% EGR rate, effectively balancing unburned ammonia, NO_x, N_2O, and GHG emission reductions. Fig. 35 [159] illustrates the EGR rate effects on CO_2 and GHG emissions, showing that both CO_2 and N_2O emissions increased with rising EGR rates, elevating overall GHG levels. At −4 °CA ATDC after the start of injection (ASOI) with a 30% EGR rate, GHG emissions exceeded diesel-only mode levels.

The same team further numerically explored liquid-ammonia diffusion combustion (LADC) based on a modified marine two-stroke engine [160]. LADC significantly increased combustion speed, reduced soot emissions by 99%, and advanced CA90 by 11.8 °CA compared with pure diesel. Optimal combustion and emission characteristics occurred at 50%–70% AER. Fig. 36 [160] shows the effects of AER on NO_x and soot emissions: Increasing AER raised NO_x while reducing soot. NO emissions decreased and N_2O increased significantly at high AER due to the lower average cylinder temperatures reducing thermal NO, with amino groups reacting with NO to form nitrogen at 1100–1400 K. The higher ammonia reaction temperatures generated fuel-type NO, decreasing NO emissions at high AER. Diesel combustion produced negligible N_2O, with elevated-temperature ammonia combustion being the primary source. Higher AER increased the liquid-ammonia injection, raising ammonia combustion and N_2O emissions while reducing soot through decreased diesel injection.

Park et al. [161] investigated efficiency improvements by introducing oxygen into the intake air of a 2.5 L ammonia-fueled DI spark-ignition engine, experimentally analyzing the combustion, exhaust, and efficiency. Liquid ammonia was injected at 15 MPa, with hydrogen and oxygen introduced via intake manifold. Oxygen addition significantly increased the combustion stability and thermal efficiency, particularly under low-speed, low-load conditions. Increasing the oxygen concentration reduced the ignition delay and accelerated the combustion speed, improving stability and efficiency. Oxygen showed more pronounced effects than hydrogen on ignition delay and combustion speed. While increasing the oxygen concentration from 25% to 30% further improved the combustion stability and reduced unburned ammonia emissions, additional efficiency improvements were insignificant.

Following their previous work, the team experimentally studied diesel post-injection timing and quantity effects on combustion, emissions, and efficiency in a 12 L ammonia–diesel dual-fuel CI single-cylinder marine engine [162]. Conducting 40% diesel post-injection near a micro-pilot injection in an ammonia–diesel dual-fuel four-stroke marine engine reduced the unburned hydrocarbons by 18.9%, unburned ammonia by 11.2%, and N_2O by 19.4% compared with conventional dual-fuel combustion, while maintaining equivalent thermal efficiency. Dual-fuel combustion

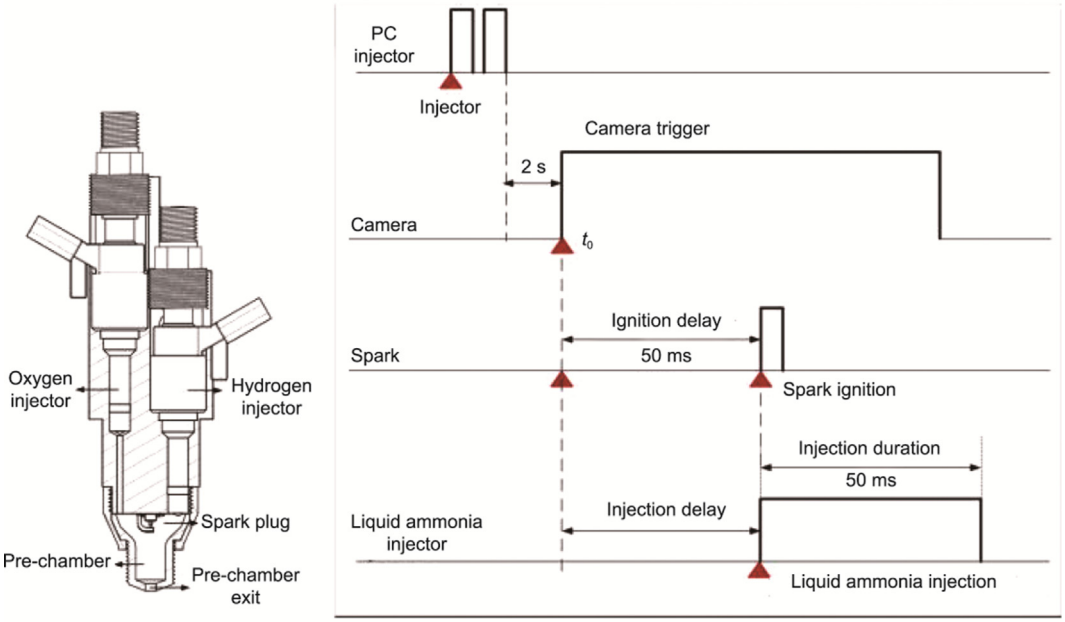

Fig. 29. Schematic diagram of reactivity-controlled turbulent jet ignition. Reproduced from Ref. [151] with permission.

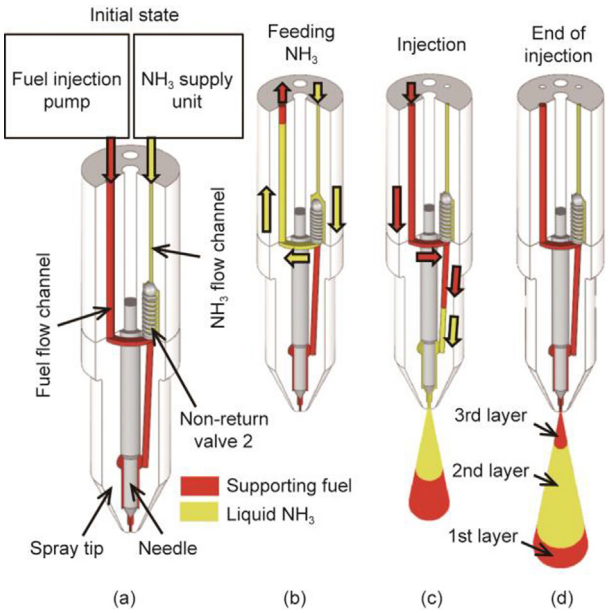

Fig. 30. Schematic of the stratified fuel injector operating principle: (a) initial state, (b) feeding NH3, (c) injection, and (d) end of injection. Reproduced from Ref. [152] with permission.

surpassed neat diesel in GWP and CO_2, NO, and CO emissions. Although post-injection slightly increased the GWP due to higher CO_2, it significantly reduced the overall NO_x emissions including N_2O and NO, improving combustion efficiency by lowering the unburned ammonia and total hydrocarbons.

Park et al. [66] conducted engine experiments comparing combustion, thermal efficiency, and exhaust emissions at various CRs using liquid-ammonia DI with pilot-ignited diesel in a 12.5 L single-cylinder marine engine. Increasing the CR in an ammonia–diesel dual-fuel marine engine significantly improved the thermal efficiency by over 5.8% and increased combustion stability. Fig. 37 [66] shows the effects of the CR on the in-cylinder pressure and HRR, demonstrating that higher CRs increased the in-cylinder pressure and temperature, accelerating combustion efficiency. While the maximum in-cylinder pressure increased with higher CR, the peak pressure timing remained consistent. Higher CR advanced heat-release initiation, although the HRR varied due to fuel atomization differences. At CR 13, lower ambient pressure and temperature produced higher premixed flame heat release than at CR 14. Maximum HRR remained consistent across CRs despite ammonia flow-rate variations. Improved diesel flame characteristics increased the initial ammonia ignition and combustion speed, with minimal impact on late combustion and unburned ammonia emissions. A higher CR improved the thermal efficiency and combustion stability, although the reduction of unburned ammonia emissions was insignificant.

In addition, engine results from Mi et al. [163] show that the ammonia post-injection strategy effectively mitigated the suppression effect of high-concentration ammonia on diesel ignition, enabling advanced ignition timing and increased peak HRR. Combined with intake heating, this approach achieved an AER of 86% at an indicated mean effective pressure (IMEP) of 4 bar while improving the ITE by 8% and substantially reducing unburned ammonia. A feasible expansion strategy for achieving high AER in liquid ammonia–diesel dual-fuel combustion is shown in Fig. 38 [163]. At IMEP = 6 bar, the ammonia post-injection strategy with a controlled SOI for diesel and second ammonia injection timing, combined with appropriate post-injection ammonia quantity, enables an 80% substitution rate. At IMEP = 4 bar, intake heating increases the in-cylinder activity, while ammonia pre-injection is employed at low AER and post-injection at high AER. This approach achieves higher thermal efficiency and lower ammonia emissions across a wide operating range with relatively low N_2O emissions.

Yang et al. [164] recently proposed an innovative ammonia thermal atmosphere compression ignition (TACI) combustion mode, as shown in Fig. 39. N-heptane is supplied to the intake manifold and enters the cylinder with the intake air during the intake stroke, where it auto-ignites under compression and undergoes homogeneous charge-compression ignition (HCCI) combustion. Following n-heptane combustion, ammonia is injected into the cylinder and auto-ignites due to the active thermal atmosphere comprising high pressure, high temperature, and active radicals. The ammonia TACI combustion mode thus consists of three stages:

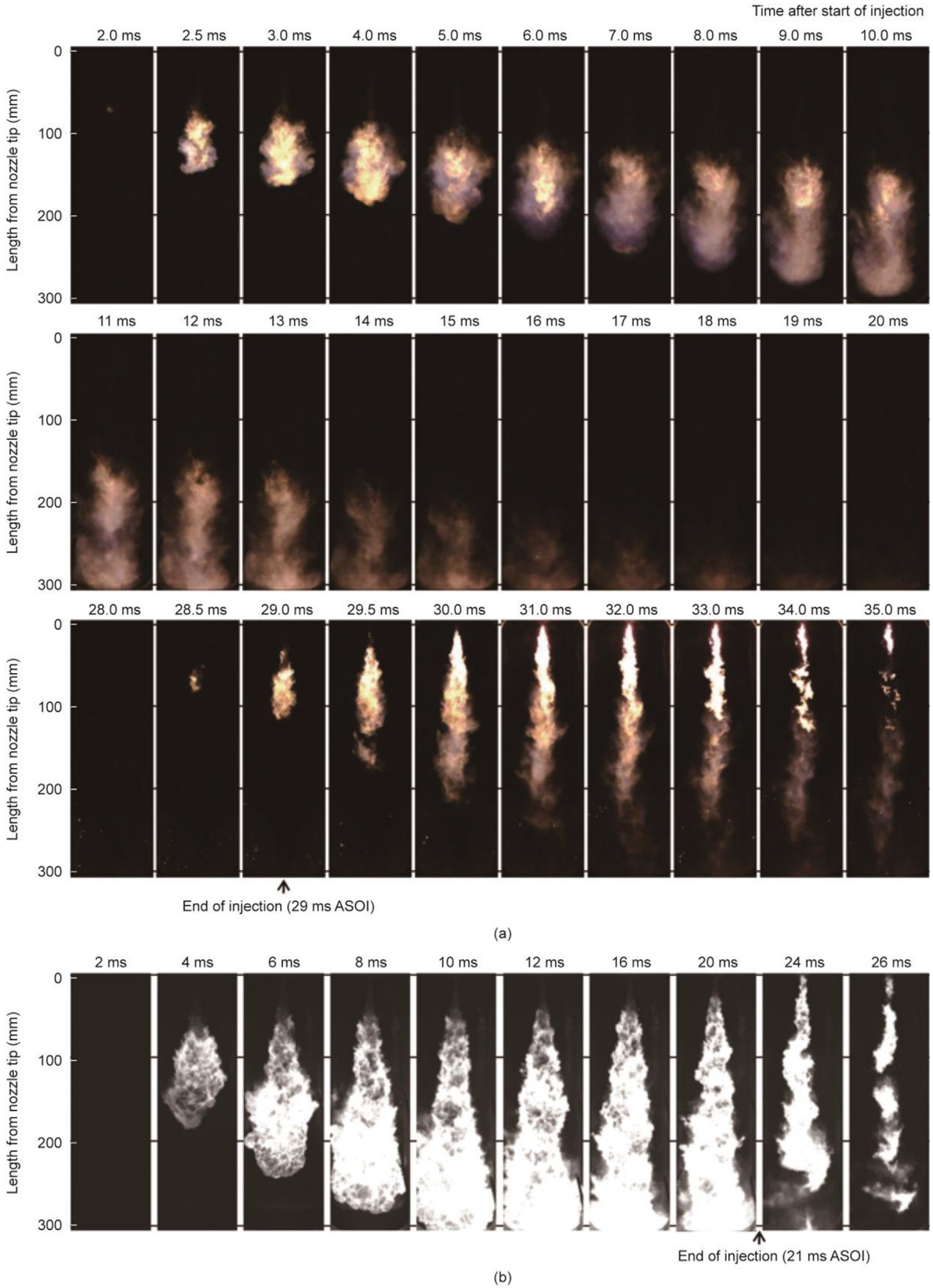

Fig. 31. High-speed direct images of (a) ammonia stratified and (b) 100% $nC_{16}H_{34}$ spray flames. Reproduced from Ref. [153] with permission.

the n-heptane low-temperature reaction, n-heptane high-temperature combustion, and ammonia diffusion combustion. The ammonia injection timing critically affects the diffusion combustion characteristics and thermal efficiency in TACI mode, with optimal timing being determined by the combustion phase. Over-delayed injections reduce stability and efficiency while

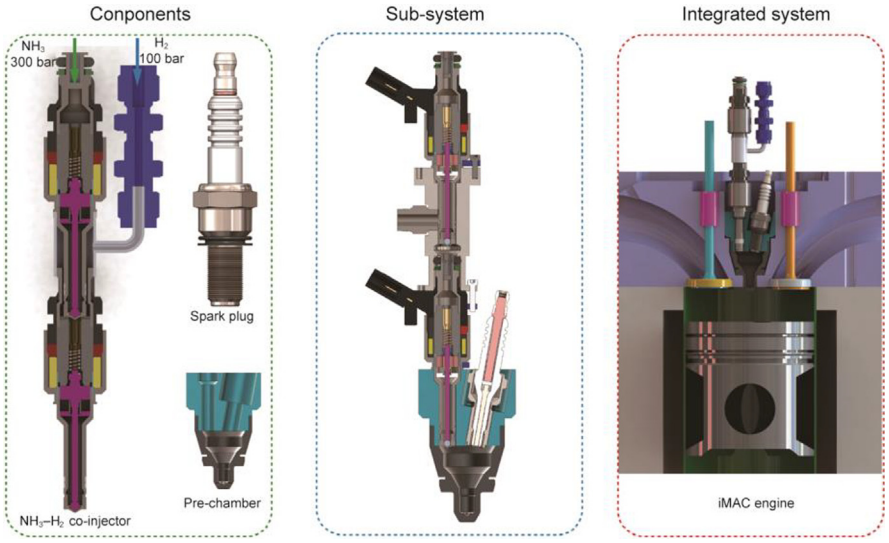

Fig. 32. Concept of a liquid and gas twin-fuel injection for NH_3–H_2 dual-fuel combustion in ICEs. Reproduced from Ref. [84] with permission.

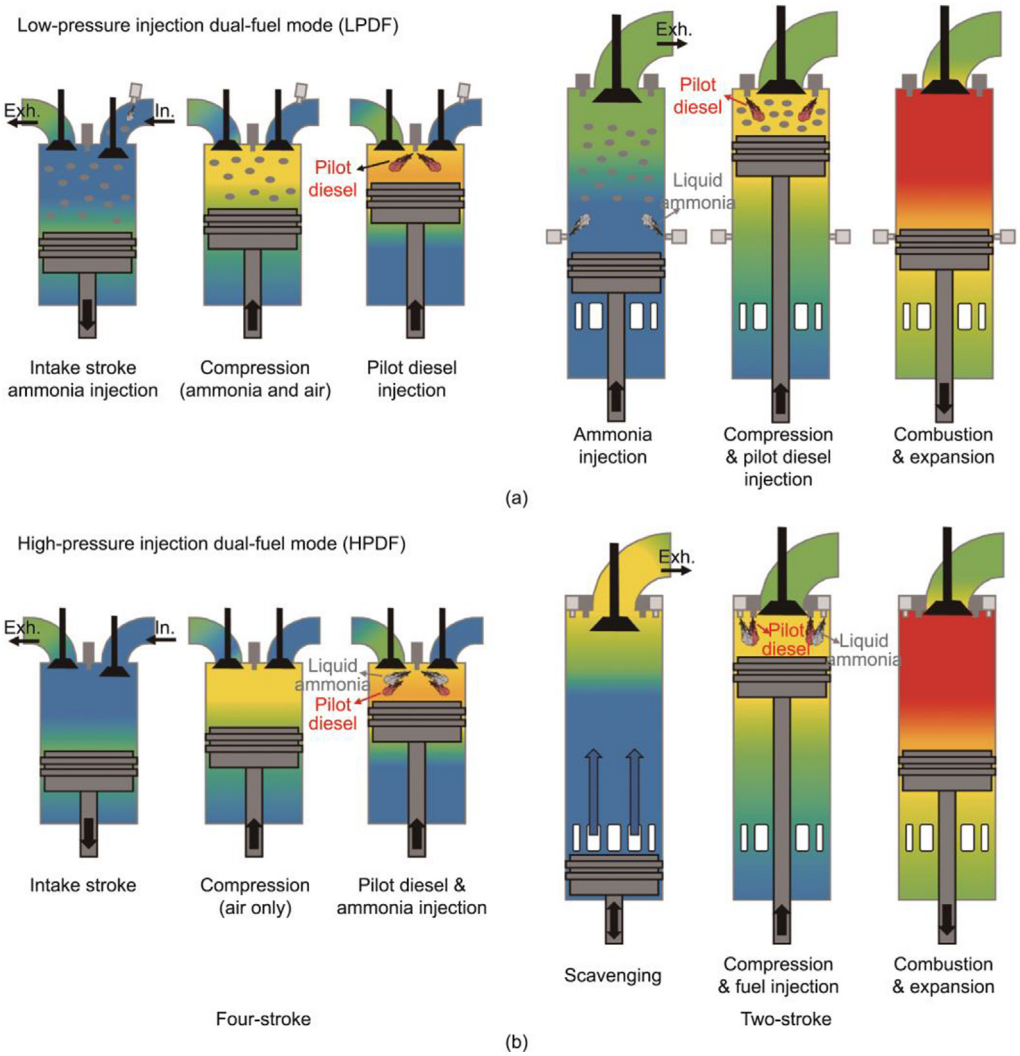

Fig. 33. Conceptual models of the pilot diesel-ignited ammonia combustion engine under both (a) LPDF and (b) HPDF modes. Reproduced from Ref. [155] with permission.

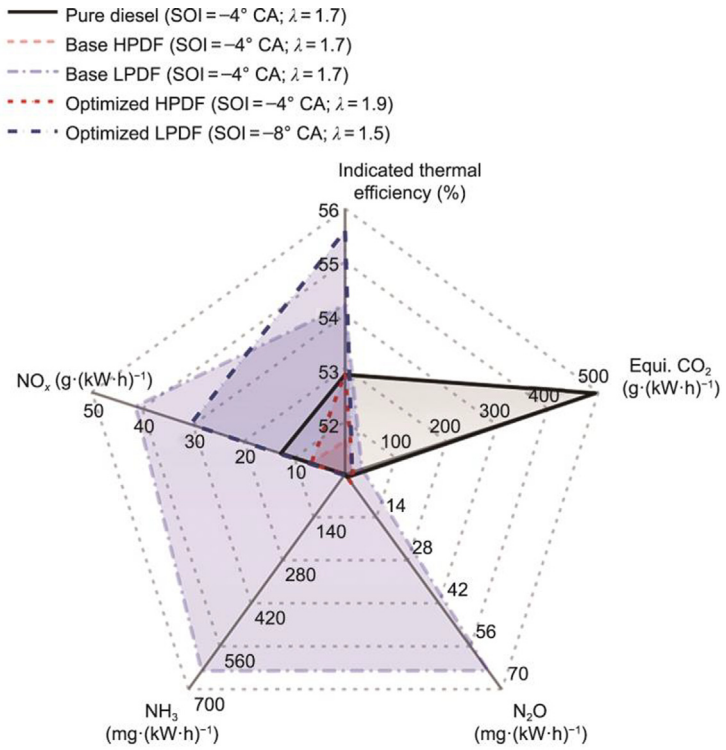

Fig. 34. Comparison of the indicated thermal efficiency and emissions among the pure diesel, LPDF, and HPDF modes. The following parameters are constant in all cases: 157 rpm engine speed, 350 K in-cylinder temperature, and 3.2 bar pressure at EVC timing. Reproduced from Ref. [155] with permission.

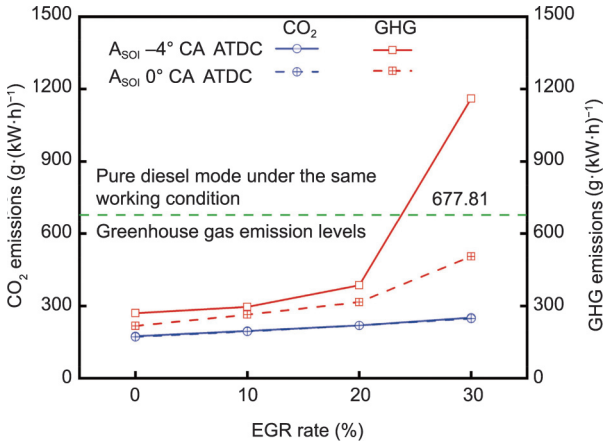

Fig. 35. Levels of GHG emissions at different EGR rates. Reproduced from Ref. [159] with permission.

increasing N_2O and NH_3 emissions. The high in-cylinder temperatures from high-reactivity fuel combustion enable ultra-low N_2O and NH_3 emissions, although CO and hydrocarbons require aftertreatment and SCR for NO_x compliance. With high ammonia substitution rates and low N_2O emissions, TACI combustion demonstrates excellent GHG reduction potential, achieving over 70% reduction.

4.2. Summary

This section examines liquid-ammonia injections in engine-application research from 2022 onward. While liquid-ammonia injection in engines demonstrates technical feasibility with the potential for 97% CO_2 reduction, significant challenges hinder its practical viability. Engine performance shows mixed results: Some studies report efficiency gains up to 5.1%, while others show 2.5% penalties compared with diesel-only operation, and all configurations require diesel pilot injection (3%–20% by energy), preventing complete carbon neutrality. Two-stroke engine tests show improved efficiency and reduced soot/CO, although NO_x increases. Numerical models indicate that spray arrangement, intake temperatures, and EGR rates can balance emissions while maintaining efficiency. Oxygen-enriched air intake improves combustion stability, especially at low speeds/loads. Higher CRs increase efficiency and stability, with minimal impact on unburned ammonia. TACI mode displays efficient ammonia diffusion combustion in a high-temperature atmosphere.

Most concerning are the emissions trade-offs: NO_x emissions increase dramatically (up to 140.6% in some modes) due to both thermal and fuel-bound nitrogen sources, while N_2O formation—with a GWP 265–298 times that of CO_2—can result in higher total GHG emissions than diesel under certain conditions. Combined with persistent ammonia-slip issues, narrow operational windows requiring precise control, and infrastructure challenges for high-pressure liquid-ammonia handling, these findings suggest that, despite its carbon-reduction potential, liquid ammonia's role in transportation may be limited to niche applications unless breakthrough emission-control technologies are developed. Critical comparisons of NO_x and N_2O mitigation strategies reveal varying levels of effectiveness:

Optimized combustion timing. Retarding ammonia injection from −25 to −10 CAD reduces NO_x by 31.4% [156] but may increase unburned ammonia. The trade-off between NO_x reduction and combustion efficiency remains a key challenge.

EGR implementation. A 20% EGR rate effectively reduces NO_x via dilution and temperature reduction [159]. However, increasing the EGR beyond 30% can elevate N_2O emissions, potentially negating GHG benefits. The optimal EGR rate appears to be 15%–25%, based on multiple studies.

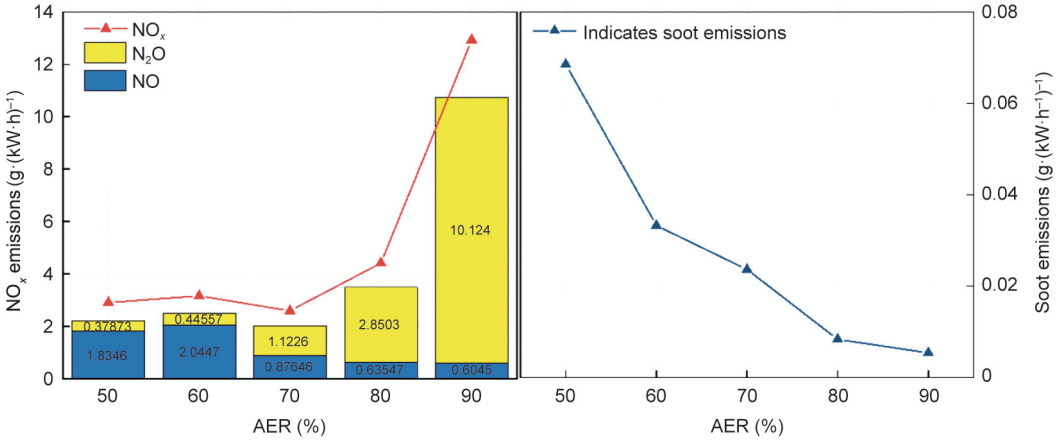

Fig. 36. Effect of AER on (a) NO_x and (b) indicate soot emissions (65/100 MPa ammonia/diesel injection pressure, 50% operational load). Reproduced from Ref. [160] with permission.

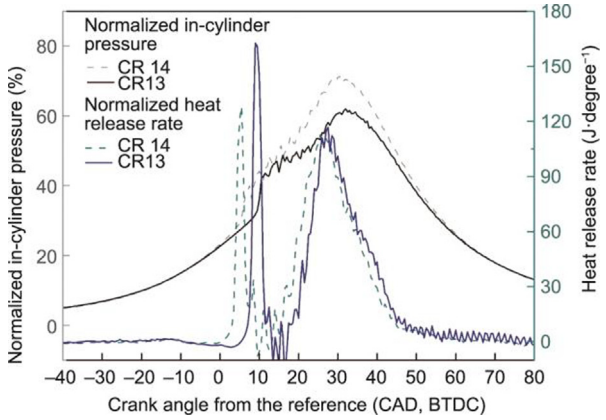

Fig. 37. Normalized in-cylinder pressure and HRR at 15 CAD, before top dead center (BTDC) of micro-pilot fuel-injection timing from the reference under different CRs. Reproduced from Ref. [66] with permission.

Stratified injection. The three-layer approach by Ichikawa et al. [152] dramatically reduces N_2O emissions by eliminating low-temperature regions. Quantitatively, N_2O emissions decreased from 150 ppm to below 20 ppm, representing an 87% reduction.

Post-injection strategies. Diesel post-injection at 40% of pilot quantity reduces N_2O by 19.4% and unburned ammonia by 11.2% [162], while maintaining thermal efficiency. This provides the best balance between emission reduction and performance.

SCR systems. While highly effective for NO_x reduction (up to 90% efficiency), SCR systems present challenges with ammonia slip and require careful temperature management (300–400 °C optimal range) for ammonia exhaust streams. EGR effectively suppresses thermal NO_x but elevates N_2O and CO_2 emissions, reducing ITE by 2%–4% [155]. Stratified injection curbs N_2O by 60% via temperature homogenization [152], yet injector complexity impedes adoption. SCR post-treatment achieves > 70% NO_x reduction [48] but requires ammonia dosing calibration to avoid ammonia slip.

5. Summaries, future research directions, and perspectives

5.1. Summaries

This review presents a comprehensive synthesis of liquid-ammonia injection research, systematically analyzing the complete spectrum from fundamental spray physics to engine implementation. It uniquely establishes critical connections between microscopic phenomena (flash boiling, cavitation, droplet dynamics) and macroscopic engine performance, demonstrating how ammonia's high latent heat causes spray core temperatures to drop, directly explaining extended ignition delays and 40% lower heat release at 900 K versus 1000 K. The review provides the first comparative evaluation of emerging injection strategies (LPDF vs HPDF, spray angles, stratified injection) with quantitative metrics, while identifying precise research gaps unique to liquid ammonia, including cavitation behavior, supercritical phase transitions, and thermal decomposition during atomization. By integrating

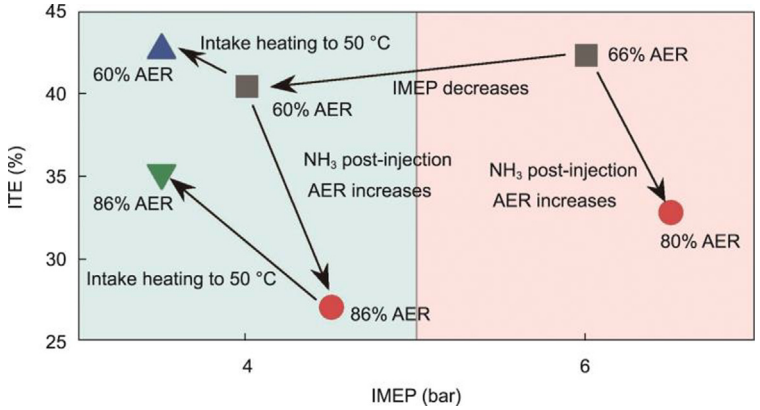

Fig. 38. Pathway for expanding to high AER at medium and low loads. Reproduced from Ref. [163] with permission.

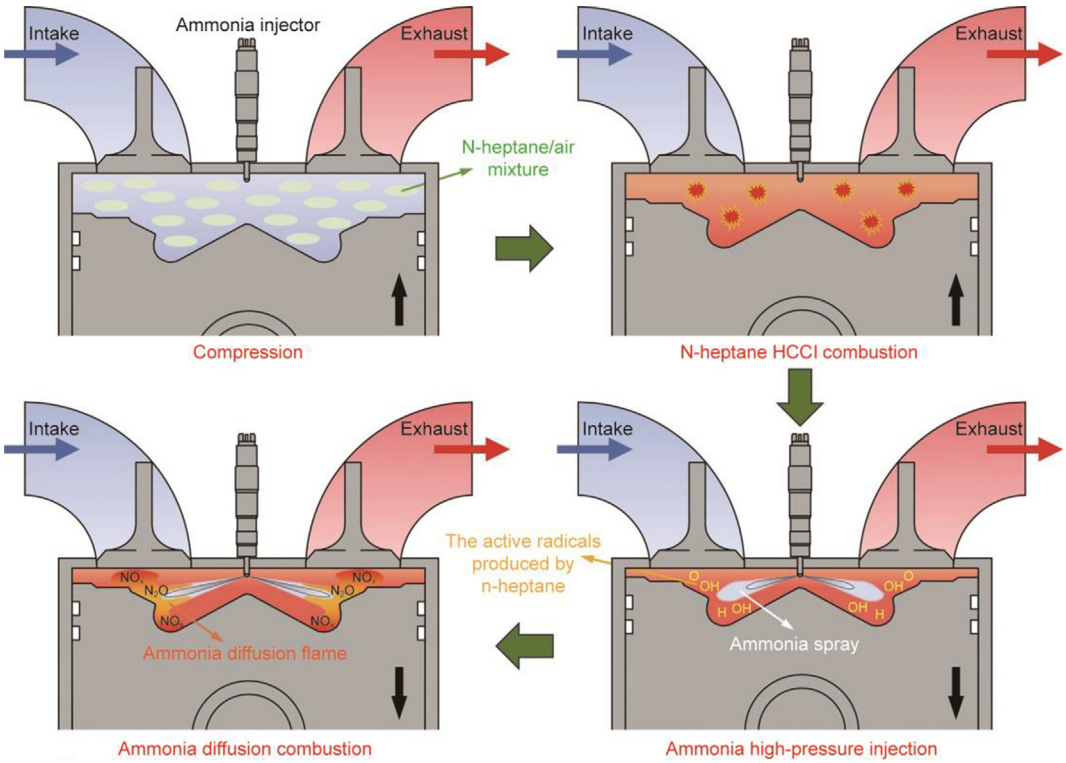

Fig. 39. Schematic diagram of the ammonia TACI combustion mode. Reproduced from Ref. [164] with permission.

breakthrough findings from 2022 to 2024, including first-ever successful auto-ignition demonstrations and novel injection and ignition strategies (TJI, stratified fuel injection, hydrogen co-injection, and TACI), this work fundamentally shows the feasibility landscape for liquid ammonia as an engine fuel and offers practical guidance beyond theoretical discussions.

5.2. Future research directions

In-depth understanding of spray dynamics. Key knowledge gaps include ammonia's unique thermophysical properties and its influence on cavitation inception and development, flash-boiling dynamics under engine conditions, supercritical phase transitions, surface tension effects on droplet breakup, evaporation kinetics in reactive environments, aerodynamic breakup mechanisms, multi-component spray behavior with fuel blends, and thermal decomposition effects during atomization.

Advanced combustion strategies. Further research is needed to develop advanced combustion strategies that can optimize the trade-offs between thermal efficiency, combustion stability, and pollutant emissions. This includes exploring novel ignition methods, such as laser ignition or advanced spark-ignition systems, to address ammonia's high ignition temperature and low reactivity.

Engine hardware and infrastructure. Research should focus on developing specialized engine hardware tailored for liquid-ammonia combustion. This includes designing injectors (prioritize cavitation suppression and an optimized aspect ratio for flash-boiling control), fuel systems, and combustion chambers that can handle ammonia's unique properties, such as its high latent heat and narrow flammability range, while ensuring reliable and efficient operation.

Emission-control technologies. Research should investigate advanced emission-control technologies to mitigate the formation of NO_x, N_2O, and unburned NH_3 during ammonia combustion. Utilizing the existing ammonia from the fuel system to replace urea in SCR can simplify the system while simultaneously reducing residual unburned ammonia and NO_x emissions. Additionally, the catalyst in SCR operates optimally at around 600–700 K, allowing effective use of engine exhaust heat to maintain catalyst temperature and achieve waste heat recovery.

Thermodynamic and fluid dynamic models. Development of more accurate thermodynamic and fluid dynamic models for ammonia sprays is essential. These models should account for ammonia's unique phase-change and resulting turbulence-chemistry interaction to improve the prediction of spray characteristics and combustion performance.

Material compatibility and safety infrastructure. Future research must develop ammonia-resistant materials for fuel injectors (nickel-based alloys, specialized polymers) and compatible seals (EPDM, fluoropolymers) capable of 10 000 + operational hours. Given ammonia's toxicity (IDLH: 300 ppm), systems require sub-second detection at < 5 ppm with automatic engine shutdown. Safety frameworks must include ventilation (6+ air changes per hour), emergency shutdown with purging systems, personal protective equipment (PPE) specifications, spill containment for liquid ammonia, and protocols for bunkering and lube-oil contamination using amine-resistant lubricants.

Long-term durability and scalability challenges. Transitioning ammonia-fueled engines from the laboratory to commercial deployment presents critical durability and scalability issues. Injector degradation occurs due to nozzle erosion from ammonia's low lubricity, requiring research into wear mechanisms, surface treatments, and maintenance schedules. Ammonia contamination neutralizes acidic oil additives, reducing lubricant effectiveness compared with diesel and necessitating ammonia-compatible formulations. Ammonium nitrate deposits from combustion differ from carbon deposits and may impact heat-transfer and CRs. Scaling to multi-cylinder engines introduces cylinder-to-cylinder ammonia distribution variations, complex dual-fuel control systems, and thermal-management challenges from non-uniform heat

release. Demonstration programs on six-plus cylinder engines are essential to validate scalability solutions.

5.3. Perspectives

The transition to liquid ammonia as a fuel represents a significant step toward decarbonizing the transportation and energy sectors. While substantial challenges remain, ongoing research and technological advancements are gradually overcoming these obstacles. Liquid ammonia's potential as a carbon-free fuel—combined with its high energy density and existing infrastructure—makes it an attractive option for future energy systems, particularly in maritime shipping and heavy-duty transportation.

Future research should prioritize the development of integrated solutions that combine advanced combustion technologies, optimized engine designs, and effective emission-control strategies. Collaboration between academia, industry, and policymakers will be crucial in driving the adoption of ammonia as a sustainable fuel alternative. By addressing the technical, economic, and safety challenges associated with liquid-ammonia combustion, we can pave the way for a cleaner and more sustainable energy future.

CRediT authorship contribution statement

Hao Wu: Writing – original draft, Visualization, Methodology, Investigation, Formal analysis. **Fahad Almatrafi:** Writing – review & editing, Investigation, Conceptualization. **Moez Ben Houidi:** Writing – review & editing, Methodology, Investigation. **Tiegang Fang:** Writing – review & editing, Supervision, Conceptualization. **William L. Roberts:** Writing – review & editing, Supervision, Resources, Funding acquisition.

Declaration of competing interest

The authors declare that they have no known competing financial interests or personal relationships that could have appeared to influence the work reported in this paper.

Acknowledgments

This work was supported by the Sustainable Marine Propulsion project from Neom Hefari and the FUELCOM program from the Saudi Aramco Research and Development Center FUELCOM program under Master Research Agreement (6600024505/01).

Appendix A. Supplementary data

Supplementary data to this article can be found online at https://doi.org/10.1016/j.eng.2025.09.008.

References

[1] Spatolisano E, Pellegrini LA, de Angelis AR, Cattaneo S, Roccaro E. Ammonia as a carbon-free energy carrier: NH_3 cracking to H_2. Ind Eng Chem Res 2023;62(28):10813–27.
[2] Wu H, Ben Houidi M, Almatrafi F, Wu B, Du J, Magnotti G, et al. Hydrogen jet characteristics with an outwardly opening piezo injector. Phys Fluids 2025;37(3):036103.
[3] David WI, Agnew GD, Bañares-Alcántara R, Barth J, Hansen JB, Bréquigny P, et al. 2023 roadmap on ammonia as a carbon-free fuel. J Phys Energy 2024;6(2):021501.
[4] MacFarlane DR, Cherepanov PV, Choi J, Suryanto BH, Hodgetts RY, Bakker JM, et al. A roadmap to the ammonia economy. Joule 2020;4(6):1186–205.
[5] Valera-Medina A, Amer-Hatem F, Azad AK, Dedoussi I, De Joannon M, Fernandes R, et al. Review on ammonia as a potential fuel: from synthesis to economics. Energy Fuels 2021;35(9):6964–7029.
[6] Ishaq H, Crawford C. Review of ammonia production and utilization: enabling clean energy transition and net-zero climate targets. Energy Convers Manag 2024;300:117869.
[7] Ammonia technology roadmap: towards more sustainable nitrogen fertiliser production. Report. Paris: International Energy Agency; 2021.
[8] Salmon N, Bañares-Alcántara R. Green ammonia as a spatial energy vector: a review. Sustain Energy Fuels 2021;5(11):2814–39.
[9] Chehade G, Dincer I. Progress in green ammonia production as potential carbon-free fuel. Fuel 2021;299:120845.
[10] Olabi A, Abdelkareem MA, Al-Murisi M, Shehata N, Alami AH, Radwan A, et al. Recent progress in green ammonia: production, applications, assessment; barriers, and its role in achieving the sustainable development goals. Energy Convers Manag 2023;277:116594.
[11] Guerra CF, Reyes-Bozo L, Vyhmeister E, Caparrós MJ, Salazar JL, Clemente-Jul C. Technical–economic analysis for a green ammonia production plant in Chile and its subsequent transport to Japan. Renew Energy 2020;157:404–14.
[12] Klerke A, Christensen CH, Nørskov JK, Vegge T. Ammonia for hydrogen storage: challenges and opportunities. J Mater Chem 2008;18(20):2304–10.
[13] Valera-Medina A, Xiao H, Owen-Jones M, David WI, Bowen P. Ammonia for power. Pror Energy Combust Sci 2018;69:63–102.
[14] Giddey S, Badwal S, Munnings C, Dolan M. Ammonia as a renewable energy transportation media. ACS Sustain Chem Eng 2017;5(11):10231–9.
[15] Dolan RH, Anderson JE, Wallington TJ. Outlook for ammonia as a sustainable transportation fuel. Sustain Energy Fuels 2021;5(19):4830–41.
[16] Schüth F, Palkovits R, Schlögl R, Su DS. Ammonia as a possible element in an energy infrastructure: catalysts for ammonia decomposition. Energy Environ Sci 2012;5(4):6278–89.
[17] Tawalbeh M, Murtaza SZ, Al-Othman A, Alami AH, Singh K, Olabi AG. Ammonia: a versatile candidate for the use in energy storage systems. Renew Energy 2022;194:955–77.
[18] Zhou X, Li T, Yang W. Ammonia–hydrogen engine with single ammonia fuel supply. Joule 2025;9(5):101922.
[19] Sun S, Jiang Q, Zhao D, Cao T, Sha H, Zhang C, et al. Ammonia as hydrogen carrier: advances in ammonia decomposition catalysts for promising hydrogen production. Renew Sustain Energy Rev 2022;169:112918.
[20] Afif A, Radenahmad N, Cheok Q, Shams S, Kim JH, Azad AK. Ammonia-fed fuel cells: a comprehensive review. Renew Sustain Energy Rev 2016;60:822–35.
[21] Morlanés N, Katikaneni SP, Paglieri SN, Harale A, Solami B, Sarathy SM, et al. A technological roadmap to the ammonia energy economy: current state and missing technologies. Chem Eng J 2021;408:127310.
[22] Machaj K, Kupecki J, Malecha Z, Morawski A, Skrzypkiewicz M, Stanclik M, et al. Ammonia as a potential marine fuel: a review. Energy Strategy Rev 2022;44:100926.
[23] An Z, Xing J, Kurose R. Recent progresses in research on liquid ammonia spray and combustion: a review. Appl Energy Combust Sci 2024:100293.
[24] Dimitriou P, Javaid R. A review of ammonia as a compression ignition engine fuel. Int J Hydrogen Energy 2020;45(11):7098–118.
[25] Starkman ES, Newhall H, Sutton R, Maguire T, Farbar L. Ammonia as a spark ignition engine fuel: theory and application. SAE Trans 1966:660155.
[26] Cornelius W, Huellmantel LW, Mitchell HR. Ammonia as an engine fuel. SAE Trans 1966:650052.
[27] Chorowski M, Lepszy M, Machaj K, Malecha Z, Porwisiak D, Porwisiak P, et al. Challenges of application of green ammonia as fuel in onshore transportation. Energies 2023;16(13):4898.
[28] Powders MT, Luqmani BA, Pidou M, Zhu M, McAdam EJ. The use of ammonia recovered from wastewater as a zero-carbon energy vector to decarbonise heat, power and transport—a review. Water Res 2024;268:122649.
[29] Notton G, Nivet ML, Voyant C, Paoli C, Darras C, Motte F, et al. Intermittent and stochastic character of renewable energy sources: consequences, cost of intermittence and benefit of forecasting. Renew Sustain Energy Rev 2018;87:96–105.
[30] Koons E. Ammonia fuel: advantages and disadvantages. Report. Energy Tracker Asia; 2023.
[31] Huang Y, Nie Z, Zhang L, Liu X, Feng J, Yin Y, et al. Ammonia fuel: a pathway for carbon-neutral of the transportation sector. Chain 2024;1(2):113–37.
[32] Kumar L, Sleiti AK. Systematic review on ammonia as a sustainable fuel for combustion. Renew Sustain Energy Rev 2024;202:114699.
[33] Ojelade OA, Zaman SF, Ni BJ. Green ammonia production technologies: a review of practical progress. J Environ Manage 2023;342:118348.
[34] Mallouppas G, Ioannou C, Yfantis EA. A review of the latest trends in the use of green ammonia as an energy carrier in maritime industry. Energies 2022;15(4):1453.
[35] Al-Aboosi FY, El-Halwagi MM, Moore M, Nielsen RB. Renewable ammonia as an alternative fuel for the shipping industry. Curr Opin Chem Eng 2021;31:100670.
[36] Fullonton A, Lea-Langton AR, Madugu F, Larkin A. Green ammonia adoption in shipping: opportunities and challenges across the fuel supply chain. Mar Policy 2025;171:106444.
[37] Kosmajac S. MAN ES presses on with project to develop four-stroke ammonia-powered engine. Report. Schiedam: Offshore Energy; 2024.
[38] Prevljak NH. Wärtsilä rolls out industry's first 4-stroke ammonia engine. Report. Schiedam: Offshore Energy; 2023.
[39] Atchison J. Hyundai Heavy Industries unveils marine ammonia engine. Report. Ashburn: Ammonia Energy Association; 2024.
[40] Xinhua. China's first medium-speed high-power ammonia-fuelled engine ignites [Internet]. Beijing: Chinadaily; 2023 Dec 7 [cited 2025 Mar 23]. Available from: https://www.chinadaily.com.cn/a/202312/07/WS65718967a31090682a5f201c.html

[41] Corporation IHI. Carbon-neutral thermal power generation using ammonia combustion technology development and boiler design to expand use of ammonia. Report. Tokyo: IHI Corporation; 2022.
[42] Yamashita T, Amari T, Urakata Y, Sumida T, Okazaki T, Takayama A. Development of ammonia co-firing technology for coal-fired boilers toward decarbonized society. Mitsubishi Heavy Ind Tech Rev 2022;59:4.
[43] Atchison J. JERA targets 50% ammonia–coal co-firing by 2030. Report. Ashburn: Ammonia Energy Association; 2022.
[44] Tian J, Wang L, Xiong Y, Wang Y, Yin W, Tian G, et al. Enhancing combustion efficiency and reducing nitrogen oxide emissions from ammonia combustion: a comprehensive review. Process Saf Environ Prot 2024;183:514–43.
[45] Verhelst S, Turner JW, Sileghem L, Vancoillie J. Methanol as a fuel for internal combustion engines. Pror Energy Combust Sci 2019;70:43–88.
[46] Yip HL, Srna A, Yuen ACY, Kook S, Taylor RA, Yeoh GH, et al. A review of hydrogen direct injection for internal combustion engines: towards carbon-free combustion. Appl Sci 2019;9(22):4842.
[47] Mazloomi K, Gomes C. Hydrogen as an energy carrier: prospects and challenges. Renew Sustain Energy Rev 2012;16(5):3024–33.
[48] Kobayashi H, Hayakawa A, Somarathne KKA, Okafor EC. Science and technology of ammonia combustion. Proc Combust Inst 2019;37(1):109–33.
[49] Lu Q, Peng Z, Zhou S, Zhang B, Chen H, Yang S. Mini-review of spray and combustion characteristics for ammonia engines. Energy Fuels 2024;38 (20):19156–73.
[50] He X, Shu B, Nascimento D, Moshammer K, Costa M, Fernandes R. Auto-ignition kinetics of ammonia and ammonia/hydrogen mixtures at intermediate temperatures and high pressures. Combust Flame 2019;206:189–200.
[51] Mounaïm-Rousselle C, Bréquigny P, Dumand C, Houillé S. Operating limits for ammonia fuel spark-ignition engine. Energies 2021;14(14):4141.
[52] El-Adawy M, Nemitallah MA, Abdelhafez A. Towards sustainable hydrogen and ammonia internal combustion engines: challenges and opportunities. Fuel 2024;364:131090.
[53] Goodman J, Dhankhar A, Date A, Lappas P. Ammonia–air laminar flame speeds from ambient to IC engine conditions: a review. Fuel 2025;383:133769.
[54] Alnajideen M, Shi H, Northrop W, Emberson D, Kane S, Czyzewski P, et al. Ammonia combustion and emissions in practical applications: a review. Carbon Neutrality 2024;3(1):1–45.
[55] Hewlett SG, Valera-Medina A, Pugh DG, Bowen PJ. Gas turbine co-firing of steelworks ammonia with coke oven gas or methane: a fundamental and cycle analysis. In: Proceedings of ASME Turbo Expo 2019: Turbomachinery Technical Conference and Exposition; 2019 Jun 17–21; Phoenix, AZ, USA. New York City: American Society of Mechanical Engineers; 2019.
[56] Feng R, Li Z. Current investigations on global N_2O emissions and reductions: prospect and outlook. Environ Pollut 2023;338:122664.
[57] Niki Y. Reductions in unburned ammonia and nitrous oxide emissions from an ammonia-assisted diesel engine with early timing diesel pilot injection. J Eng Gas Turbine Power 2021;143(9):091014.
[58] Eyisse EF, Nadimi E, Wu D. Ammonia combustion: internal combustion engines and gas turbines. Energies 2024;18(1):29.
[59] Zhou L, Zhong L, Liu Z, Wei H. Toward highly-efficient combustion of ammonia–hydrogen engine: prechamber turbulent jet ignition. Fuel 2023;352:129009.
[60] Koike M, Miyagawa H, Suzuoki T, Ogasawara K. Ammonia as a hydrogen energy carrier and its application to internal combustion engines. J Combust Soc Jpn 2016;58(184):99–106.
[61] Yamashita H, Hayakawa A, Oku K, Colson S, Reibel G, Chen Y, et al. Visualization of liquid ammonia spray using 2p-SLIPI and comparison of liquid ammonia spray and gaseous ammonia combustion in a swirl combustor at atmospheric pressure. Fuel 2024;371:131833.
[62] Angelilli L, Hernández Pérez FE, Im HG, Ciottoli PP, Valorani M. Evaporation and clustering of ammonia droplets in a hot environment. Phys Rev Fluids 2022;7(11):114301.
[63] Wang X, Bu H, Chen H, Liu J, Chen Z, Gao J. Numerical investigation of diesel spray combustion characteristics in the ammonia/air atmosphere. J Energy Inst 2024;116:101718.
[64] Xu L, Dong P, Zhang Z, Bu J, Tian J, Long W, et al. Impact of spray interaction on ammonia/diesel dual-fuel combustion and emission under engine relevant conditions. Proc Combust Inst 2024;40(1–4):105751.
[65] Wang B, Yang C, Wang H, Hu D, Duan B, Wang Y. Study on injection strategy of ammonia/hydrogen dual fuel engine under different compression ratios. Fuel 2023;334:126666.
[66] Park C, Jang I, Kim M, Park G, Kim Y. Effect of high compression ratio on thermal efficiency and unburned ammonia emissions of a dual-fuel high-pressure direct injection marine ammonia engine. Appl Therm Eng 2025;261:125183.
[67] Okafor EC, Yamashita H, Hayakawa A, Somarathne KKA, Kudo T, Tsujimura T, et al. Flame stability and emissions characteristics of liquid ammonia spray co-fired with methane in a single stage swirl combustor. Fuel 2021;287:119433.
[68] Liu J, Zhang M, An Z, Wang J, Huang Z. Effect of preheated air temperature on a liquid ammonia flash spray in a swirl combustor. Droplet 2025;4(1):e159.
[69] Scharl V, Lackovic T, Sattelmayer T. Characterization of ammonia spray combustion and mixture formation under high-pressure, direct injection conditions. Fuel 2023;333:126454.
[70] Scharl V, Sattelmayer T. Ignition and combustion characteristics of diesel piloted ammonia injections. Fuel Commun 2022;11:100068.
[71] Elbaz AM, Wang S, Guiberti TF, Roberts WL. Review on the recent advances on ammonia combustion from the fundamentals to the applications. Fuel Commun 2022;10:100053.
[72] Otomo J, Koshi M, Mitsumori T, Iwasaki H, Yamada K. Chemical kinetic modeling of ammonia oxidation with improved reaction mechanism for ammonia/air and ammonia/hydrogen/air combustion. Int J Hydrogen Energy 2018;43(5):3004–14.
[73] Okafor EC, Naito Y, Colson S, Ichikawa A, Kudo T, Hayakawa A, et al. Experimental and numerical study of the laminar burning velocity of CH_4–NH_3–air premixed flames. Combust Flame 2018;187:185–98.
[74] Cai T, Zhao D, Gutmark E. Overview of fundamental kinetic mechanisms and emission mitigation in ammonia combustion. Chem Eng J 2023;458:141391.
[75] Xiao H, Valera-Medina A, Bowen PJ. Study on premixed combustion characteristics of co-firing ammonia/methane fuels. Energy 2017;140:125–35.
[76] Li J, Lai S, Chen D, Wu R, Kobayashi N, Deng L, et al. A review on combustion characteristics of ammonia as a carbon-free fuel. Front Energy Res 2021;9:760356.
[77] Wang Y, Wang X, Zeng W, Wang W, Song Z. Advancements in turbulent combustion of ammonia-based fuels: a review. Int J Hydrogen Energy 2024;88:1332–55.
[78] Zhang M, Wei X, An Z, Okafor EC, Guiberti TF, Wang J, et al. Flame stabilization and emission characteristics of ammonia combustion in lab-scale gas turbine combustors: recent progress and prospects. Prog Energy Combust Sci 2025;106:101193.
[79] Valera-Medina A, Marsh R, Runyon J, Pugh D, Beasley P, Hughes T, et al. Ammonia–methane combustion in tangential swirl burners for gas turbine power generation. Appl Energy 2017;185:1362–71.
[80] Wei D, Fang H, Tang H, Wang Y, Wei G, Zhou H. Experimental study of combustion instability and emission characteristics of ethanol/ammonia co-firing swirl flame. Fuel 2024;362:130786.
[81] Zhang X, Tian J, Li X, Yin S, Cui Z, Yang H, et al. Fundamental study on the factors influencing the stability of ammonia combustion and the effects of pre-chamber on the combustion characteristics. Appl Therm Eng 2024;254:123812.
[82] Zhu X, Du J, Yu Z, Cheng YB, Wang Y. NO_x emission and control in ammonia combustion: state-of-the-Art review and future perspectives. Energy Fuels 2023;38(1):43–60.
[83] Chiong MC, Chong CT, Ng JH, Mashruk S, Chong WWF, Samiran NA, et al. Advancements of combustion technologies in the ammonia-fuelled engines. Energy Convers Manag 2021;244:114460.
[84] Cheng Q, Muhammad A, Kaario O, Ahmad Z, Martti L. Ammonia as a sustainable fuel: review and novel strategies. Renew Sustain Energy Rev 2025;207:114995.
[85] Kang L, Pan W, Zhang J, Wang W, Tang C. A review on ammonia blends combustion for industrial applications. Fuel 2023;332:126150.
[86] Pan S, Ma J, Chen X, Yang W, Liang C. A simplified reaction model for combustion of ammonia. Fuel 2025;383:133818.
[87] Zhu Y, Curran HJ, Girhe S, Murakami Y, Pitsch H, Senecal K, et al. The combustion chemistry of ammonia and ammonia/hydrogen mixtures: a comprehensive chemical kinetic modeling study. Combust Flame 2024;260:113239.
[88] Mathieu O, Petersen EL. Experimental and modeling study on the high-temperature oxidation of ammonia and related NO_x chemistry. Combust Flame 2015;162(3):554–70.
[89] Stagni A, Cavallotti C, Arunthanayothin S, Song Y, Herbinet O, Battin-Leclerc F, et al. An experimental, theoretical and kinetic-modeling study of the gas-phase oxidation of ammonia. React Chem Eng 2020;5(4):696–711.
[90] Sher E, Bar-Kohany T, Rashkovan A. Flash-boiling atomization. Pror Energy Combust Sci 2008;34(4):417–39.
[91] Bar-Kohany T, Levy M. State of the art review of flash-boiling atomization. At Sprays 2016;26(12):1259–305.
[92] Wang L, Wang F, Fang T. Flash boiling hollow cone spray from a GDI injector under different conditions. Int J Multiph Flow 2019;118:50–63.
[93] Xu M, Zhang Y, Zeng W, Zhang G, Zhang M. Flash boiling: easy and better way to generate ideal sprays than the high injection pressure. SAE Int J Fuel Lubr 2013;6(1):137–48.
[94] Polanco G, Holdø AE, Munday G. General review of flashing jet studies. J Hazard Mater 2010;173(1–3):2–18.
[95] Chang M, Lee Z, Park S, Park S. Characteristics of flash boiling and its effects on spray behavior in gasoline direct injection injectors: a review. Fuel 2020;271:117600.
[96] Li X, Wang S, Yang S, Qiu S, Sun Z, Hung DL, et al. A review on the recent advances of flash boiling atomization and combustion applications. Pror Energy Combust Sci 2024;100:101119.
[97] Wang S, Qiu S, Li X, Zhang P. Modeling non-monotonic variation of plume angle with superheat index of flash boiling spray. Energy 2024;306:132515.
[98] Du J, Mohan B, Sim J, Fang T, Roberts WL. Study of spray structure under flash boiling conditions using 2phase-SLIPI. Exp Fluids 2021;62(1):1–17.
[99] Zeng W, Xu M, Zhang G, Zhang Y, Cleary DJ. Atomization and vaporization for flash-boiling multi-hole sprays with alcohol fuels. Fuel 2012;95:287–97.
[100] Li S, Li T, Wang N, Zhou X, Chen R, Yi P. An investigation on near-field and far-field characteristics of superheated ammonia spray. Fuel 2022;324:124683.

[101] Li S, Li T, Wang N, Zhou X, Yi P, Chen R. Effect of near-field characteristics on the two-phase distribution of superheated ammonia spray. Int J Engine Res 2023;24(10):4373–81.
[102] Ma Y, Zhong W, Lai S, Chen J, Pachiannan T, Zhang L, et al. Experimental study on the flash boiling spray characteristics and jet fluctuation of high-pressure direct injection liquid ammonia. Appl Therm Eng 2024;257:124032.
[103] Fang Y, Ma X, Zhang Y, Li Y, Zhang K, Jiang C, et al. Experimental investigation of high-pressure liquid ammonia injection under non-flash boiling and flash boiling conditions. Energies 2023;16(6):2843.
[104] Fang Y, Zhang K, Ma X, Zhang Y, Xu L, Li Y, et al. Droplet measurement of high-pressure liquid ammonia injection using PDPA. SAE Technical Paper; 2023:2023–01–1637.
[105] Liu X, Yao X, Wang Z, Tang C. Single hole ammonia spray macroscopic and microscopic characteristics at flare and transition flash boiling regions. Appl Therm Eng 2023;235:121443.
[106] Li S, Liu S, Wang N, Li T, Chen R, Yi P, et al. Atomization and evaporation characteristics of liquid ammonia spray under engine intake stroke conditions. Energy 2025;316:134589.
[107] Zhong W, Chen J, Li C, Huang Y, Pachiannan T, Jiang Z, et al. Visualization study on flash boiling spray characteristics of high-pressure liquid ammonia with different nozzle diameters. Fuel 2024;367:131525.
[108] Shen L, Leach F. Effect of ambient pressure on ammonia sprays using a single hole injector. SAE Tech Pap 2024:2024–01–618.
[109] Colson S, Yamashita H, Oku K, Somarathne KDKA, Kudo T, Hayakawa A, et al. Study on the effect of injection temperature and nozzle geometry on the flashing transition of liquid ammonia spray. Fuel 2023;348:128612.
[110] Desclaux A, Pelé R, Hespel C, Mounaïm-Rousselle C. Liquid Ammonia injection on single hole injector: effect of initial conditions on flash boiling process. In: Proceedings of 32nd European Conference on Liquid Atomization and Spray System; 2023 Sep 4–7; Napoli, Italy. 2023. Hannover: TIB; 2023.
[111] Bjørgen KO, Desclaux A, Mounaïm-Rousselle C, Hespel C. Experimental characterization of superheated ammonia spray from a single-hole ECN spray M injector. J Eng Gas Turbines Power 2025;147(8):081018.
[112] Hiroyasu H, Arai M. Structures of fuel sprays in diesel engines. SAE Tech Pap 1990. 900475.
[113] Naber JD, Siebers DL. Effects of gas density and vaporization on penetration and dispersion of diesel sprays. SAE Tech Pap 1996:960034.
[114] Wu H, Zhang F, Zhang Z. Fundamental spray characteristics of air-assisted injection system using aviation kerosene. Fuel 2021;286:119420.
[115] Huang Z, Wang H, Luo K, Fan J. Large eddy simulation investigation of ammonia spray characteristics under flash and non-flash boiling conditions. Appl Energy Combust Sci 2023;16:100220.
[116] An Z, Xing J, Kurose R. Numerical study on the phase change and spray characteristics of liquid ammonia flash spray. Fuel 2023;345:128229.
[117] Wang J, Wang H, Zheng Z, Yao M. Numerical analysis of flash-boiling spray characteristics with liquid ammonia. Phys Fluids 2024;36(6):063327.
[118] Zhou X, Li T, Wang N, Wu Z, Cao J, Chen R, et al. Similarity of high-pressure direct-injection liquid ammonia spray for different-sized engines. Energy 2024;310:133267.
[119] Pelé R, Mounaïm-Rousselle C, Bréquigny P, Hespel C, Bellettre J. First study on ammonia spray characteristics with a current GDI engine injector. Fuels 2021;2(3):253–71.
[120] Akram MS, Cheng Q, Kaario O, Larmi M. Superheated fuel sprays: a comparative study of flash boiling ammonia fuel sprays with methanol, ethanol, and gasoline for multi-hole fuel injection. Case Stud Therm Eng 2024;61:105110.
[121] Scharl V, Bjørgen KOP, Emberson DR, Løvås T. Investigation of fuel temperature and injection timing effects on ammonia direct injection in an optical engine. Appl Energy Combust Sci 2024;20:100299.
[122] Zembi J, Battistoni M, Pandal A, Rousselle C, Pelè R, Brequigny P, et al. Numerical study of ammonia spray with a GDI engine injector. J Ammonia Energy 2023;1:59–73.
[123] Hu Y, Li J, Chen H, Zhang F, Wang L. Numerical study on spray characteristics of liquid ammonia based on variable model constants. Appl Therm Eng 2024;261:125166.
[124] Rachakonda SK, Goette D, Schmidt DP. Near-nozzle flash-boiling flow of iso-octane, methanol, and ammonia in the engine combustion network spray G injector. Phys Fluids 2024;36(11):113371.
[125] Zembi J, Battistoni M, Pandal A, Pelé R, Brequigny P, Hespel C, et al. Lagrangian CFD modeling of ammonia sprays: a correlation across flash boiling and evaporative conditions. Int Commun Heat Mass Transf 2024;158:107866.
[126] Payri R, García-Oliver JM, Bracho G, Cao J. Experimental characterization of direct injection liquid ammonia sprays under non-reacting diesel-like conditions. Fuel 2024;362:130851.
[127] Zhang Y, Xu L, Zhu Y, Xu S, Bai XS. Numerical study on liquid ammonia direct injection spray characteristics under engine-relevant conditions. Appl Energy 2023;334:120680.
[128] Wu H, Du J, Houidi MB, Aljohani B, Cenker E, AlRamadan AS, et al. Spray and combustion characterization under an ultra-high-density condition–multi-fuel comparison. Proc Combust Inst 2024;40(1–4):105555.
[129] Wang N, Li T, Zhou X, Li S, Chen R. Characteristics of high-pressure ammonia spray combustion under diesel-like conditions. Appl Therm Eng 2024;257:124335.
[130] Li S, Wang N, Li T, Chen R, Yi P, Huang S, et al. Experimental investigation on liquid length of direct-injection ammonia spray under engine-like conditions. Energy 2024;301:131758.
[131] Yang R, Tang Q, Cheng H, Zhang S, Zhang Y, Yao M. Experimental study on the spray characteristics of high-pressure liquid ammonia under different ambient conditions. J Energy Inst 2024;117:101771.
[132] Wu H, Mi S, Qian Y, Zhang T, Zhang J, Pan C, et al. Spray and evaporation characteristics of high-pressure liquid ammonia injection under flash-boiling and evaporating conditions. Fuel 2025;381:133627.
[133] Wu H, Qian Y, Zhang T, Zhu J, Lu X. Ignition and flame development of high-pressure liquid ammonia spray combustion with simultaneous high-speed OH^* and NH_2^* chemiluminescence imaging. Combust Flame 2025;272:113899.
[134] Matsuura Y, Banno A, Mikami M. Single ammonia droplet combustion in a high-pressure environment in microgravity. Proc Combust Inst 2024;40(1–4):105503.
[135] Scharl V, Sattelmayer T. Spectroscopic investigation of diesel-piloted ammonia spray combustion. Fuel 2024;358:130201.
[136] Zhang X, Tian J, Cui Z, Yin S, Ye M, Yang H, et al. Visualization study on the flame propagation and distribution characteristics and exploration of optimal injection strategy in ammonia/diesel dual direct injection mode. Energy 2024;307:132499.
[137] Wu H, Qian Y, Mi S, Zhang T, Lu X. Ammonia–PODE dual-fuel direct-injection spray combustion: an optical study of spray interaction, ignition and flame development. J Clean Prod 2024;487:144647.
[138] Pathak U, Scharl V, Krnac D, Sattelmayer T. Numerical investigation on temperature dependence of flame behavior in high pressure direct injection combustion of diesel piloted liquid ammonia sprays. In: Proceedings of Internal Combustion Engine Division; 2024 Oct 20–23; San Antonio, TX, USA. New York City: ASME; 2024.
[139] Zhang J, Chen D, Li X, Li J, Huang H, Kobayashi N. Large eddy simulation of ammonia–diesel dual fuel spray combustion: effects of ambient condition on ignition characteristics. Chem Eng J 2024;501:157698.
[140] Yu W, Wei Y, Dong D, Zhou M, Mi X, Zhang Z, et al. Characteristics of $NO/NO_2/N_2O$ Formation and distribution in ammonia/n-heptane dual-fuel spray combustion under different ammonia concentrations. Energy Fuels 2024;38(17):16882–95.
[141] Tian J, Zhang X, Cui Z, Ye M, Wang Y, Xu T, et al. Visualization study on ammonia/diesel dual direct injection combustion characteristics and interaction between sprays. Energy Convers Manag 2024;299:117857.
[142] Chen Z, He H, Wu J, Wang L, Lou H, Zhao P, et al. An experimental study the cross spray and combustion characteristics diesel and ammonia in a constant volume combustion chamber. Energy 2024;293:130733.
[143] Zhang Z, Long W, Cui Z, Dong P, Tian J, Tian H, et al. Visualization study on the ignition and diffusion combustion process of liquid phase ammonia spray ignited by diesel jet in a constant volume vessel. Energy Convers Manag 2024;299:117889.
[144] Sharma P, Brouzet D, Chung WT, Ihme M. Examining diesel-spray assisted ignition of ammonia under reactivity-controlled conditions using large-eddy simulations. Proc Combust Inst 2024;40(1–4):105317.
[145] Haputhanthri SO, Maxwell TT, Fleming J, Austin C. Ammonia and gasoline fuel blends for internal combustion engines. J Energy Res Technol 2015;137(6):062201.
[146] Ryu K, Zacharakis-Jutz GE, Kong SC. Performance characteristics of compression-ignition engine using high concentration of ammonia mixed with dimethyl ether. Appl Energy 2014;113:488–99.
[147] Gross CW, Kong SC. Performance characteristics of a compression-ignition engine using direct-injection ammonia–DME mixtures. Fuel 2013;103:1069–79.
[148] Xu L, Xu S, Bai XS, Repo JA, Hautala S, Hyvönen J. Performance and emission characteristics of an ammonia/diesel dual-fuel marine engine. Renew Sustain Energy Rev 2023;185:113631.
[149] Lang M, Su Y, Wang Y, Zhang Y, Wang B, Chen S. Experimental study on the effects of pilot injection strategy on combustion and emission characteristics of ammonia/diesel dual fuel engine under low load. Energy 2024;303:131913.
[150] Shi T, Pei Y, Jin S, Zi Z, Zhang F, Wu B. An investigation into particulate emission and the formation mechanism of soot precursors in ammonia–diesel dual-fuel engines. Fuel 2025;391:134734.
[151] Zhong L, Zhao W, Wei H, Shu G, Zhou L. A novel concept of pre-chamber turbulent jet ignition-induced liquid ammonia spray flame. Phys Fluids 2024;36(12):126107.
[152] Ichikawa Y, Niki Y, Takasaki K, Kobayashi H, Miyanagi A. NH_3 combustion using three-layer stratified fuel injection for a large two-stroke marine engine: experimental verification of the concept. Appl Energy Combust Sci 2022;10:100071.
[153] Ichikawa Y, Niki Y, Takasaki K, Kobayashi H, Miyanagi A. Experimental study of combustion process of NH_3 stratified spray using imaging methods for NH_3 fueled large two-stroke marine engine. Appl Energy Combust Sci 2023;13:100119.
[154] Bakir AH, Ge H, Zhang Z, Zhao P. Computational investigation on spray autoignition of liquid ammonia with dissolved hydrogen in spray D configuration. Fuel 2024;371:132124.

[155] Zhou X, Li T, Wang N, Wang X, Chen R, Li S. Pilot diesel–ignited ammonia dual fuel low-speed marine engines: a comparative analysis of ammonia premixed and high-pressure spray combustion modes with CFD simulation. Renew Sustain Energy Rev 2023;173:113108.
[156] Nadimi E, Przybyła G, Løvås T, Peczkis G, Adamczyk W. Experimental and numerical study on direct injection of liquid ammonia and its injection timing in an ammonia–biodiesel dual injection engine. Energy 2023;284:129301.
[157] Nadimi E, Przybyła G, Løvås T, Adamczyk W. Effects of biodiesel injector configuration and its injection timing on performance, combustion and emissions characteristics of liquid ammonia dual direct injection engine. J Energy Inst 2024;114:101605.
[158] Zhang Z, Long W, Dong P, Tian H, Tian J, Li B, et al. Performance characteristics of a two-stroke low speed engine applying ammonia/diesel dual direct injection strategy. Fuel 2023;332:126086.
[159] Dong P, Liu K, Zhang L, Zhang Z, Long W, Tian H. Study on the synergistic control of nitrogenous emissions and greenhouse gas of ammonia/diesel dual direct injection two-stroke engine. Energy 2024;307:132657.
[160] Dong P, Chen S, Zhang L, Zhang Z, Long W, Wang Q, et al. Ammonia diffusion combustion and emission formation characteristics in a single cylinder two stroke engine. Energy 2024;311:133432.
[161] Park C, Jang I, Park G, Min C, Kim M, Kim Y, et al. Effect of oxygen concentrations in intake air on combustion characteristics of ammonia direct injection SI engine. Fuel 2024;376:132643.
[162] Lee J, Park C, Jang I, Kim M, Park G, Kim Y. Experimental research on the effect of diesel post-injection conditions on the efficiency and global warming potential in a single-cylinder four-stroke marine engine fueled with ammonia and diesel. Energy 2025;314:134244.
[163] Mi S, Zhang J, Shi Z, Wu H, Zhao W, Qian Y, et al. Optimization of direct-injection ammonia–diesel dual-fuel combustion under low load and higher ammonia energy ratios. Fuel 2024;375:132611.
[164] Yang R, Yue Z, Zhang S, Lv Z, Yao M. Ammonia thermal atmosphere compression ignition combustion mode to achieve efficient combustion and low greenhouse gas emissions. Energy Convers Manag 2025;325:119427.
[165] Li Z, Fan Y, Li J, Wu K, Zhang Z, Ren F, et al. Stratified charge assisted jet ignition mode (SCAJI) for low-speed two-stroke Otto cycle ammonia marine engine. Fuel 2025;379:133037.
[166] Mi S, Zhang J, Shi Z, Wu H, Qian Y, Zhu L, et al. Investigation of low carbon emission and high thermal efficiency of diesel engine combined with high-pressure direct injection of hydrogen carrier: ammonia. Int J Hydrogen Energy 2024;88:86–96.
[167] Mi S, Shi Z, Zhang J, Wu H, Qian Y, Lu X. Exploration of ultra-low carbon heavy-duty commercial vehicle technology: liquid ammonia–diesel dual fuel high-pressure direct injection. Int J Engine Res 2024;26(7):1029–43.
[168] Xiong Q, Zhao B, Wan Z, Liang D, Liu L. Effect of ammonia jet strategy and intake air temperature on mixing characteristics in ammonia/diesel dual-fuel marine engine. Appl Therm Eng 2025;262:125192.
[169] Wang Y, Zhou X, Liu L. Feasibility study of hydrogen jet flame ignition of ammonia fuel in marine low speed engine. Int J Hydrogen Energy 2023;48(1):327–36.
[170] Lin Z, Liu S, Liu W, Wang W, Cai K, Qi Y, et al. Numerical investigation of ammonia-rich combustion produces hydrogen to accelerate ammonia combustion in a direct injection SI engine. Int J Hydrogen Energy 2024;49:338–51.
[171] Li T, Zhou X, Wang N, Wang X, Chen R, Li S, et al. A comparison between low- and high-pressure injection dual-fuel modes of diesel-pilot-ignition ammonia combustion engines. J Energy Inst 2022;102:362–73.
[172] Cui J, Chen W, Wang B, Fan Y, Tian H, Long W, et al. Effects of relative position of injectors on the performance of ammonia/diesel two-stroke engines. Energy 2024;309:133085.